ABSTRACT

Title of dissertation: CHARACTERIZATION AND CLASSIFICATION OF FACES ACROSS AGE PROGRESSION

Narayanan Ramanathan, Doctor of Philosophy, 2008

Dissertation directed by: Dr. Rama Chellappa
Department of Electrical and Computer Engineering

Facial aging, a new dimension that has recently been added to the problem of face recognition, poses interesting theoretical and practical challenges to the research community . How do humans perceive age ? What constitutes an age-invariant signature for faces ? How do we model facial growth across different ages ? How does facial aging effects impact recognition performance ? This thesis provides a thorough overview of the problem of facial aging and addresses the aforementioned questions.

We propose a craniofacial growth model that characterizes growth related shape variations observed in human faces during formative years (0 - 18 yrs). The craniofacial growth model draws inspiration from the 'revised' cardioidal strain transformation model proposed in psychophysics and further, incorporates age-based anthropometric evidences collected on facial growth during formative years. Identifying a set of fiducial features on faces, we characterize facial growth by means of growth parameters estimated on the fiducial features. We illustrate how the growth related transformations observed on facial proportions can be studied by means of linear and non-linear equations in facial growth parameters, which subsequently help in computing the growth parameters. The proposed growth model implicitly accounts for factors such as gender, ethnicity, the individual's age group etc. Predicting one's appearance across ages, performing face verification across ages etc. are some of the intended applications of the model.

Next, we propose a two-fold approach towards modeling facial aging in adults. Firstly, we develop a shape transformation model that is formulated as a physically-based parametric muscle model that captures the subtle deformations facial features undergo with age. The model implicitly accounts for the physical properties and geometric orientations of the individual facial muscles. Next, we develop an image gradient based texture transformation function that characterizes facial wrinkles and other skin artifacts often observed during different ages. Facial growth statistics (both in terms of shape and texture) play a crucial role in developing the aforementioned transformation models. From a database that comprises of pairs of

age separated face images of many individuals, we extract age-based facial measurements across key fiducial features and further, study textural variations across ages. We present experimental results that illustrate the applications of the proposed facial aging model in tasks such as face verification and facial appearance prediction across aging.

How sensitive are face verification systems to facial aging effects ? How does age progression affect the similarity between a pair of face images of an individual ? We develop a Bayesian age difference classifier that classifies face images of individuals based on age differences and performs face verification across age progression. Further, we study the similarity of faces across age progression. Since age separated face images invariably differ in illumination and pose, we propose pre-processing methods for minimizing such variations. Experimental results using a database comprising of pairs of face images that were retrieved from the passports of 465 individuals are presented. The verification system for faces separated by as many as 9 years, attains an equal error rate of 8.5%.

CHARACTERIZATION AND CLASSIFICATION OF FACES ACROSS AGE PROGRESSION

by

Narayanan Ramanathan

Dissertation submitted to the Faculty of the Graduate School of the
University of Maryland, College Park in partial fulfillment
of the requirements for the degree of
Doctor of Philosophy
2004

Advisory Committee:
Dr. Rama Chellappa, Chair/Advisor
Dr. P.S. Krishnaprasad
Dr. Prakash Narayan
Dr. Larry Davis
Dr. Amitabh Varshney

DEDICATION

To Sudha, Amma and Appa.

Acknowledgments

I would like thank my advisor Dr. Rama Chellappa for all his guidance and continued support all through my life at graduate school. He was a great source of inspiration without whom my journey in graduate school would not have been as memorable. I am greatly indebted to him for having provided me with financial assistance all through my degree. I would like to thank him wholeheartedly for having sent me to many conferences and workshops which helped significantly in expanding my horizon in the area of research. In addition, I would like to thank him for having provided me with an opportunity to be a teaching assistant for his course on Pattern Recognition.

I would like to thank Dr. Amit K. Roy Chowdhury for his guidance on the HID project and the National Geographic project. The many discussions I had with him played a crucial role in initiating me into research. I would like to thank Dr. David Jacobs for the discussions we have had on my thesis. I would like to thank Dr. Krishnaprasad, Dr. Prakash Narayan, Dr. Larry Davis and Dr. Amitabh Varshney for serving on my defense committee. Their suggestions and remarks played a crucial role in refining my thesis. I would like to thank Mr. Phil Horvitz from Apptis Inc. for having provided the 'Horvitz Fellowship'.

The years I spent at graduate school would not have been as lively and as invigorating without the company of my labmates, Gaurav Aggarwal and Ashok Veeraraghavan. The innumerable discussions I have had with them greatly helped me in making advances on my thesis. I would also like to thank Aravind Sun-

daresan, Aswin Sankaranarayanan, Jagan Sankaranarayanan, Sameer Shirdonkar, Haibin Ling, Kevin Zhou, Naresh Cuntoor, Amit Kale, Amit Agrawal, Mahesh Ramachandran, Yang Ran and my other fellow CFAR graduate students for the memorable years I happened to spend at A.V.Williams. My heartfelt thanks to my roommates Prasanth, Somashekar, Shiv Naga, Raghav Kashyap, Indrajith, Arunesh Mishra and Harish for their inimitable support and friendship.

I would like to thank Dr. Nikhil Gagvani (CTO, Cernium) for his constant support and guidance. Chipotle and Noodles & Company deserve a special mention. They fed me well for the most part of my graduate life. Finally, I would like to express my heartfelt gratitude to my wife, Sudha, for all her support all through the thick and thin. I dedicate this thesis to her.

Table of Contents

List of Tables

List of Figures

Chapter 1

Introduction

Human faces comprise a special class of 3D objects that have long been of interest to computer vision and psychophysics communities. Apart from playing a crucial role in human identification, human faces convey a significant amount of information on one's age, gender, ethnicity, his / her emotional state etc. Over the past decade, researchers from computer vision and psychophysics have contributed significantly towards a better understanding of the perception of human faces and towards developing computational models that help characterize facial appearances. Apart from the numerous holistic and feature based approaches that have been proposed towards face recognition from 2-D images, many algorithms have been proposed for face recognition from video and from 3-D scans of human faces. Zhao et al. [13] provide a qualitative analysis of the different face recognition algorithms. Decades of dedicated research coupled with the standardization of face recognition algorithms through evaluation methodologies such as FERET [14,15] and FRVT [16] have enhanced the commercial significance of face recognition systems.

While today's face recognition systems perform commendably well in controlled environments, there is a notable drop in their performance in uncontrolled environments. Factors such as illumination variations, pose variations, facial expressions, facial occlusions etc. affect recognition performance significantly. Zhao

et al. [13] discuss the effects of non-uniform illumination and pose variations on face recognition. [17], [18], [19], [20], [21], [22], [23], [24] are some of the notable approaches proposed towards recognizing faces across illumination and pose variations. Facial Action Coding systems [25] has contributed significantly towards facial expression characterization. [26], [27], [28], [29] propose approaches towards recognizing facial expressions from face images.

In recent years, a new dimension has been added to the problem of face recognition. *Age* as an attribute related to human faces is being increasingly studied and there has been a growing interest in problems such as face recognition across ages, automatic age estimation from face images, appearance prediction across ages etc. Some of the motivations behind working on the problem of facial aging are listed below.

1.1 Motivation

Characterizing the progressive, but subtle variations in facial appearances as humans age has many significant implications. Some of the interesting applications of studying age progression in human faces are discussed below.

- Developing face recognition systems that are robust to age progression would enable the successful deployment of face recognition systems in public places. Such systems would be highly beneficial to homeland security applications. Further, developing systems that verify face images across age progression would annul the necessity of periodically updating large face databases with

more recent images.

- Since different individuals age differently, developing automatic age progression systems that could predict the many different ways a person could have aged would have a significant impact in finding missing individuals.

- Ethological studies have revealed that the perceived age of an individual significantly affects the type and amount of behavior directed towards him/her by other individuals. Hence, building systems that could reliably estimate the age of individuals, would be useful for developing human-robot interaction systems and human-computer interaction systems.

- Changes in facial appearances have a significant psychosocial impact on an individual [30]. Studies related to craniofacial growth are bound to help surgeons and orthodontists in treating disfigurements and deformities in faces.

1.2 Problem Statement

From a computer vision perspective, facial aging offers many an exciting challenges. Figure 1.1 illustrates the face images of an individual taken during different ages, from infancy until the later stages of adulthood. The figure illustrates the many forms by which facial aging effects are manifested across ages. The different forms of manifestations could be described as (a) rapid increase in facial size and a loss in facial fat during infancy (b) a gradual, but well pronounced, increase in facial size during teenage years (c) subtle changes in facial shape during adulthood

Figure 1.1: A compilation of multiple images of an individual taken during different ages. The images were collected from the FG-NET aging database. [2]

(d) the appearance of facial wrinkles during the later stages of adulthood (e) Hair growth or hair loss etc.

1.3 Contributions made in this thesis

Providing formal characterizations to such facial appearance variations and improving the performance of face recognition systems when presented with age separated face images of individuals are the primary focuses of this thesis. In this thesis

- We propose a facial growth model that characterize facial characterizes growth related shape variations commonly observed during formative years. The model draws inspiration from the certain facial growth models that were studied in psychophysics and further, incorporates age-based anthropometric measurements in characterizing facial appearances.

- Next, we propose a physically based model that characterizes the shape and textural variations that are observed in adult faces as a result of aging. We propose a facial muscle model that helps characterize the drift in facial features commonly observed in adulthood. We also propose methods to characterize facial textural variations such as wrinkles and other skin artifacts.

- We propose a subspace-based approach towards performing face verification across age progression. We also illustrate how the proposed approach could be used to estimate the age separation between a pair of age separated face images of an individual.

Chapter 2 provides an in-depth account of the previous work on the topic of facial aging. Chapters 3 and 4 detail computational approaches towards characterizing facial aging effects during formative years and during adulthood respectively. Chapter 5 addresses the problem of verifying one's identity from his or her age separated face images. Chapter 6 illustrates some of my intended future in a topic quite related to this thesis.

Chapter 2

Literature Survey

Human perception studies reveal that attributes derived from one's appearance such as *one's emotional state*, *attractiveness*, *perceived age* etc. tend to significantly influence interpersonal behavior [31]. Hence, for many decades human faces have been closely studied in computer vision and psychophysics with the objective of characterizing the many factors that induce appearance variations and subsequently unearthing information pertaining to an individual from his / her varying facial appearances. This chapter provides a thorough analysis on problems related to facial aging and further offers a complete account on the many research initiatives pertaining this problem.

We discuss some of the interesting studies performed on the topic of facial aging in *Psychophysics and Human Perception* and in *Computer Vision* focusing on problems such as age estimation, facial appearance modeling, face verification across aging etc. Finally, the chapter introduces some of the face databases that provide age separated face images of individuals.

2.1 Contributions from Human Perception and Psychophysics

The ability of humans to perceive age-related changes in facial appearances and their readiness in judging the relative age differences even from sparse repre-

sentations of faces such as 'schematic faces', prompted numerous researchers from human perception and psychophysics to study the natural phenomenon of facial aging. D'arcy Thompson's study of morphogenesis [32] played a critical role in understanding the morphological changes associated with growth in biological forms. Thompson based his study of morphogenesis on identifying the constraints (forces) that biological forms were subjected to and in understanding their role in maintaining the structural and physiological integrity of biological forms despite the morphological changes. He embedded biological forms within a coordinate framework and employed coordinate transformations in studying different morphogenetic events. The graphic depictions of such morphogenetic events that he presented, highlighted the effects of natural constraints on the global morphology of organisms. Figure 2.1 illustrates the morphological changes induced on a human skull image as a result of coordinate transformations.

In the 1970s, there was considerable interest in experimental psychology in the topic of event perception. Events invariably involved change and hence, event perception studies sought to analyze the patterns of change in characterizing events. Delineating the perceptual information specific to a class of events and knowing *apriori* the external environment where the events occur were identified as critical aspects of event perception. Robert Shaw studied *facial growth* as an event perception problem [33] as against those who believed facial growth to be a problem of cognition. Shaw sought to identify the *transformational invariants* and *structural invariants* that are associated with facial growth, with the objective of identifying the factors that were responsible for similar patterns of change each time the event

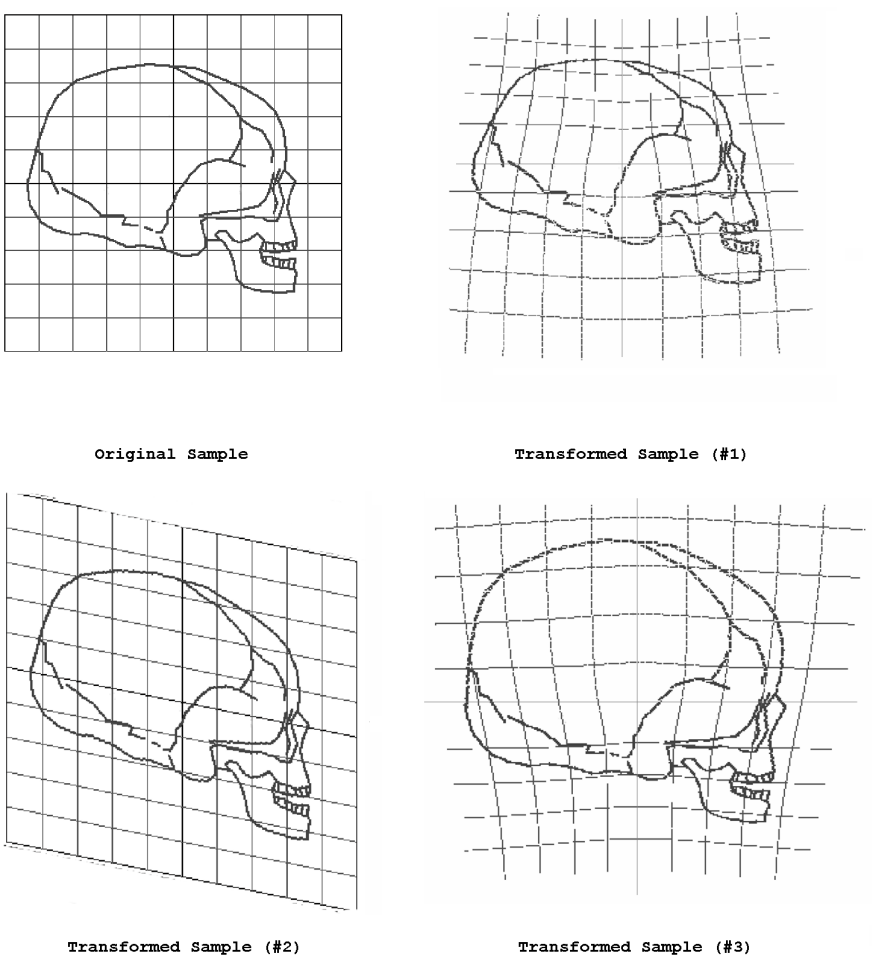

Figure 2.1: Morphological changes that are induced on biological forms (human, in the case above) as a result of applying coordinate transformations is illustrated.

was manifested. He observed that the *structural invariants* associated with facial growth were responsible for preserving the identity of individuals over the course of facial growth.

Drawing inspiration from Thompson's work, Shaw *et al.* [33] sought to identify mathematical transformations that help characterize the facial growth event. They discovered two transformations that could be applied on the outer contour of faces in the 'profile view' namely,

- Cardioidal strain : Stretches the face downward and outward
- Affine shear : When applied in the right proportion, introduces a protrusion in the jaw and a backward slant in the forehead

Pittenger and Shaw [34] revisited the above approach and investigated the relative importance of three force configurations namely, the *shear* forces, the *strain* forces and the *radial* forces in inducing facial growth. Observers were asked to identify the age-level of facial profiles that were altered by different force configurations. They observed that the age-level estimates from facial profiles altered by 'cardioidal strain' forces (which implicitly incorporates the radial force component) were far more consistent than that altered by 'shear forces' and proposed that 'cardioidal strain' transformation were effective in characterizing morphological changes in the human cranium as a result of growth. Fig. 2.2 illustrates the effects of applying combinations of strain transformations and shear transformations on profile faces.

Todd *et al.* [7] proposed the hydrostatic model, also called as the 'revised' cardioidal strain transformation model to characterize facial growth. Drawing analogies between human head growth and the modeling of a fluid-filled spherical object with pressure, they performed a hydrostatic analysis of the effects of gravity on a growing head. Their approach was based on the notion that a biological structure remodeled in accordance with the amount and direction of forces the structure was subjected to.

Mark *et al.* [1] hypothesized that the perceptual information associated with any recognizable style of change were contained in the geometric invariants asso-

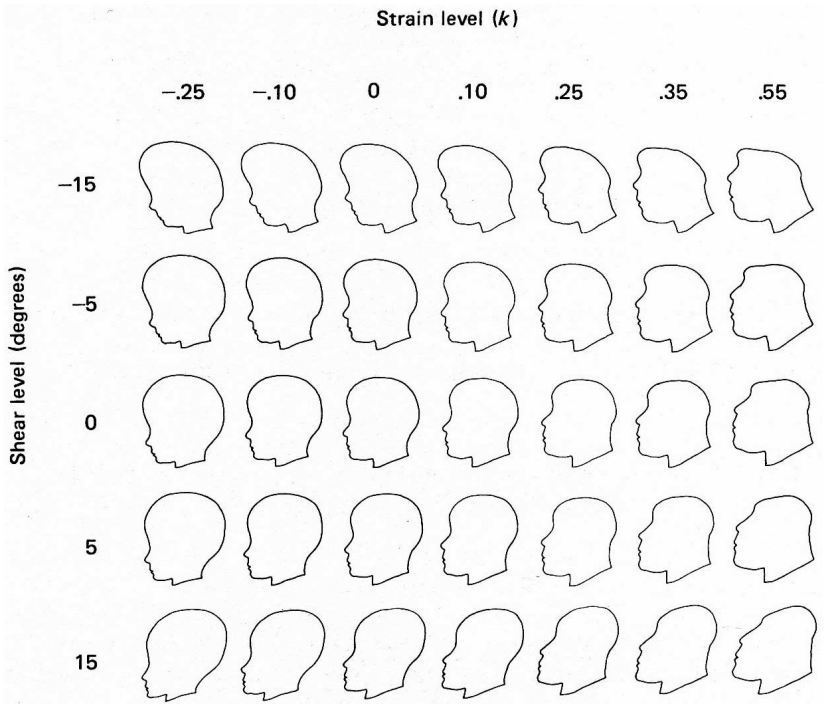

Figure 2.2: Transformation functions that were proposed to model craniofacial growth : The 'revised' cardioidal strain transformation was observed to be most effective in performing the task.)

.

ciated with the event. They sought to identify the geometric invariants that are characteristic of growth, the invariants that were common to the myriad of structures that could be recognized as growing. Three geometric invariants were identified in relation to facial growth, namely

- Type I : The angular coordinates of features being preserved
- Type II : Bilateral symmetry about the vertical axis being preserved
- Type III : Continuity of all contours and their directions of curvature being preserved

Mark *et al.* [1] further hypothesized that for any transformation to be identified as that which induces growth related changes, the aforementioned attributes had to be preserved across transformation. Delineation of such invariants provided a framework for selecting different transformation functions for study in perceptual tests related to facial growth. Table 2.1 and Table 2.2 illustrate the mathematical form of some of the transformation functions that were studied as being relevant to facial growth and further illustrates which geometric invariants (discussed above) are preserved by each transformation function.

Table 2.1: Geometric transformations that were studied under the context of craniofacial growth

Transformation function	**Mathematical Form**	**Invariants**		
		I	II	III
Rigid Rotation (polar coordinates)	$\theta_{t+1} = \theta_t + \phi$ $R_{t+1} = R_t$	×	×	✓
Reflected Shear (Cartesian coordinates)	$Y_{t+1} = Y_t$ $X_{t+1} = X_t + kY_t\ (\frac{X_t}{\lvert X_t \rvert})$	×	✓	✓
Affine Shear (Cartesian coordinates)	$Y_{t+1} = Y_t$ $X_{t+1} = X_t + kY_t$	×	✓	✓
Spiral strain (polar coordinates)	$\theta_{t+1} = \theta_t$ $R_{t+1} = R_t(1 + k\lvert\theta_t\rvert)$	✓	✓	✓

Table 2.3 illustrates the growth ratings that were recorded for each transfor-

Table 2.2: First set of geometric transformations that were studied under the context of craniofacial growth

Transformation function	**Mathematical Form**	**Invariants**		
		I	II	III
Cardioidal strain (polar coordinates)	$\theta_{t+1} = \theta_t$ $R_{t+1} = R_t(1 - k\cos(\theta_t))$	✓	✓	✓
Revised Cardioidal Strain (polar coordinates)	$\theta_{t+1} = \theta_t$ $R_{t+1} = R_t(1 + k(1 - \cos(\theta_t)))$	✓	✓	✓

mation function. The growth ratings, which originally appeared in [1] were compiled as described below : Subjects were provided with pairs of face profiles with each pair reflecting the transformation induced by each function. The growth ratings were computed by taking the mean of the scores that were assigned to each transformation function. To give a perspective of the scale of such ratings : The growth ratings that were assigned for 'Actual Growth' (the case when the pair of face profiles actually were retrieved from growing faces) and that for 'No Change' (the case where the pair of face profiles were identical) were 3.8 and 0.1 respectively. Figure 2.3 illustrates the effects of four of the transformation functions that were studied in relation to facial growth. Table 2.4 and Table 2.5 summarize some of the other contributions in this topic from Psychophysics, Human Perception and related fields. A concise account of the above mentioned studies is provided in Pittenger [35] and Mark [36].

Table 2.3: Second set of growth ratings that were assigned to different transformation functions in Mark *et al.* [1]

Transformation function	**Growth Rating**
Rigid Rotation	0.05
Reflected Shear	0.3
Affine Shear	0.8
Spiral strain	3.0
Cardioidal strain	3.6
Revised Cardioidal Strain	-NA-

2.2 Contributions from Computer Vision

In recent years, there has been a growing interest in the computer vision community in addressing the many problems related to facial aging such as : age estimation, appearance modeling, face recognition / verification across ages etc. From a computer vision perspective, the problem of facial aging can be described as follows :

- *Shape vs. Texture* : Facial aging can be described as a problem of characterizing facial shape and facial texture as functions of time. Since aging effects induce progressive variations in facial appearances, models characterizing the same need to account for the temporal nature of the induced variations.

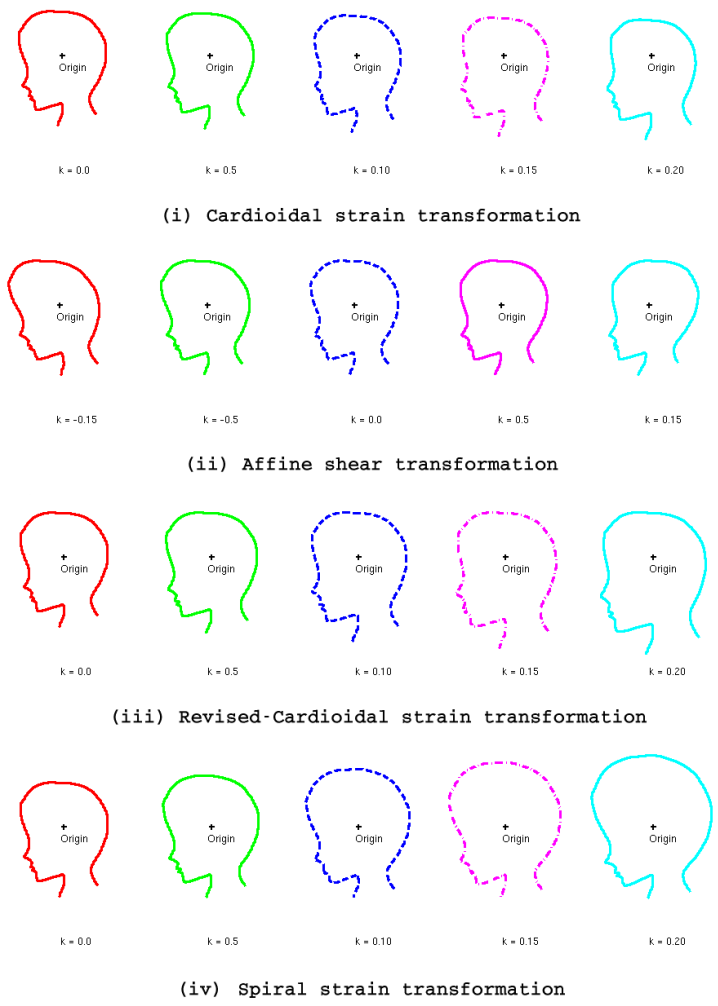

Figure 2.3: An illustration of the effects of applying different transformation functions on 'profile faces'. An illustration of this nature originally appeared in [1].

- *Feature selection* : Developing facial growth models or building characterizations of facial aging begins with identifying the appropriate form of data that provide a fair description of the event. The data could be *individual-specific* or *population-specific*. Fiducial features (2D or 3D) extracted from age separated faces, 2D facial imagery or 3D facial scans extracted from individuals across different ages, face anthropometric measurements extracted from a population

Table 2.4: Some Contributions from Psychophysics, Human Perception, Physiology, Paleontology etc. in the topic of Facial Aging

Reference	**Summary of contributions**
Enlow [37]	Provided a detailed account of neonatal growth and observed disproportionate changes in the dimensions of the head and the face, across growth.
Gerasimov [38]	Developed explicit procedures to infer a detailed structure of human faces from their bare skulls. His accurate reconstructions led to the hypothesis that bone growth was largely controlled by the soft-tissue
Pittenger and Shaw [39]	Interestingly, observed that the cardioidal strain transformation was effective in altering the perceived age of cartoon drawings of monkeys, birds, dogs and inanimate objects such as the 'Volkswagen' beetle.

etc. are some of forms of data that can help characterize facial growth.

- *Factors* : Apart from biological factors such as bone growth, loss in elasticity of facial muscles, facial fat atrophy etc., numerous other factors such as one's ethnicity, gender, dietary habits and climatic conditions have been shown to contribute to facial aging effects [6] . Further, facial appearances get altered with increase in age due to factors such as loss of hair. Hence, the proposed

Table 2.5: Additional Contributions from Psychophysics, Human Perception, Physiology, Paleontology etc. in the topic of Facial Aging

Reference	**Summary of contributions**
Mark *et al.* [40]	Age estimates were obtained from faces whose shape and degree of skin wrinkling were changed. Both the variables affected the perceived age of faces.
Mark and Todd [41]	Extended the 2D cardioidal strain transformation model into 3D and demonstrated its effectiveness in characterizing facial growth in 3D
Bruce *et al.* [42]	Observed that a subject's sensitivity to cardioidal strain related changes in 3D faces were comparable, when viewed in pairs of
O'Toole *et al.* [3], [43]	Applied a facial caricaturing algorithm on 3D faces. Noted that an exaggeration or a de-emphasis of facial creases, increased or decreased the perceived age of faces respectively. Fig. 2.4 illustrates the same.

characterization of facial aging effects should ideally account for the multiple factors that have been identified to induce aging effects.

Table 2.6 summarizes computer vision approaches towards facial aging based on the nature of the approach. Table 2.7 and Table 2.8 summarize them based on the problem that was addressed for different age groups. In subsequent sections, we provide a concise account of each of of the contributions mentioned in Table 2.6.

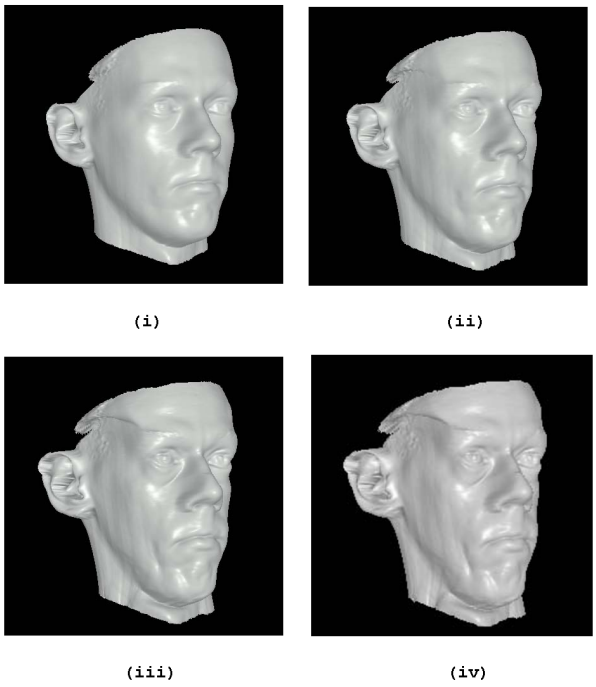

Figure 2.4: The effects of inducing wrinkles and facial creases on 3D caricatures of human faces is illustrated. Sub-figure (i) corresponds to the original 3D Face. Sub-figures (ii), (iii) and (iv) correspond to the 3D faces that were generated upon exaggerating facial crease. The illustration has been derived from [3] and has been included with due permission from the authors.

2.2.1 Age Estimation

Age estimation techniques were often based on shape-based cues and texture-based cues that were extracted from faces. While feature-based approaches used anthropometric distances extracted from different facial regions in estimating one's age, holistic approaches typically adopted subspace methods to reduce the dimensionality of faces and subsequently used regression techniques to estimate one's age from his or her face images.

Table 2.6: A summary of contributions from computer vision in the topic of facial aging

Approach	**Reference(s)**
Subspace based	Lanitis *et al.* [44], [45], Geng *et al.* [46], [47] Fu *et al.* [48], Guo *et al.* [49]
Model based	Suo *et al.* [50], Unsang *et al.* [51]
Machine Learning	Gandhi and Levine [52], Ling *et al.* [53] Yang and Ai [54]
Image / Feature driven	Kwon and Lobo [55], Burt and Perrett [4] Tiddeman *et al.* [5], Biswas *et al.* [56]

Kwon and Lobo [55] proposed an age classification approach that identifies the age group a face image belongs to, based on the anthropometry of the face and the density of its wrinkles. They considered three age groups in their study, namely, that of *infants*, *young adults* and *senior adults*. Observing that the lower and upper halves of faces grow at different rates during formative years, [7], they used ratios of facial measurements in distinguishing images of infants from those of adults. They identified 6 ratios (eye-eye : eye-nose, eye-eye : eye-mouth etc.) for their study. Further, they proposed the use of *snakelets* [59] in characterizing facial wrinkle density in predesignated facial regions, which was used to classify the images of young adults from that of senior adults.

Table 2.7: A summary of computer vision approaches : Based on the problem addressed for different age groups

Reference	**Objective**	**Age group**
Kwon and da Lobo [55], [57]	Age based classification	Infants, young adults and and senior adults
Burt and Perrett [4]	Age transformation, Age perception	Adults
Wu *et al.* [58]	Age transformation	Adults
O'Toole *et al.* [3]	Age perception	Adults
Tiddeman *et al.* [5]	Age transformation, Age perception	20 yrs - 60 yrs
Lanitis *et al.* [44]	Age transformation, Face recognition across age	0 yrs - 30 yrs

Adopting the Active Appearance Model (AAM) [60] approach, Lanitis *et al.* [44], [45] devised a combined shape and intensity model to represent face images. Face images were represented by means of model parameters, which are nothing but the principal components from the eigenspaces that correspond to facial shape and facial intensity. They proposed the following approaches to estimate one's age from such low-dimensional representations of faces. Let the model parameters of faces be designated as $\mathbf{b}$.

Table 2.8: A summary of computer vision approaches : Based on the problem addressed for different age groups

Reference	**Objective**	**Age group**
Lanitis *et al.* [45]	Age based classification of face images	0 yrs - 30 yrs
Gandhi [52]	Age transformation Age estimation	15 yrs and above
Geng *et al.* [47]	Age estimation	All ages
Suo *et al.* [50]	Age transformation	Adults

- Regression functions : Modeling age as a function of the model parameters $\mathbf{b}$, age $= f(\mathbf{b})$, they modeled f as linear, quadratic and cubic functions. The age of an unknown face was estimated using the identified function f.

- Age-based Distribution functions : Identifying a distribution function for the model parameters corresponding to each age, the age of unknown faces is estimated by means of the Mahanalobis distance computed between the model parameters of the unknown face and the centroid of the age-based distribution functions.

- Neural Networks : Supervised and unsupervised neural networks were built

on the model parameters to estimate one's age from face images.

Geng *et al.* [46], [47] proposed the 'Aging pattern subspace : AGES' approach to perform age estimation from face images. Defining the 'aging pattern' as a sequence of personal face images ordered in time, AGES is designed to characterize the temporal nature of the underlying data and thereby capture the appearance variations commonly observed in aging faces. Since obtaining a 'complete aging pattern' for each individual is difficult (the case when an individual's face images are available for all the ages of interest), they developed the 'aging pattern subspace' drawing inspiration from methods that develop an eigenspace [61] using incomplete data (data with missing features). Upon developing the subspace, the aging pattern and the age of a previously unseen face is determined by the projection in the subspace that best reconstructs the face.

Fu and Huang [48] construct a low-dimensional manifold from a set of age-separated face images using different manifold learning approaches such as LPP (Locality Preserving Projections), OLPP (Orthogonal Locality Preserving Projections), CEA (Conformal Embedding Analysis) etc., and use linear and quadratic regression functions on the low-dimensional feature vectors from the respective manifolds, in estimating the age of a face. Along very similar lines, Guo *et al.* [49] adopt the manifold learning approach and use Support Vector Regression [61] to estimate the age from the low-dimensional representation of faces. They report that local adjustments made on the regression result lead to improved accuracy in age estimation.

Yang and Ai [54] proposed a learning-based approach towards classifying face images based on their age group. They used the LBP (Local Binary Pattern) [62] as an image operator and extracted the LBP histogram which was subsequently used for texture characterization. Adopting the AdaBoost technique [61], they identified a sequence of local features which when combined into a strong classifier performs the task of age classification successfully.

Table 2.9 lists the different databases on which age estimation results were reported.

2.2.2 Computational Models for Age Progression

Modeling facial appearances across different ages amounts to building computational models for facial aging that account for a multitude of factors such as (i) age group (ii) gender (iii) ethnicity (iv) weight loss / gain etc.

Burt and Perrett's [4] focusing on age-related visual cues associated with faces, offered many insights into the task of modeling facial aging in adults. Considering face images from 7 age groups [20-24 years, 25-29 years, ... and 50-54 years], they identified a set of fiducial features from every face image in order to characterize the facial shape. By averaging the shape and skin color (in RGB space) from face images belonging to the same age group, they created *composite faces* for each age group. They observed that by incorporating the differences between composite faces (in both shape and skin-color) from different age groups onto real face images, the perceived age of the transformed face images increased. Interestingly, the averaging

Table 2.9: Databases that were used for the task of age estimation

References	**Database**
Kwon and da Lobo [55]	A private database comprising of 47 images of infants and adults
Lanitis *et al.* [44]	FG-NET Aging Database [2] 330 images in the age range 0 to 35 years.
Geng *et al.* [47]	FG-NET Aging Database [2]
Fu and Huang [48] Guo *et al.* [49]	(i) FG-NET Aging Database [2] (ii) UIUC-IFP-Y Aging Database A private database comprising of 8000 images of 1600 individuals
Yang and Ai [54]	FERET Database [14], PIE Database [11]

operation involved in creating the composite faces was observed to smoothen facial creases and result in composite faces appearing younger than those from their own age groups.

Tiddeman *et al.* [5] extended the above study and incorporated wavelet based methods for prototyping facial textures and subsequently, creating the *composite faces* for different age groups. A locally weighted measure of edge strength in small regions was used to retain the edges in composite faces leading to better age trans-

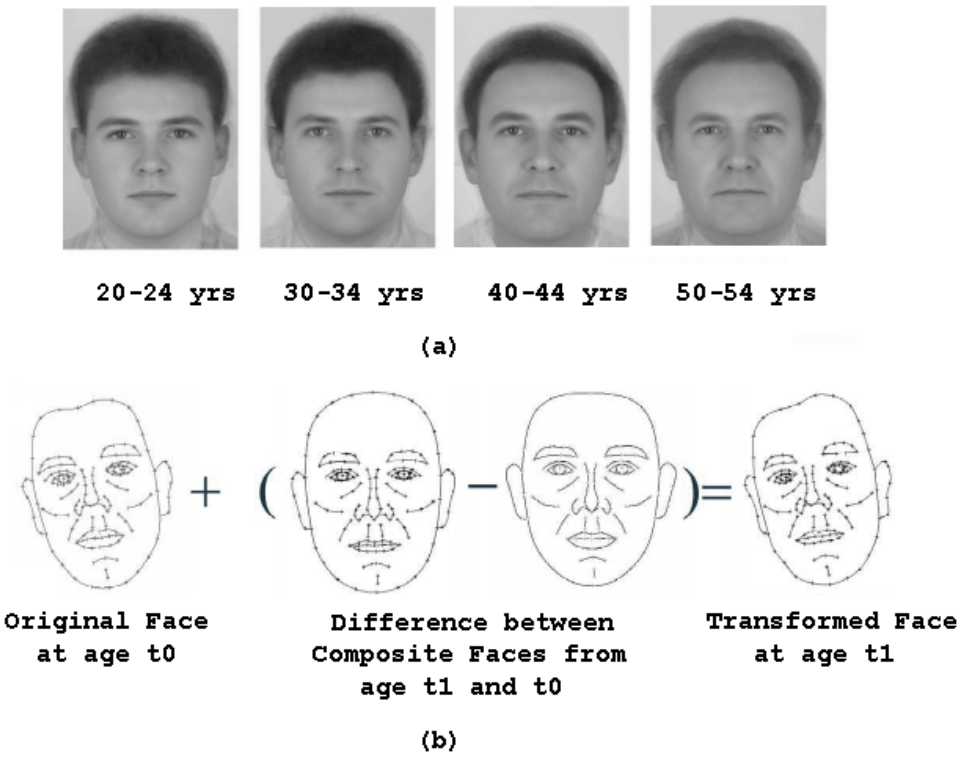

Figure 2.5: (a) An illustration of the 'Composite faces' that were constructed for four age groups (b) An illustration of the age-based shape transformation approach proposed by [4] and [5]. (The above illustration was derived from [5] and has been published with permission from the authors)

formation in a manner identical to that described in [4]. Figure 2.5 illustrates the composite faces that were created for different age groups and further illustrates the age-based shape transformation approach prescribed by [4] and [5].

Suo *et al.* [50] adopted the multi-resolution grammatical face model proposed in [63] and augmented the model with age and hair features. Faces are represented by means of And-Or graphs, where the 'And-nodes' correspond to the course to fine representation of faces and the 'Or-nodes' correspond to the alternative configura-

tions in facial components in each resolution. Facial aging was modeled by means of a dynamic Markov process on the And-Or graph representation. They create a dictionary of different facial components and regions across five age groups (20-30 years, 30-40 years, 40-50 years, 50-60 years and 60-70 years). The transitional probabilities comprised in the dynamic model are computed by means of 'geometric distances' and 'photometric distances' computed between facial components from different age groups. The following attributes related to facial aging are accounted for, in three different resolutions of the face image.

- Global appearance variations in facial shape, hair style, skin color etc. are addressed at the lowest resolution.
- Deformations in facial components are addressed in the next resolution.
- Finally, finer aspects such as wrinkles, skin pigments etc. are accounted for in the highest resolution.

2.2.3 Face verification across age progression

On a broad scale, the different methods that were proposed to perform face verification across ages can be classified as 'generative' and 'non-generative' in nature. Verification methods under the former category, typically introduce appearance transformations on one of the test images to reduce the facial appearance difference due to age separation. Generative approaches typically involve a computational model for facial aging which is subsequently employed for a face verification task. The face recognition / verification tasks are described in Lanitis *et al.* [44].

On the other hand, non-generative approaches derive an age-invariant signature from faces and use the same to perform face verification across age progression. The approaches proposed by Ling *et al.* [53] and Biswas *et al.* [56] fall under the latter category. Ling *et al.* [53] proposed an face operator derived based on the image gradient orientations derived from multiple resolutions and used Support Vector Machines [61] to perform face verification across ages. They offered insight into why image gradient orientations tend to be robust to appearance changes introduced as a result of facial aging.

Biswas *et al.* [56] proposed *coherency* in facial feature drifts across ages as a measure to perform face verification across ages. Their approach is based on the idea that while facial feature drifts observed across age separated face images of the same individual follow a coherent drift pattern, the same might not be true for age separated face images of two different individuals. Since fiducial features extracted on the outer contour tend to be very sensitive to head pose variations, they limited their study to fiducial features that were derived from interior facial regions.

2.3 Aging Databases and Growth Related Data

Over the years, numerous face databases [64] have been collected to help study the different problems related to face recognition. Given the difficulty in compiling face datasets that comprise of age-separated face images, there are very few publicly available datasets that specifically address facial aging in comparison to the datasets that address other problems in face recognition. There are three publicly available

databases that comprise of age separated face image samples namely, the MORPH Database [65], [66], the FG-NET Aging Database [2] and the FERET Database [14]. Here, we provide a concise account on each of the three databases, in relation to facial aging.

2.3.1 The MORPH Database

The MORPH Database comprises face images of adults taken during different ages. The database has been organized into two albums : 'MORPH Album 1' and 'MORPH Album 2'. 'MORPH Album 1' comprises of 1690 digitized images of 515 individuals in the age range $15 - 68$ years. 'MORPH Album 2' comprises of 15204 images of nearly 4000 individuals. Apart from the face images, the database also provides meta-information that is critical for the task of studying age progression such as age, sex, ethnicity, height and weight. Table 2.10 provides a quick overview of the MORPH database.

2.3.2 FG-NET Aging Database

The FG-NET (Face and Gesture Recognition Research Network) aging database [2] comprises of 1002 images of 82 subjects ($6 - 18$ images per subject) in the age range $0 - 69$ years. The database also provides 68 landmark features that were identified manually, on all the face images. In addition, the following meta-information is available for all the images in the dataset namely : *image size*, *age*, *gender*, *spectacles*, *hat*, *mustache*, *beard*, *horizontal pose* and *vertical pose*. Since the images were

Table 2.10: MORPH Database : Age based Data

MORPH Album 1									
Gender	**Age Group**					**# Samples**			
	<18	18-29	30-39	40-49	50+	#1	#2	#3	#4+
Male	142	803	345	93	22	519	289	67	9
Female	15	182	70	18	0	105	58	13	2
MORPH Album 2									
Gender	**Age Group**					**# Samples**			
	<18	18-29	30-39	40-49	50+	#1	#2	#3	#4+
Male	0	29	5371	5679	1905	3440	1954	1192	2958
Female	0	4	964	1017	235	599	322	200	500

retrieved from real-life albums of different subjects, aspects such as illumination, head pose, facial expressions etc. are uncontrolled in this dataset. Nevertheless, this database is the only publicly available resource that provides quite a few age separated face images of individuals in the age range $0 - 18$ years. Further, the database also has adult face images.

Table 2.11: MORPH Database : Ethnicity based data

Gender	**MORPH Album 1**			**MORPH Album 2**		
	AA	C	O	AA	C	O
Male	1037	365	3	10283	2650	51
Female	216	69	0	1665	550	5

2.3.3 FERET Database

The FERET Database [14], a comprehensive database that addresses multiple problems related to face recognition such as illumination variations, pose variations, facial expressions etc., also comprises of a few hundred age separated face images of subjects (the age separation amounting to 18 months or more). The FERET dataset, pertaining to facial aging, can be described as below :

- Gallery-set : Comprises of 1196 images
- Duplicate I Probe-set : Comprises of 722 images of subjects whose gallery match was taken $0 - 1031$ days beforehand.
- Duplicate II Probe-set : Comprises of 234 images of subjects whose gallery match was taken $540 - 1031$ days beforehand.

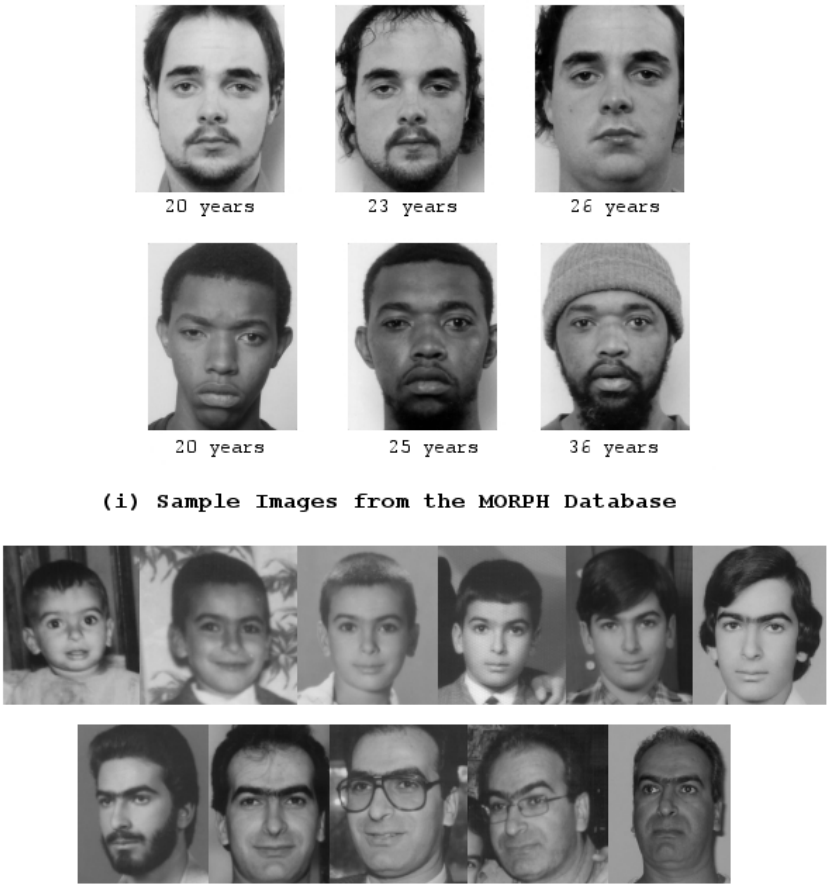

Figure 2.6: Sample images from the MORPH Database and the FG-NET Database

2.3.4 Face Anthropometry

Face anthropometry, the science of measuring sizes and proportions on human faces, has the potential to play a crucial role in developing facial aging models. Such studies provide a quantitative description of the craniofacial complex at different ages and hence, provide a plethora of options for learning based approaches to be adopted to characterize facial aging. Face anthropometric studies provide dense measurements taken between key landmarks on human faces across different ages and have played a critical role in surgical procedures employed on the faces of

growing children [67]. Farkas [6] provides a comprehensive overview of face anthropometry and its many significant applications. He defines face anthropometry in terms of measurements taken from 57 carefully selected landmarks on human faces spread across 6 regions in the craniofacial complex (head, face, orbits, nose, lips and mouth, ear). The facial measurements are of three kinds : (i) projective measurements (shortest distance between two landmarks)(ii) tangential measurements (distance between two landmarks measured along the skin surface) (iii) angular measurements. Figure 2.7

Age (years)	Male			Female		
	N	Mean	SD	*N*	Mean	SD
0–5 months	8	70.0	4.5	5	68.0	4.5
6–12 months	20	70.5	4.8	8	72.7	4.4
1	18	80.6	4.8	20	77.2	4.9
2	31	87.5	3.5	31	83.8	3.9
3	30	88.5	3.5	30	86.9	2.4
4	30	96.4	4.3	30	92.6	3.6
5	30	96.7	3.5	30	96.5	4.6
6	50	98.5	5.0	50	95.7	4.4
7	50	99.5	5.0	50	98.3	3.7
8	51	101.8	4.9	51	98.1	5.4
9	51	102.7	5.3	50	101.3	5.3
10	50	105.2	4.5	49	103.9	5.0
11	50	107.1	6.0	51	104.7	5.0
12	52	109.1	5.4	53	108.2	4.6
13	50	111.6	5.7	49	109.1	5.0
14	49	114.1	6.5	51	110.7	5.3
15	50	119.1	5.7	51	111.0	5.1
16	50	120.9	4.6	51	113.5	6.0
17	49	120.9	7.1	51	112.0	4.7
18	52	121.3	6.8	51	111.8	5.2
19–25	109	124.7	5.7	200	111.4	4.8

(a)

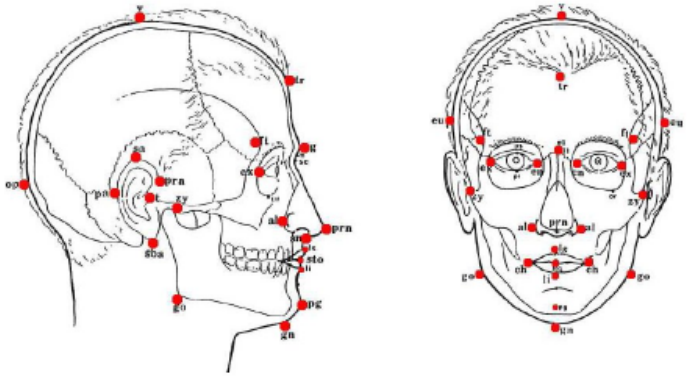

(b)

Figure 2.7: (a) Sample measurements extracted across fiducial features designated by 'n' and 'sn' from ages 0 to 18 years on boys and girls are illustrated (Appears in [6]). (b) An illustration of the different facial features that are studied in anthropometric studies

Chapter 3

Modeling facial aging during formative years

Developing computational models that help emulate humans in their remarkable ability in recognizing faces, despite the many different facial appearance variations, has been one of the primary objectives of studies related to human facial analysis. Computational models that characterize facial appearances should ideally account for factors that are inherent to human faces such as (i) the 3D structure of human faces (ii) the reflective properties of facial skin (iii) the degrees of freedom associated with different facial features that result in local deformations (iv) the bilateral symmetry in the configuration of facial features etc. In addition, scene-centric attributes as illumination, head-pose and other external sources of variations such as facial occlusions, facial hair need to be taken into account. The focus of this chapter is in proposing a facial aging model that characterizes growth related changes observed in one's facial appearance as a result of aging, during formative years (0 - 18 years).

Facial aging effects are manifested in different forms in different ages. During formative years, they are predominantly manifested in the form of facial shape variations and during adulthood, as a combination of gradual variations in facial shape and texture. Factors such as gender, ethnicity, age group etc. are often attributed to playing a significant role in affecting facial growth. Since textural variations tend

to be subtle during formative years, the proposed model primarily addresses shape variations that are characteristic of aging faces in their formative years. Predicting the appearance of children across ages and improving the performance of face verification systems on age-separated face images of children are some of the model's intended applications. Fig. 3.1 shows examples of age separated face images of individuals from the FG-Net aging database [8].

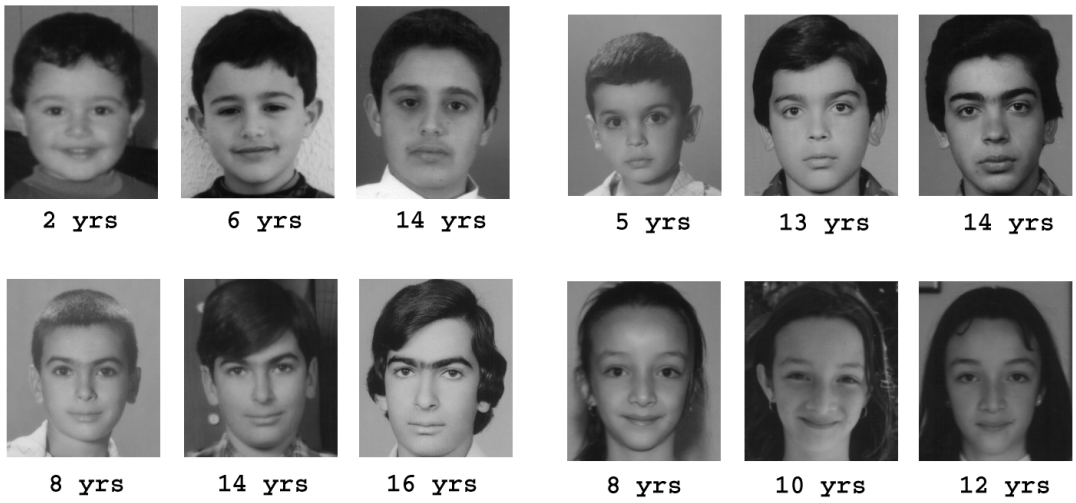

Figure 3.1: Age separated face images of children (from the FG-Net database [2]

Apart from the regular challenges encountered in performing recognition on adult face images, recognizing children from their face images is posed with an added complication : age separated face images of children differ in their physical sizes. Hence, the preprocessing approaches that are typically applied on adult faces to reduce mis-alignment of features such as aligning the pair of eyes, the facial mid-axis etc. cannot be adopted to align age separated face images of children. Developing computational models that characterize the facial shape variations during formative years is crucial to successfully perform face verification / recognition on age

separated face images of children.

The following section provides an overview of the craniofacial growth model and highlights the importance of incorporating age-based anthropometric face measurements in developing the model. In subsequent sections, we discuss face anthropometry in relation to studying age progression in human faces and provide a mathematical framework for computing the craniofacial growth model, respectively. Further, we detail the experiments results and discuss some of the strengths and limitations of the proposed craniofacial growth model.

3.1 Craniofacial Growth Model

We propose a craniofacial growth model that draws inspiration from the 'revised' cardioidal strain transformation model proposed by Todd *et al.* [7]. Reintroducing the 'revised' cardioidal strain transformation model discussed in the previous chapter, the model is mathematically expressed as :

$$P_i^{t_0} \propto R_i^{t_0}(1 - \cos(\theta_i^{t_0})) \tag{3.1}$$

$$R_i^{t_1} = R_i^{t_0}[1 + k_i^{t_0 t_1}(1 - \cos(\theta_i^{t_0}))]$$

$$\theta_i^{t_1} = \theta_i^{t_0} \tag{3.2}$$

where $P_i^{t_0}$ denotes the pressure (directed radially outward) applied at the i'th fiducial feature on the surface of the spherical object at age t_0 yrs, ($R_i^{t_0}$, $\theta_i^{t_0}$) and ($R_i^{t_1}$, $\theta_i^{t_1}$) denote the angular co-ordinates of the i'th fiducial feature at t_0 yrs and t_1 yrs respectively and $k_i^{t_0 t_1}$ denotes a growth related constant. The model assumes

knowledge of the origin of reference for the transformation model. Fig. 3.2(a) illustrates the pressure distribution within a fluid filled spherical object. Fig. 3.2(b) illustrates the different face profiles that were generated upon applying the 'revised' cardioidal strain transformation on face profiles of children. With an increase in the value of parameter 'k', one can observe an increase in the perceived age of the resultant face profiles.

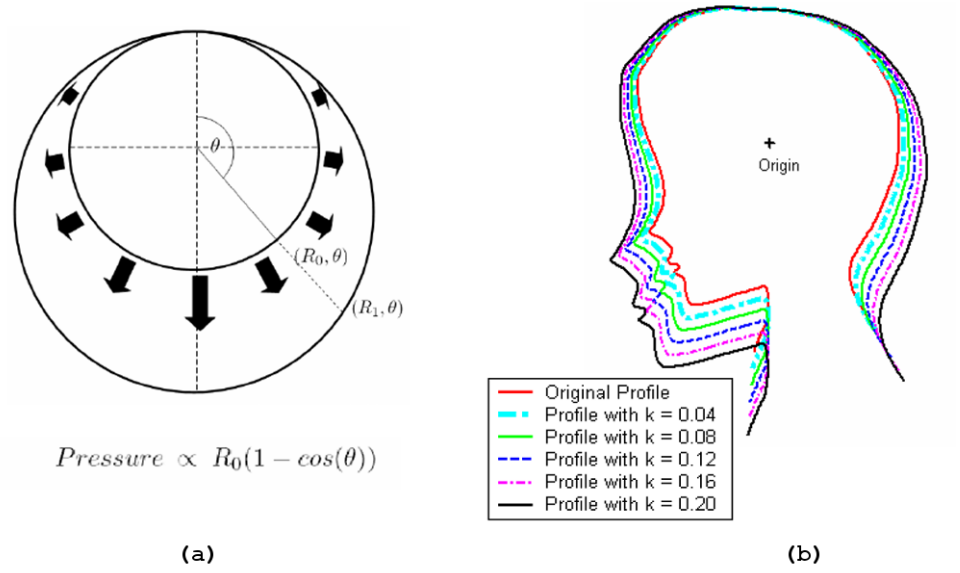

Figure 3.2: (a) Pressure distribution within a fluid filled spherical object is illustrated. (b) Facial growth simulated on the profile of a child's face using the 'revised' cardioidal strain transformations. An illustration similar to the one above originally appeared in [7]

Interestingly, the three geometric invariants that were identified by Mark *et al.* [1] as those characteristic of objects undergoing growth, are well preserved in objects undergoing transformations induced by the 'revised' cardioidal strain transformation

model. Re-examining the geometric invariants in relevance to the 'revised' cardioidal strain transformation model, we observe the following.

- *Angular coordinates of the fiducial features on an object are preserved* : The pressure applied on fiducial features are directed radially outward, hence preserving their angular coordinates.

- *Bilateral symmetry about the vertical axis is maintained* : The pressure distribution being bilaterally symmetric about the vertical axis preserves the bilateral symmetry of objects upon transformation.

- *Continuity of object contours is preserved* : In the proposed model, the pressure distribution changes gradually throughout the object and hence continuity of object contours is preserved.

But, directly employing the afore-mentioned age transformational model on frontal face images reveals some of the short comings of the model. Fig. 3.3 illustrates the face images obtained by applying the 'revised' cardioidal strain transformation model. In each of the two instances illustrated in fig. 3.3, we observe that while the age transformation is perceivable in the initial few transformations, the aspect ratio of faces obtained for large age transformations seem unnatural. For large values of k, which essentially implies larger age transformations, the aspect ratios between different regions of the transformed faces were less preserved. Face anthropometric studies report that different facial regions reach maturation at different years and hence a few facial features change relatively less when compared to other facial features, as age increases.

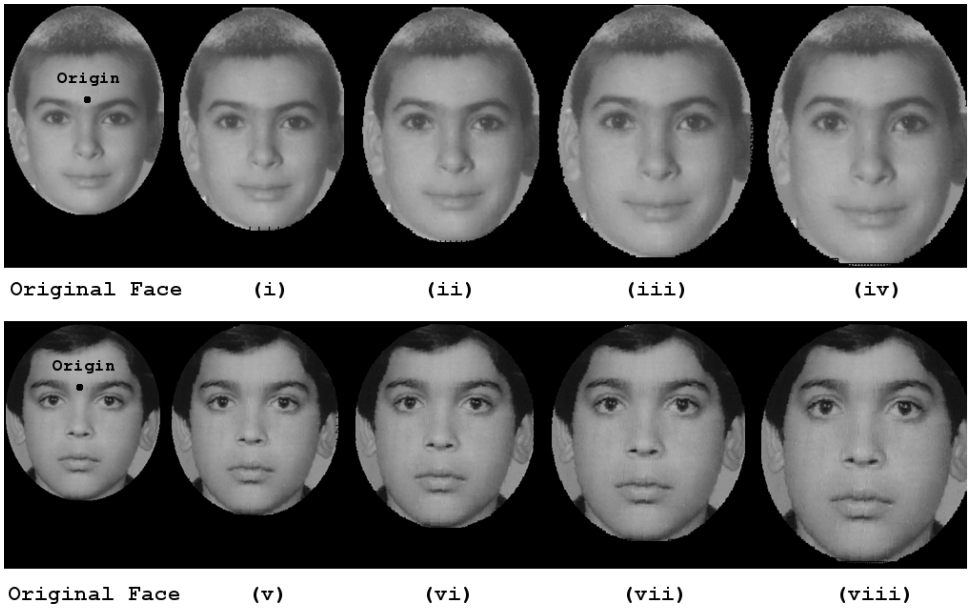

Figure 3.3: Age transformation results obtained by applying the 'revised' cardioidal strain transformation on real-life face images of two individuals (8 years and 13 years of age respectively). The growth parameters chosen for each of the 8 instances were (i) $k = 0.06$ (ii) $k = 0.12$ (iii) $k = 0.18$ (iv) $k = 0.21$ (v) $k = 0.06$ (vi) $k = 0.12$ (vii) $k = 0.18$ (viii) $k = 0.27$. The original images belong to the FG-Net aging database [2].

Some of the factors that need to be taken into consideration while developing the model are :

- Facial growth rates at different ages : Face anthropometric studies [6] provide considerable evidences on the different growth rates observed over different facial features across years. Different facial features attain saturation in growth at different stages and hence, facial growth models should implicitly account for such variabilities. Growth parameters designated as $k_i^{t_0 t_1}$ in eq. 3.1 play a

crucial role in controlling the amount of growth observed over the i'th fiducial feature from ages t_0 years to t_1 years and hence, identifying the growth parameters for each fiducial feature across different age transformations is crucial towards the success of the model.

- Gender-based and ethinicity-based facial growth rates : Again, face anthropometric studies have proven that facial growth rates depend heavily on the individual's gender and ethinicity. Hence, accounting for such factors is a crucial aspect in developing facial growth models.

We use age-based anthropometric data (in the form of measurements extracted across different features) in developing the proposed facial growth model.

3.1.1 Face Anthropometry

Face anthropometric studies provide a quantitative description of the craniofacial complex by means of measurements taken between key landmarks on human faces across ages and are often used in characterizing normal and abnormal facial growth. Facial measurements collected across individuals from the same ethnic background and gender across different ages, provide significant information on facial growth patterns that are commonly observed on individuals from the. We incorporate such evidences on facial growth in computing the facial growth parameters and hence, implicitly account for factors such as gender, ethnicity, adolescence etc. that affect facial growth. Face anthropometry has been successfully used in computer graphics applications by DeCarlo *et al.* [68] in developing geometric models for hu-

man faces and by Kahler [69] in simulating growth on human head models. Next, we elaborate the nature of face anthropometric data that was used in our approach towards developing a craniofacial growth model.

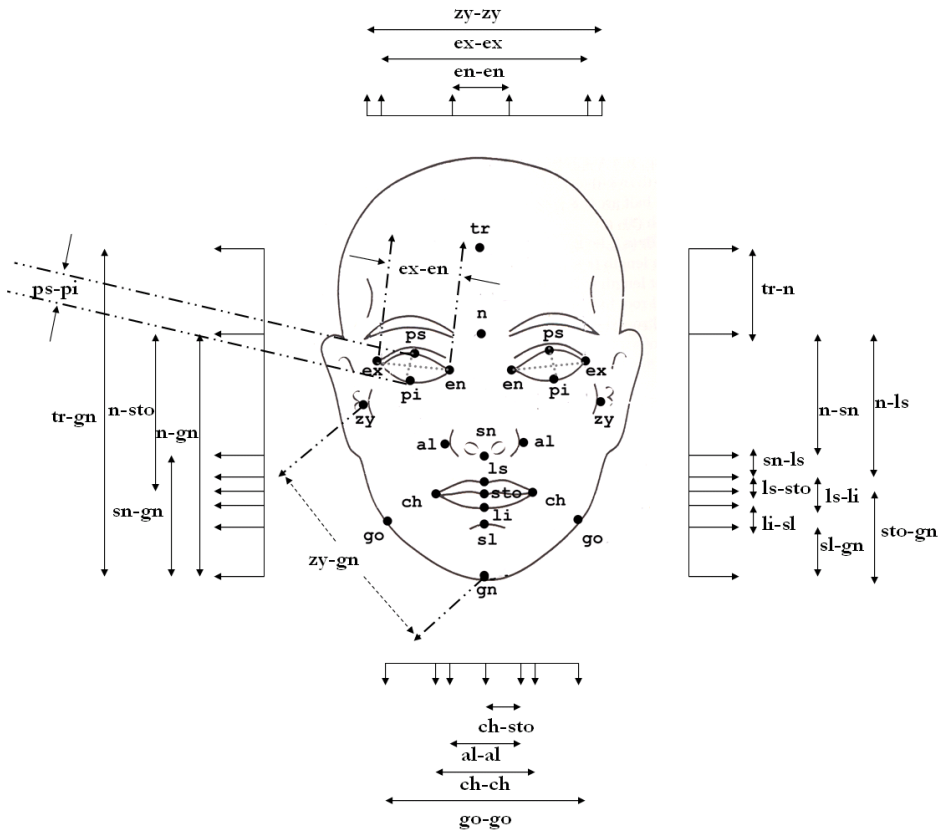

Figure 3.4: The 24 facial landmarks identified on frontal faces and the different facial measurements that were used in developing the model are illustrated.

Farkas [6], [67] identifies a set of facial landmarks that can be reliably located on human faces (both from real-life faces and frontal / profile face images) and extracts facial measurements across different landmarks on Caucasian faces (male/female) belonging to ages 1 - 18 years. For each of the ages 1 to 18 years, facial measurements were extracted from 50 subjects (of the same gender and ethinic

origin) and the means and standard deviations across such measurements are tabulated in [6]. Facial measurements extracted across landmarks are generally of three kinds : (i) projective measurements (shortest distance between two landmarks) (ii) tangential measurements (distance between two landmarks measured along the skin surface) (iii) angular measurements. For the proposed application, we select 24 facial landmarks that can be reliably located on frontal faces and use a set of projective measurements extracted across these landmarks to characterize facial growth. Fig. 3.4 illustrates the 24 landmarks and the relevant facial measurements that are used in our study. The radial and angular coordinates of different facial landmarks across ages are illustrated in Fig. 3.5, below.

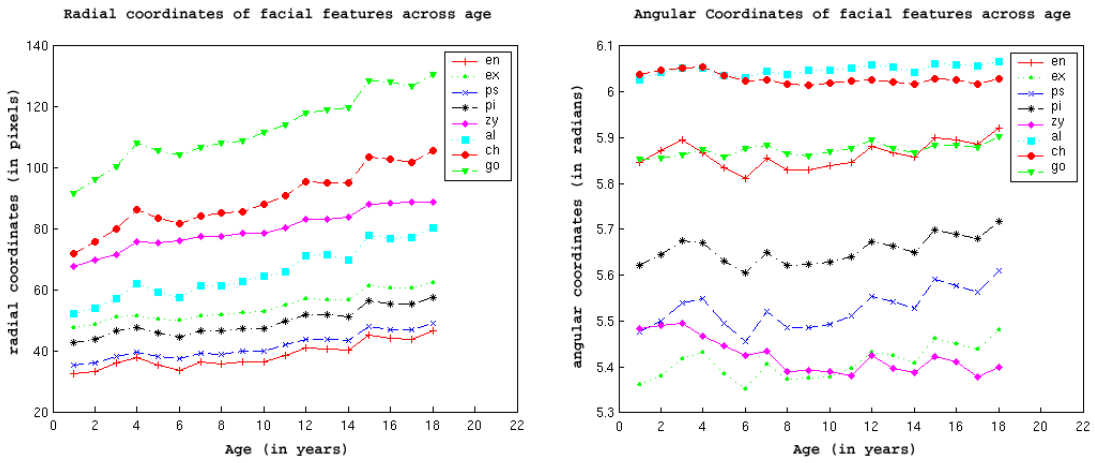

Figure 3.5: The radial and angular coordinates of fiducial features are plotted across different ages. They were derived from the facial measurements that were provided by Farkas [6].

Facial proportion index, defined as the ratio of a pair of facial measurements, is a commonly adopted metric in analyzing facial growth [67]. Clinical studies

related to craniofacial disorders are said to identify a set of facial proportion indices while studying abnormalities in facial growth. Further, an inherent advantage of using facial proportion indices in our application is that the unknown scale factor from an individual's face images can be discounted while studying the variations in facial measurements across ages. We identify 52 such facial proportion indices in developing the craniofacial growth model. Some of the proportion indices that were used are listed here :(i) Facial index ($\frac{n-gn}{zy-zy}$) (ii) Mandibular index ($\frac{sto-gn}{go-go}$) (iii) Intercanthal index ($\frac{en-en}{ex-ex}$) (iv) Orbital width index ($\frac{ex-en}{en-en}$) (v) Eye fissure index ($\frac{ps-pi}{ex-en}$) (vi) Nasal index ($\frac{al-al}{n-sn}$) etc.

3.2 Model Computation

This section details the computational aspects involved in developing the facial growth model. Two kinds of growth models are developed : (i) A 'generic' growth model that is learnt from 'population-based' facial growth patterns (ii) A 'personalized' growth model that is learnt upon incorporating individual specific facial attributes with the 'population-based' facial growth data, in the computational process. The objective behind both the 'generic' growth model and the 'personalized' growth model is to compute the facial growth parameters k_i (eq. 3.1) across a set of fiducial features (as illustrated in Fig. 3.4) and subsequently across the entire facial region (face pixels).

3.2.1 Step I : Identifying the Origin of Reference

The craniofacial growth model described in eq. 3.1 implicitly assumes knowledge of its origin of reference. Hence, in order to successfully apply the model on face images, identifying one on face images is critical. Let the rescaled facial measurements be denoted as $\Omega_i = (\omega_1^{(i)}, \omega_2^{(i)}, \ldots, \omega_N^{(i)})$ where i corresponds to the age $(1 \leq \mathrm{i} \leq 18)$ and N corresponds to the number of facial measurements used in our study. Prototype faces are built by identifying the coordinates of the 24 facial landmarks for each of the ages : $(\Omega_i \mapsto (\mathbf{x}_i, \mathbf{y}_i), 1 \leq i \leq 18)$. Subsequently, the facial feature drifts observed across different ages can be used to determine the optimal origin of reference for the proposed craniofacial growth model. The following cues help in identifying the origin of reference for the proposed model.

- The craniofacial growth model defined in eq. 3.2 is such that the facial features with angular coordinates $\theta = 0$ remain static and features with θ such that $|\theta| \leq \epsilon$, where ϵ is a small number, grow minimally. Further, from eq. 3.2 we observe that facial feature growth is directly proportional to the radial coordinates of feature points.

- 'Relative total increment' (RTI(%)) is a measure that quantifies the growth observed across different landmarks. It is defined as $\frac{l_{18}-l_1}{l_1} \times 100$, where $l_1,\ l_{18}$ correspond to the facial measurements extracted across a pair of facial landmarks at ages 1 and 18 years. Farkas [6] cites that the 'relative total increment' computed across landmarks 'tr' and 'n' (in the forehead region) is much less than that computed across other pairs of facial landmarks.

The above cues suggests that the origin of reference for the craniofacial growth model should ideally be located between landmarks 'tr' and 'n' on the axis of bilateral symmetry. Fig. 3.6(i) illustrates the prototype faces for ages 2 yrs, 5 yrs, 8 yrs, 12 yrs, 15 yrs and 18 yrs and further illustrates the flow of facial features with increase in age.

The optimal origin of reference for the craniofacial growth model is estimated as explained below. Let (x_{ij}, y_{ij}) correspond to the coordinates of the i'th feature at age 'j' years ($1 \leq i \leq 24$, $1 \leq j \leq 18$). Let (x_0, y_0) correspond to the origin of reference for the growth model. y_0 corresponds to the facial mid-axis and hence is known a-priori. The origin of reference for the craniofacial growth model is to be identified such that the growth constraints imposed on the radial and angular coordinates of facial features are best accounted for. The growth constraints imposed on the angular coordinates of facial features imply that the 'x' and 'y' coordinates of facial features across age, follow a linear relationship. We compute x_0 and m_i, $1 \leq i \leq 24$, the slopes of lines that best fit the facial feature coordinates across years by solving the underlying least squares problem :

$$\min_{w.r.t\ m_i,\ x_0} \{\sum_{i=1}^{m} \sum_{j=1}^{n} (x_{ij} - m_i(y_{ij} - y_0) - x_0)^2\} \tag{3.3}$$

By solving the above problem, we observe that the optimal origin of reference for the model is located between landmarks 'tr' and 'n' (on the forehead). The low rates of growth observed on forehead regions for boys (11.8%) and girls (2.25%) [6] further validate the above solution. Fig. 3.6(ii) illustrates the growth observed over different facial features for boys and girls (using average measurements) and

illustrates the located origin of reference.

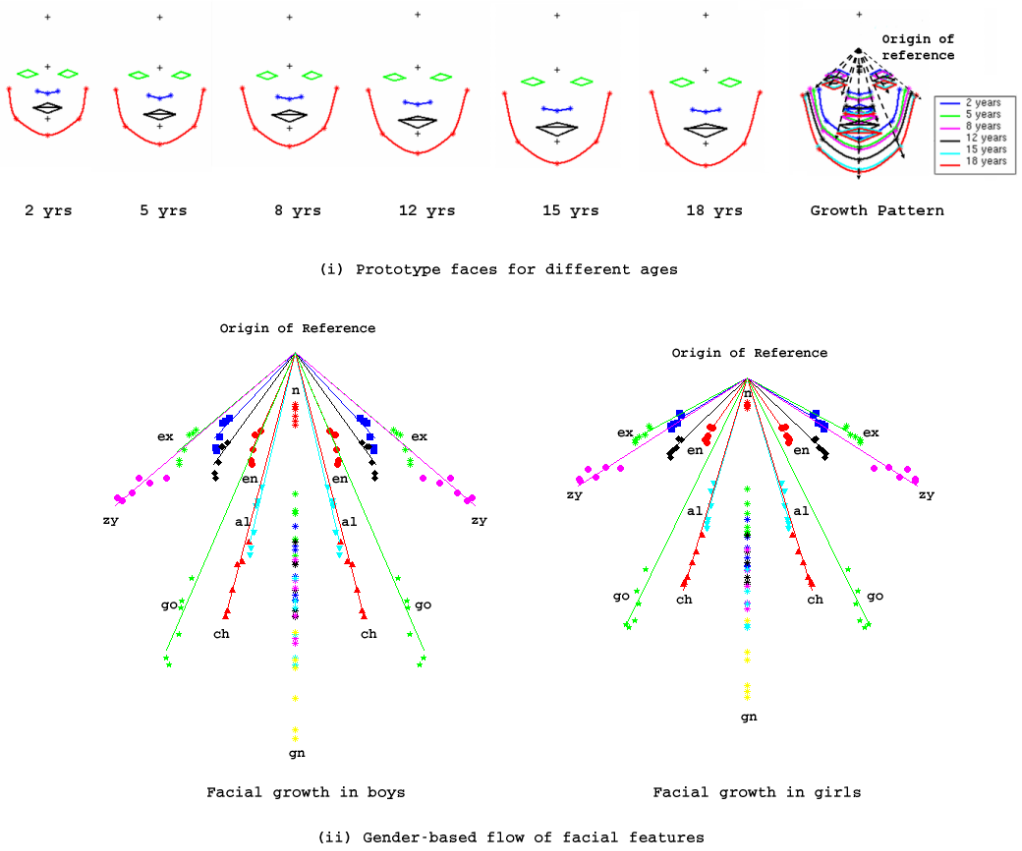

Figure 3.6: (i) Prototype faces for different ages and the flow of facial features across age are illustrated (ii) The origin of reference computed from age-based facial measurements from boys and girls are illustrated.

3.2.2 Step II : Computing Facial Growth Parameters

Upon computing the origin of reference for the craniofacial growth model, the facial landmarks for different ages are represented in polar coordinates $((\mathbf{x}_i, \mathbf{y}_i) \leftrightarrow (\mathbf{r}_i, \Theta_i)$ where 'i' corresponds to the feature index and 'j' corresponds to the age in years. Let the growth parameters corresponding to facial landmarks designated by

$[tr,\ n,\ sn,\ ls,\ sto,\ li,\ sl,\ gn,\ en,\ ex,\ ps,\ pi,\ zy,\ al,\ ch,\ go]$ be $\mathbf{k} = [k_1,\ k_2,\ \cdots\ k_{16}]$, respectively. Assuming bilateral symmetry of faces, symmetric facial features share the same growth parameters and hence the 24 facial features result in 16 unique growth parameters. The 52 proportion indices that were discussed in the previous section, play a fundamental role in computing the facial growth parameters. By studying the transformation in proportion indices from ages 'u' years to 'v' years, we can compute the facial growth parameters corresponding to the specific age transformation. The age-based proportion indices translate into linear and non-linear equations in facial growth parameters. Proportion indices derived from facial measurements that were extracted across facial features that lie on the same horizontal or vertical axis, result in linear equations in the respective growth parameters and those extracted across features that do not lie on the same horizontal or vertical axis, result in non-linear equations in growth parameters.

For example, the age based transformation observed in the proportion index $\frac{n-gn}{zy-zy}$ on features 'n', 'gn' and 'zy', for an age transformation from 'u' years to 'v' years, results in a linear equation in the relevant growth parameters. The following equations illustrate the same. (R^u_n, θ^u_n, R^u_{gn}, θ^u_{gn}, R^u_{zy}, θ^u_{zy} and c_v were derived from the projective facial measurements provided in [6]).

$$\frac{(n\_gn)_v}{(zy\_zy)_v} \ = \ c_v \ \Rightarrow \ \frac{R^v_{gn} - R^v_n}{2 \times R^v_{zy} \times \cos(\theta_{zy})} \ = \ c_v \ \Rightarrow \tag{3.4}$$

$$\begin{aligned} R^u_{gn}(1 + k_{gn}(1 - \cos(\theta_{gn}))) - R^u_n(1 + k_n(1 - \cos(\theta_n))) \\ = 2 \times c_v \times \cos(\theta_{zy}) \times R^u_{zy}(1 + k_{zy}(1 - \cos(\theta_{zy}))) \\ \Rightarrow \alpha_1 k_{gn} + \alpha_2 k_n + \alpha_3 k_{zy} = \beta_1 \end{aligned} \tag{3.5}$$

Similarly, the age based transformation observed in the proportion index $\frac{sto-gn}{gn-zy}$ on features 'sto', 'gn' and 'zy', for an age transformation from 'u' years to 'v' years, results in a non-linear equation in the relevant growth parameters, as illustrated below. (Again, R^u_{gn}, θ^u_{gn}, R^u_{sto}, θ^u_{sto}, R^u_{zy}, θ^u_{zy} and d_v were derived from the projective facial measurements provided in [6]).

$$\frac{(sto\_gn)_v}{(gn\_zy)_v} = d_v \Rightarrow$$

$$\frac{R^v_{sto} - R^v_{gn}}{\sqrt{(R^v_{gn} - R^v_{zy} \times \sin(\theta_{zy}))^2 + (R^v_{zy}\cos(\theta_{zy}))^2}} = d_v \Rightarrow$$

$$R^u_{sto}(1 + k_{sto}(1 - \cos(\theta_{sto}))) - R^u_{gn}(1 + k_{gn}(1 - \cos(\theta_{gn}))) =$$

$$\{[R^u_{gn}(1 + k_{gn}(1 - \cos(\theta_{gn}))) - R^u_{zy}(1 + k_{zy}(1 - \cos(\theta_{zy})))$$

$$\times \sin(\theta_{zy})]^2 + [R^u_{zy}(1 + k_{zy}(1 - \cos(\theta_{zy})))\cos(\theta_{zy})]^2)\}^{\frac{1}{2}} \times d_v$$

$$\Rightarrow \alpha_1 k_{sto} + \alpha_2 k_{gn} + \alpha_3 k_{zy} + \alpha_4 k^2_{sto} + \alpha_5 k^2_{gn}$$

$$+ \alpha_6 k^2_{zy} + \alpha_7 k_{sto} k_{gn} + \alpha_8 k_{gn} k_{zy} = \beta_2$$

Thus, the set of 52 proportion indices that were identified for our study, result in a set of linear and non-linear equations on growth parameters solving which one can identify the growth parameters for specific age transformations.

Let the constraints derived using proportion indices be denoted as $r_1(\mathbf{k}) = \beta_1$, $r_2(\mathbf{k}) = \beta_2$, $\cdots$, $r_{52}(\mathbf{k}) = \beta_{52}$. The objective function $f(\mathbf{k})$ that needs to be minimized w.r.t $\mathbf{k}$ is defined as

$$f(\mathbf{k}) = \frac{1}{2}\sum_{i=1}^{52}(r_i(\mathbf{k}) - \beta_i)^2 \tag{3.6}$$

The following equations illustrate the constraints that were derived using different facial proportion indices.

$$
\begin{aligned}
r_1 \;&:\; \Big[\frac{n-gn}{zy-zy} = c_1\Big] \equiv \alpha_1^{(1)}k_1 + \alpha_2^{(1)}k_7 + \alpha_3^{(1)}k_{12} = \beta_1 \\
r_2 \;&:\; \Big[\frac{al-al}{ch-ch} = c_2\Big] \equiv \alpha_1^{(2)}k_{13} + \alpha_2^{(2)}k_{14} = \beta_2 \\
r_3 \;&:\; \Big[\frac{li-sl}{sto-sl} = c_3\Big] \equiv \alpha_1^{(3)}k_4 + \alpha_2^{(3)}k_5 + \alpha_3^{(3)}k_6 = \beta_3 \\
r_4 \;&:\; \Big[\frac{sto-gn}{gn-zy} = c_4\Big] \equiv \alpha_1^{(4)}k_4 + \alpha_2^{(4)}k_7 + \alpha_3^{(4)}k_4^2 + \alpha_4^{(4)}k_7^2 \\
&\quad +\alpha_5^{(4)}k_{12} + \alpha_6^{(4)}k_{12}^2 + \alpha_7^{(4)}k_4\ k_7 + \alpha_8^{(4)}k_7\ k_{12} = \beta_4
\end{aligned}
$$

(α_j^i and β_i are constants. c_i is the proportion index value computed from the ratios of mean values of facial measurements corresponding to the target age, which were obtained from [6].) To compute the growth parameters $\mathbf{k}$, we minimize the objective function in an iterative fashion using the Levenberg-Marquardt non-linear optimization algorithm [70]. We use the craniofacial growth model defined in eq. 3.2 to compute the initial estimate of the facial growth parameters. The initial estimates are obtained using the age-based facial measurements provided for each facial landmark, individually. The iterative step involved in the optimization process is defined as

$$
\begin{aligned}
\mathbf{k}_{i+1} &= \mathbf{k}_i - (\mathbf{H} + \lambda diag[\mathbf{H}])^{-1}\nabla f(\mathbf{k}_i) \\
\nabla f(\mathbf{k}_i) &= \sum_{i=1}^{N} r_i(\mathbf{k})\nabla r_i(\mathbf{k})
\end{aligned}
$$

where $\mathbf{H}$ corresponds to the Hessian matrix of f evaluated at $\mathbf{k}_i$. At the end of each iteration, λ is updated as illustrated in [70]. Since, the computation of $\mathbf{k}$

discussed above is based on the average facial measurements tabulated in [6] and does not involve facial measurements from test face images, such computations can be performed offline.

On each of the test face images, we locate the 24 facial features illustrated in fig. 3.4 in a semi-automatic manner. We adopt the face detection and feature localization approach proposed by Moon *et al.* [71] to detect facial features. Facial features such as eyes, mouth and the outer contour of the face are located by fitting ellipses as proposed by Moon *et al.* [71]. This operation enables the location of the following facial landmarks (tr, gn : forehead and chin), (en, ex, ps, pi : eyes) and (ch, sto, ls, li : mouth). Other features designated as n, zy, go etc. do not correspond to corners or edges on faces and hence were located manually. We enforce bilateral symmetry while locating facial features. In our observation, minor errors in feature localization do not affect the proposed method to compute facial growth parameters.

3.2.3 Interpolation of growth parameters

Next, using the growth parameters computed over selected facial landmarks $\mathbf{k}$, we compute the growth parameters over the entire facial region. This is formulated as a scattered data interpolation problem [72]. On a Cartesian coordinate system defined over the face region, the growth parameters $\mathbf{k} = [k_1, k_2, \cdots, k_n]$ correspond to parameters obtained at facial landmarks located in $(x_1, y_1), (x_2, y_2), \cdots, (x_n, y_n)$.

Our objective is to find an interpolating function $f : R^2 \rightarrow R$ such that

$$g(\mathbf{x}_i) = k_i \qquad i = 1, \ldots, n \tag{3.7}$$

where $\mathbf{x}_i = (x_i, y_i)$ and the thin-plate energy functional $\mathbf{E}$, a measure of the amount of 'bending' in the surface, is minimized. The thin-plate energy functional is defined as

$$\mathbf{E} = \int\int_{\Omega} g_{xx}^2(\mathbf{x}) + 2g_{xy}^2(\mathbf{x}) + g_{xx}^2(\mathbf{x}) d\mathbf{x} \tag{3.8}$$

where Ω is the region of interest (face region, in our case). Using the method of radial basis function, the interpolating function that minimizes the energy functional can be shown to take the form

$$g(\mathbf{x}) = c_0 + c_1 x + c_2 y + \sum_{i=1}^{n} \lambda_i \phi(|\mathbf{x} - \mathbf{x}_i|) \tag{3.9}$$

where λ_i's are real numbers, $|.|$ is the Euclidean norm in R^2 and the linear polynomial $c_0 + c_1 x + c_2 y$ accounts for affine deformations in the system. We adopt the thin plate splines functions defined as $\phi(\mathbf{x}) = |\mathbf{x}|^2 \log(|\mathbf{x}|)$ as the basis functions. As illustrated in [72], to remove affine contributions from the basis functions, we introduce additional constraints $\sum_{i=1}^{n} \lambda_i = \sum_{i=1}^{n} \lambda_i x_i = \sum_{i=1}^{n} \lambda_i y_i = 0$. Eqs. 3.7 and 3.9 coupled with the constraints above, results in the following linear system of equations, the solution of which yields the interpolating function g. The linear system of equations is

$$\left(\begin{array}{c|c} \mathbf{A}_{n\times n} & \mathbf{P}_{n\times 3} \\ \hline \mathbf{P}_{3\times n}^T & \mathbf{0}_{3\times 3} \end{array}\right) \left(\begin{array}{c} \Lambda_{n\times 1} \\ \hline \mathbf{c}_{3\times 1} \end{array}\right) = \left(\begin{array}{c} \mathbf{k} \\ \\ \mathbf{0} \end{array}\right) \tag{3.10}$$

where $\mathbf{A}$ is a matrix with entries $A_{i,j} = \phi(|\mathbf{x}_i - \mathbf{x}_j|)\ i, j = 1, \ldots, n$, $\mathbf{P}$ is a matrix with rows $(1, x_i, y_i)$, $\Lambda = (\lambda_1, \cdots, \lambda_n)^T$ and $\mathbf{c} = (c_0, c_1, c_2)^T$. Thus, the growth parameters computed at selected facial features using age based anthropometric data is used to compute the growth parameters over the entire facial region. Upon computing the facial growth parameters over the facial region, the craniofacial growth model can be applied in a pixel-wise manner, to transform facial appearances.

The proposed transformation model can be used both to predict one's facial appearance in the coming years and to derive one's appearance in the yesteryears. The transformation models for both the kinds of transformations are illustrated in table 3.1.

Table 3.1: Age transformation models

Age transformation	**Growth Model**
From t_0 years to t_1 years $(t_1 > t_0)$	$R_i^{t_1} = R_i^{t_0}[1 + k_i^{t_0 t_1}(1 - \cos(\theta_i^{t_0}))]$ $\theta_i^{t_1} = \theta_i^{t_0}$
From t_0 years to t_1 years $(t_1 < t_0)$	$R_i^{t_1} = \frac{R_i^{t_0}}{[1+k_i^{t_1 t_0}(1-\cos(\theta_i^{t_0}))]}$ $\theta_i^{t_1} = \theta_i^{t_0}$

3.2.4 Personalized Growth Model

The 'generic' growth model proposed above is built upon the average facial measurements obtained across different ages. Hence, the facial growth parameters $\mathbf{k}_{t_0 t_1}$ that correspond to an age transformation from t_0 years to t_1 years, remain the

same for all individuals irrespective of their facial geometries. Though the interpolation procedure in computing the facial growth parameter across all the 'facial pixels' incorporates the individual facial geometries, the facial growth parameters corresponding to the fiducial features remain the same across all individuals belonging to the same gender and undergoing the same age transformations.

Different individuals have different facial aspect ratios. We propose a 'personalized' growth model that takes into account the individual's facial aspect ratios in the process of computing the facial growth parameters. Facial aspect ratios reflect attributes such as the 'ovalness' or the 'flatness' of individual faces. In order to develop a quantitative characterization of an individual's facial aspect ratio, we study the deviations of horizontal and vertical measurements extracted from an individual's face from that of an average face that corresponds to the same age as that of the individual. Farkas [6] tabulates the first and the second order statistics of different facial measurements extracted across ages. We derive quantitative measures of one's aspect ratio by means of two parameters (ϵ_1, ϵ_2), the deviations corresponding to the horizontal and vertical measurements extracted from the face respectively. Of the 23 facial measurements that constitute our study, we identify 10 facial measurements (6 horizontal measurements (en-en, ex-ex, go-go, zy-zy, al-al, ch-ch) and 4 vertical measurements (tr-n, n-sn, sn-gn, sto-gn)) that are most representative of facial dimensions, to compute the deviation measures. We make the assumption that all the horizontal and vertical measurements exhibit similar deviations respectively, from the average faces and hence limit our characterization to a couple of deviation parameters. To reliably estimate the deviation measures,

it is important to determine the scale differences between face images and average faces. Fig. 3.7 illustrates the different aspect ratios faces belonging to the same age (15 years, in the illustrated example) appear in.

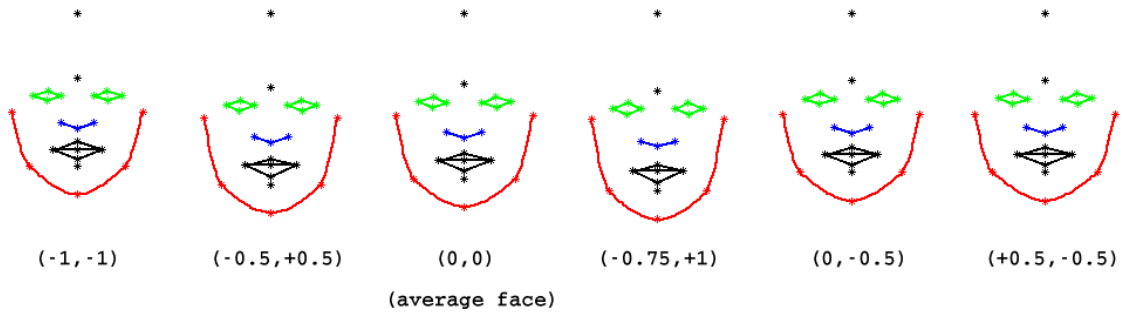

Figure 3.7: An illustration of the different aspect ratios observed in faces belonging to the same age (15 years). The deviation parameters (ϵ_h, ϵ_v) corresponding to each of the different aspect ratios of faces are mentioned.

Let $\mathbf{h} = (m_1, m_2, \ldots, m_6)$ correspond to the 6 horizontal measurements and $\mathbf{v} = (m_7, m_8, m_9, m_{10})$ correspond to the 4 vertical measurements extracted from an individual's face image. Let t_0 correspond to the individual's age. Let $(\mu_i, \sigma_i),\ i = (1, 2, \ldots, 10)$ correspond to the means and standard deviations of the 10 facial measurements corresponding to age t_0 (obtained from [6]). Let $\mathbf{X} = (s, \epsilon_1, \epsilon_2)$ denote the scale factor and the deviation measures that are to be estimated from an individual's face image. Each measurement can be expressed in terms of four parameters : (mean, standard deviation, deviation measure and scale). For instance, the i'th horizontal measurement h_i can be expressed in terms of $(\mu_i, \sigma_i, \epsilon_1, s)$ as follows :

$$\mu_{hi} + \epsilon_h \sigma_{hi} = s \times h_i \quad 1 \leq i \leq 6 \tag{3.11}$$

The 10 facial measurements lead to the following set of linear equations

$$\begin{pmatrix} m_1 & -\sigma_1 & 0 \\ m_2 & -\sigma_2 & 0 \\ \vdots & & \vdots \\ m_6 & -\sigma_6 & 0 \\ m_7 & 0 & -\sigma_7 \\ \vdots & & \vdots \\ m_{10} & 0 & -\sigma_{10} \end{pmatrix} \begin{pmatrix} s \\ \epsilon_1 \\ \epsilon_2 \end{pmatrix} = \begin{pmatrix} \mu_1 \\ \mu_2 \\ \vdots \\ \mu_6 \\ \mu_7 \\ \vdots \\ \mu_{10} \end{pmatrix}$$

which is written as $\mathbf{AX} = \mathbf{b}$. We solve the the linear system above, by forumalating the problem as a constrained least squares problem. We impose a non-negativity constraint on the scale factor s and inequality constraints on each of the deviation measures ϵ_i, $1 \leq i \leq 2$, that constitute $\mathbf{X}$. The optimal scale and deviation parameters ($\mathbf{X}^*$) are estimated as follows :

$$\begin{aligned} \mathbf{X}^* &= \arg\min_{\mathbf{X}} \left|\left|(\mathbf{AX} - \mathbf{b})^2\right|\right| \\ s.t &\quad -\alpha_i \leq \epsilon_i \leq \alpha_i \\ and &\quad \min_j \frac{\mu_j - \alpha_j \sigma_j}{m_j} \leq s \leq \max_j \frac{\mu_j + \alpha_j \sigma_j}{m_j} \end{aligned}$$

where, α_i corresponds to 'n' standard deviations away from the mean value (we set $\alpha_i = 4$). We used the MATLAB function 'lsqlin' to solve the constrained linear least squares problem mentioned above.

Upon computing the deviation measures from different facial regions, we rescale the age-based anthropometric measurements tabulated in [6] and obtain facial measurements that are more representative of the individual's facial measurements at

different ages.

3.2.5 Computational complexity

The nonlinear optimization process involved in computing the facial growth parameters corresponding to fiducial features converges in roughly 50 iterations. The thin plate spline interpolation process involved in computing the facial growth parameters over the entire face results in a linear problem. On a Pentium 2.4GHz processor, the MATLAB computations span a couple of minutes in performing age transformation of a face image. The computational complexity involved in estimating the facial growth parameters for the generic growth model can be reduced considerably by using the underlying recursive formulation. Using the age-based anthropometric data, we compute the growth parameters $k_i^{t,t+1}$, where $1 \leq t \leq 17$ and 'i' corresponds to a pixel on the face for different sets of aspect ratios, apriori. The growth parameters $k_i^{t_0,t_1}$ for any t_0 and t_1 such that $1 \leq t_0 < t_1 \leq 18$, can be computed as follows :

$$\begin{aligned}
R_i^{(y)} &= R_i^{(y-1)}(1 + k_i^{(y-1,y)} \cos(\theta_i)) \\
&= R_i^{(y-2)}(1 + k_i^{(y-2,y-1)} \cos(\theta_i))(1 + k_i^{(y-1,y)} \cos(\theta_i)) \\
&= \cdots \\
&= R_i^{(x)} \prod_{j=x}^{y-1}(1 + k_i^{(j,j+1)} \cos(\theta_i)) \quad \Rightarrow \\
k_i^{(x,y)} &= \frac{\prod_{j=x}^{y-1}(1 + k_i^{(j,j+1)} \cos(\theta_i)) - 1}{\cos(\theta_i)}
\end{aligned}$$

3.3 Experimental Results

In this section we discuss the experiments that were performed on a database of age separated face images using the proposed facial aging models. We performed three experiments using the 'generic' and the 'personalized' facial growth models : (i) Facial feature match accuracy across age progression (ii) Appearance prediction across ages (iii) Face recognition across age progression. Age separated face images from the FG-NET aging database were used in our experiments. Since the FG-NET database comprises of real-life images of individuals taken across years, images tend to differ significantly in factors such as illumination conditions, head pose, facial expressions etc. apart from the ages at which the images were taken. Hence, images with poor illumination conditions and non-frontal head pose orientations were discarded. In effect, our database comprised on 286 pairs of age separated face images of 133 individuals.

3.3.1 Accuracy in facial feature matches across age progression

One of the biggest challenges involved in performing face recognition on age separated face images of children is being able to account for the inherent shape transformations faces undergo during formative years. Since the drifts observed on facial features are far from being uniform, trivial pre-processing approaches adopted for adult faces such as eye-alignment, facial mid-axis alignment etc. do not suffice in terms of reducing facial feature mismatches in the case of age separated images of children. The following experiment performed on the age-based face prototypes that

were reconstructed from the average facial measurements for different age groups [6] illustrates the importance of developing facial aging models in reducing facial feature mismatches between age separated face images.

Let the fiducial features corresponding to ages 2 yrs, 5 yrs, 8 yrs, 12 yrs, 15 yrs, 18 yrs be designated as $\mathbf{x}_u$, $u = 1, 2, \ldots, 6$. We apply two different transformations on the fiducial features corresponding to the age-based face prototypes, with the objective of studying the best fiducial feature matches across different ages. The transformation functions correspond to that proposed by the 'generic' craniofacial growth model and a generic scale based transformation function and let the transformation functions be designated as $\mathbf{T}_u^v$ and $\mathbf{S}_u^v$ respectively. $((u, v) \in (2, 5, 8, 12, 15, 18)$ correspond to the base age and the target age). The scale based transformation function aligns the eyes of facial prototypes (as typically performed on adult faces by most face recognition algorithms). The fiducial features corresponding to a particular facial prototype, $\mathbf{x}_u$ for instance, are transformed into that corresponding to every other facial prototype by applying both kinds of transformation functions. Under each kind of transformation, $\mathbf{x}_u$ undergoes five different transformations.

$$\begin{aligned} \mathbf{T}_u^v(\mathbf{x}_u) &= \mathbf{y}_u^v \quad v \in \{2, 5, 8, 12, 15, 18\} - \{u\} \\ \mathbf{S}_u^v(\mathbf{x}_u) &= \mathbf{z}_u^v \quad v \in \{2, 5, 8, 12, 15, 18\} - \{u\} \end{aligned}$$

where $\mathbf{y}_u^v$ and $\mathbf{z}_u^v$ correspond to the fiducial features of the transformed prototypes (from base age $u \rightarrow$ target age v) induced by the 'generic' craniofacial growth model and generic scale based transformation methods. We compute the Euclidean distance between the original and the transformed fiducial features for each age trans-

formation. Let $\xi_u^v = \frac{1}{N}|\mathbf{y}_u^v - \mathbf{x}_v|$ and $\psi_u^v = \frac{1}{N}|\mathbf{z}_u^v - \mathbf{x}_v|$ be the Euclidean distances computed in each of the transformations. Table 3.2 illustrates the distance measures that were computed by repeating the above operations in a round-robin fashion. We observe that the 'generic' craniofacial growth model performs consistently better than the generic scale based transformation methods in aligning facial features across age transformations.

Next, we performed a similar analysis on the image pairs that were selected from the FG-NET aging database. Facial features were transformed from the base age to the target age using three different transformations : (i) 'generic' craniofacial growth based transformation (designated as $\mathbf{T}_u^v$) (ii) personalized craniofacial growth based transformation (designated as $\mathbf{R}_u^v$) (iii) generic scale based transformation (designated as $\mathbf{S}_u^v$), where u and v correspond to the base age and the target age respectively. Let the fiducial features corresponding to each image pair be addressed as $\mathbf{x}_{i1}$ and $\mathbf{x}_{i2}$ respectively and let (u_i, v_i) , $u_i \neq v_i$, be their respective ages. ($i = 1, 2, \ldots, 286$). Upon applying the transformation functions, we arrive at

$$\mathbf{R}_{u_i}^{v_i}(\mathbf{x}_{i1}) = \mathbf{y}_{i1}, \quad \mathbf{S}_{u_i}^{v_i}(\mathbf{x}_{i1}) = \mathbf{z}_{i1}, \quad \mathbf{T}_{u_i}^{v_i}(\mathbf{x}_{i1}) = \mathbf{w}_{i1}$$

where $\mathbf{y}_{i1}$, $\mathbf{z}_{i1}$, $\mathbf{w}_{i1}$ are the age transformed fiducial features under each transformation function. We compute the Euclidean distance between the age transformed fiducial features and the original fiducial features (at the target age) and study the effectiveness of the applied transformations in modeling facial growth. $\rho_i = \frac{1}{N}|\mathbf{x}_{i2} - \mathbf{y}_{i1}|$, $\tau_i = \frac{1}{N}(|\mathbf{x}_{i2} - \mathbf{z}_{i1}|)$, $\psi_i = \frac{1}{N}|\mathbf{x}_{i2} - \mathbf{w}_{i1}|$, $i = 1, 2, \ldots, 286$ correspond to the sets of euclidean distances between fiducial features upon applying each model. We study the

accuracy in facial feature matches for each of the following age difference categories ($1 \leq A < 3, 3 \leq A < 6, 6 \leq A < 9, 9 \leq A < 12, 12 \leq A < 15, 15 \leq A < 18$) where A corresponds to the intra-pair age difference. Fig. 3.8 displays the proportion of image pairs under each age difference category where better feature matches were obtained upon performing 'generic' and personalized craniofacial growth transformations as against generic scale based transformations. Fig. 3.8 illustrates that the

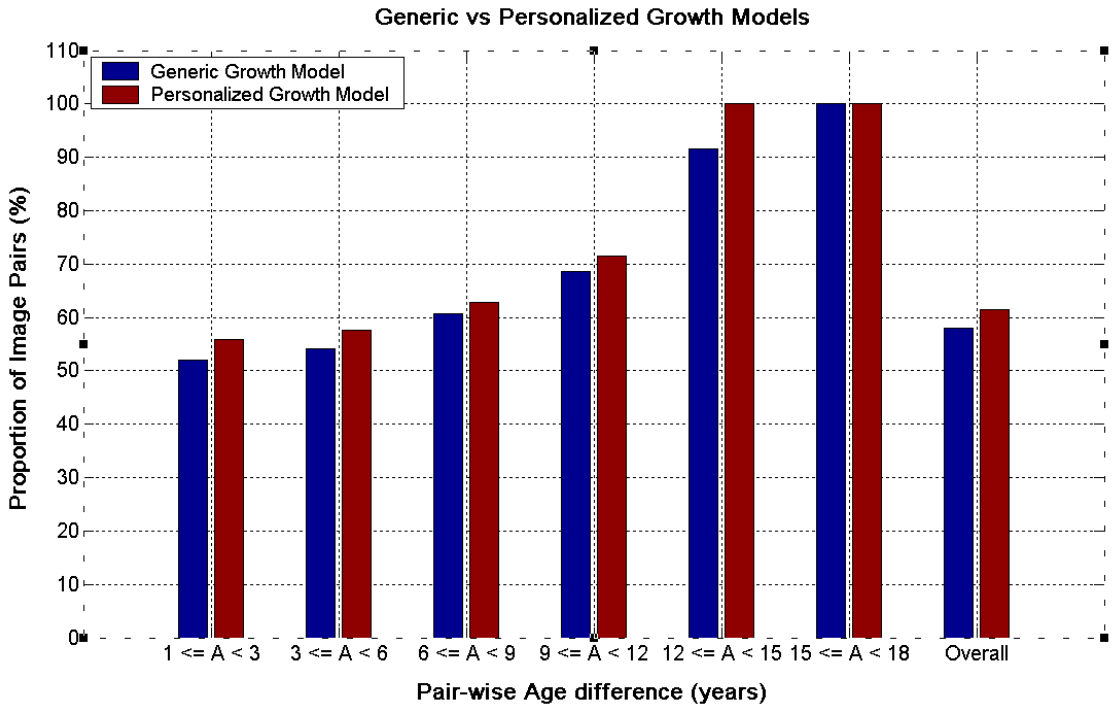

Figure 3.8: Generic growth model vs Personalized growth model

personalized growth model performs consistently better than the 'generic' growth model under all the age difference categories. As expected, the age transformation functions performed progressively better with increase in the intra-pair age separation.

3.3.2 Appearance prediction across ages

The proposed craniofacial growth model finds direct applications in predicting the appearances of children across different ages. Fig. 3.9 illustrates the original age separated image pairs of different subjects and the age transformed face image that was obtained using the 'personalized' growth model. Further, the facial growth parameters corresponding to the specific age transformation on each subject are illustrated, in the form of range maps. The varying intensities observed in the range maps reflect the different growth rates observed across different facial features across ages. One can identify certain gender-based facial growth patterns that are similar across subjects undergoing a similar age transformation. For instance, one can observe that while facial features along the outer contour of the face grow rapidly in the initial few years, their growth rate reduces beyond 15 years of age. Further, fig. 3.10 illustrates multiple age transformed images that were obtained from a single face image of two individuals. The growth parameters associated with each age transformation are illustrated as well.

3.3.3 Face recognition across age progression

Next, for the face recognition experiment, we create the gallery and the probe sets from the database such that the gallery set comprises of a single image per individual and the probe set comprises of either single or multiple images per individual. One of the challenges involved in recognizing face images of children across age progression is to account for growth related shape variations in children's faces.

Most face recognition systems process face images as 2D vectors of fixed dimensions $M \times N$. Such a constraint if imposed on pairs of age separated face image of children, would result in the face recognition system comparing pairs of face images with misaligned facial features that were scaled without due considerations on facial growth. Hence, to perform recognition across age separated face images of children, a better approach to handle the differences in the size of faces would be to employ an age transformation such that pairs of images that are to be compared are transformed to the same ages and hence presumably have comparable sizes.

To highlight the importance of performing an age transformation on pairs of age separated face images before performing face recognition across age progression, we designed the following experiment. Let the images comprising the gallery set and probe set be designated as $\mathbf{G} : \{G_1^{x_1}, G_2^{x_2}, \cdots, G_m^{x_m}\}$ and $\mathbf{P} : \{P_1^{y_1}, P_2^{y_2}, \cdots, P_n^{y_n}\}$ respectively. Let $(x_1, \cdots, x_m, y_1, \cdots, y_n)$ correspond to the different ages of individuals present in the gallery and the probe sets. Under the first setting, the images in the gallery and the probe sets are scaled and cropped such that they are all of dimensions $M \times N$ and the eyes are aligned across all images. Under the second setting, given a probe image $P_i^{y_i}$, we perform an age transformation operation using the 'generic' growth model on all the gallery images and generated the gallery images for age y_i years. Finally, we repeat the same operation using the 'personalized' growth model. Such an operation is repeated for all the probe images $P_i^{y_i}$, $i = 1 \ldots n$. Using eigenfaces [73], we perform face recognition under both the settings. The recognition results tabulated in Table 3.3 show that better recognition rates can be achieved when age transformation operations are performed on pairs

of age separated face images of individuals before performing recognition. We observed many age separated face images in our database to differ from one another in factors such as illumination, head pose, facial expressions etc. apart from age related variations and hence the rank 1 recognition scores are low.

3.4 Summary and Conclusions

We have proposed a craniofacial growth model that takes into account both psychophysical evidences on how humans perceive age progression in faces and anthropometric evidences on facial growth. We have demonstrated the effectiveness of the proposed model in predicting one's appearance across age and in improving recognition results across age separated face images of individuals. To discuss some of the strengths and weaknesses of the proposed method :

- The craniofacial growth model that we propose is unique for each individual. The personalized growth model accounts for different aspect ratios observed in faces of different individuals of the same age.

- The model accounts for gender based differences in facial growth as it was developed using anthropometric data pertaining to men and women separately. The growth spurts observed during adolescense in boys and girls are well captured by the proposed model.

- Further, the craniofacial growth model can be adapted to characterize facial growth on people from different origins by using anthropometric data pertaining to people from those origins. In this work, the anthropometric data used to

develop the model was obtained from facial measurements taken on Caucasian faces and hence, we expect our model to work better on Caucasian faces.

- The proposed approach lacks a textural model and does not account for textural variations across age. Hence facial hair and other commonly observed textural variations in teenagers are not accounted for. Further, it does not account for changes in the amount of fat tissue in the face. The model retains 'baby fat' and hence the age transformation results obtained on toddlers were poor.

Table 3.2: Average mismatch in fiducial feature upon transformation

Age	2 years		5 years		8 years		12 years		15 years		18 years	
	ξ_2	ψ_2	ξ_5	ψ_5	ξ_8	ψ_8	ξ_{12}	ψ_{12}	ξ_{15}	ψ_{15}	ξ_{18}	ψ_{18}
2 yrs	-	-	0.8	1.3	1.45	2.32	1.91	3.38	2.34	4.37	3.13	4.94
	-	-	0.95	1.8	1.35	2.34	1.65	3.89	1.55	3.68	2.2	3.84
5 yrs	0.68	1.16	-	-	0.94	1.48	1.68	2.63	2.25	3.76	3.01	4.18
	0.91	1.59	-	-	1.54	1.43	1.75	2.39	1.44	2.59	2.14	2.58
8 yrs	1.36	1.94	0.93	1.39	-	-	1.75	1.47	2.44	2.62	2.83	2.87
	1.16	1.98	1.41	1.37	-	-	0.78	1.58	0.54	1.39	0.95	1.53
12 yrs	1.64	2.69	1.51	2.34	1.56	1.39	-	-	0.81	1.23	1.36	1.47
	1.43	3.05	1.59	2.12	0.8	1.47	-	-	0.7	1.23	0.92	1.06
15 yrs	1.85	3.22	1.79	3.1	1.88	2.32	0.73	1.14	-	-	0.96	1.14
	1.15	2.78	1.41	2.22	0.56	1.25	0.69	1.19	-	-	0.75	0.91
18 yrs	2.38	3.56	2.42	3.38	2.27	2.47	1.22	1.34	0.78	1.1	-	-
	1.79	2.89	1.73	2.2	0.88	1.36	0.94	1.02	0.84	0.9	-	-

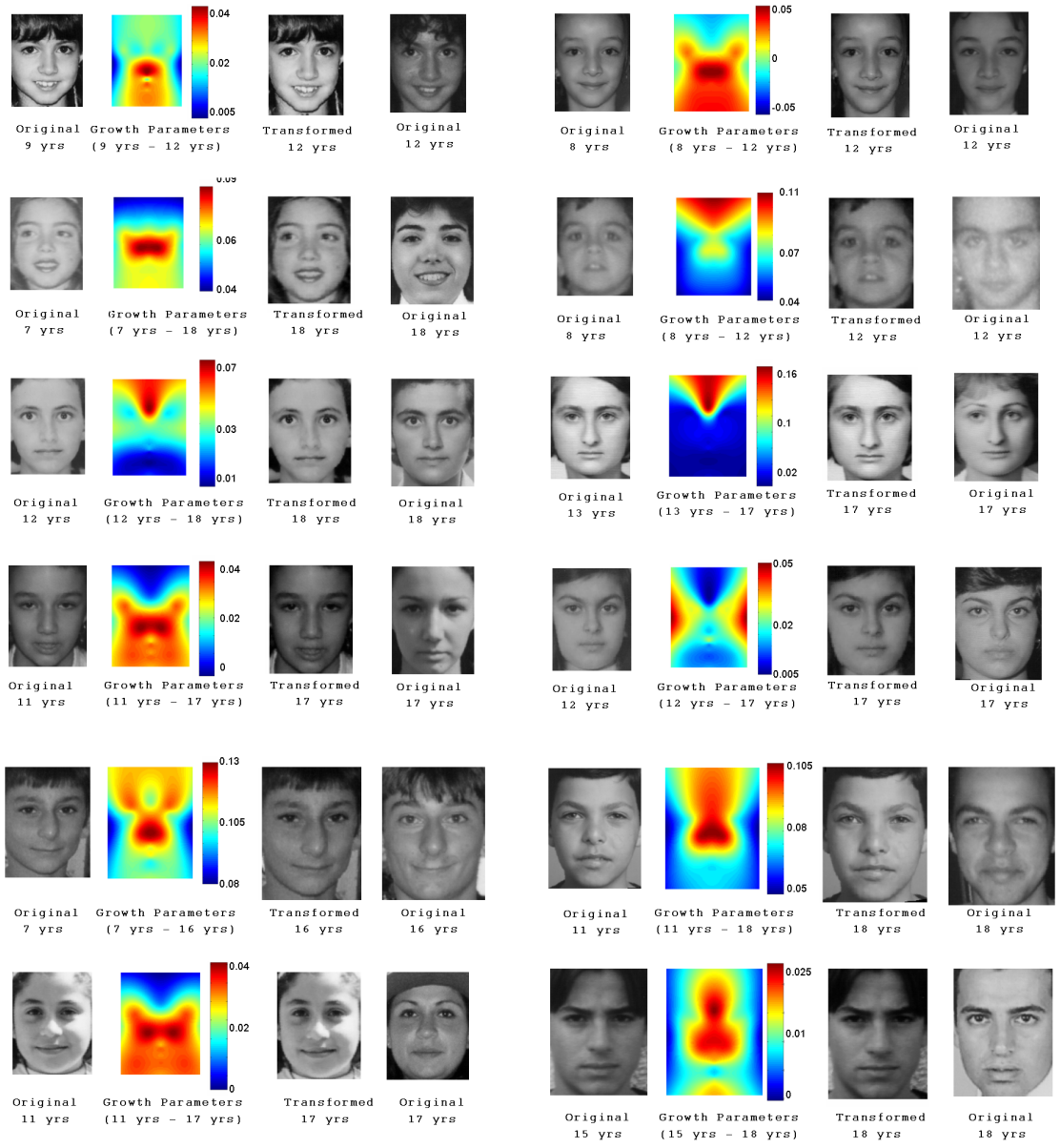

Figure 3.9: Age transformation results on different individual. (The original images shown above were taken from the FG-Net database [8].)

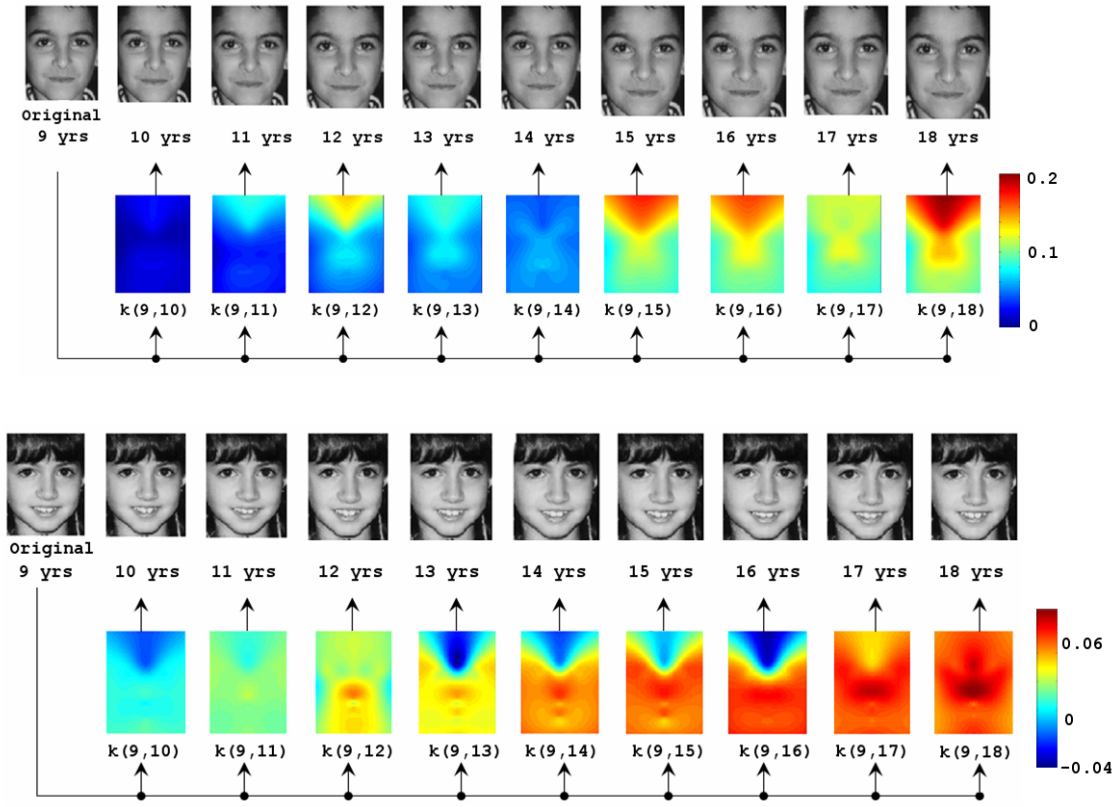

Figure 3.10: Age transformation results on different individual. (The original images shown above were taken from the FG-Net database [8].)

Table 3.3: Recognition results (%) before and after age transformation

Approach	**Rank 1**	**Rank 5**	**Rank 10**
No transformation	8	28	44
Age transformed [Generic]	15	37	58
Age transformed [Personalized]	16	37	58

Chapter 4

Modeling Facial Aging in Adults

Perceiving human faces and modeling the distinctive features of human faces that contribute most towards face recognition are some of the challenges faced by computer vision and psychophysics researchers. While there has been considerable interest in developing face recognition systems that are robust to pose variations, facial expressions, illumination variations etc., the appearance variations induced as a result of aging effects are rarely accounted for in such systems. In the previous chapter, we had discussed a computational model that characterizes facial growth during formative years. The focus of the proposed model was predominantly on characterizing facial shape variations that are well pronounced in that age group. Taking a step ahead, in this chapter we propose a computational model that characterizes the shape and textural variations adult faces undergo with age. During adulthood, facial aging effects induce subtle variations in facial shape and textural variations in the form of facial creases and wrinkles with varying degrees of intensity.

The chapter is organized as described below: The following section details the shape variation model. A physically based parametric muscle model for faces that helps characterize the subtle shape variations adult faces undergo, across different age groups is discussed in this section. The next section discusses a texture variation model that characterizes facial wrinkles across different age. The final section

illustrates the experimental results obtained using the proposed facial aging model and offers certain conclusions.

4.1 Shape Transformation

Facial shape variations due to aging are often observed by means of subtle drifts in facial features and progressive variations in the shape of facial contours, across ages. We propose a facial shape variation model that represents facial feature deformations as that driven by the changing physical properties of the underlying facial muscles. The model is based on the assumption that the degrees of freedom associated with facial feature deformations are directly related to the physical properties and geometric orientations of the underlying facial muscles. Further, since factors such as weight-loss or weight-gain across ages can influence facial feature deformations, the proposed shape variation model has been formulated such that it implicitly accounts for such external factors.

Drawing inspirations from the 'revised' cardioidal strain transformation model [7] that was proposed to model the shape variations human faces (in profile views) undergo during formative years (0 to 18 yrs), we propose a shape variation model for adult faces that takes the following generic form :

$$\begin{aligned} x_{t_1}^{(i)} &= x_{t_0}^{(i)} + k^{(i)} \left[P_{t_0}^{(i)}\right]_x \\ y_{t_1}^{(i)} &= y_{t_0}^{(i)} + k^{(i)} \left[P_{t_0}^{(i)}\right]_y \end{aligned} \tag{4.1}$$

where $(x_{t_0}^{(i)}, y_{t_0}^{(i)})$ and $(x_{t_1}^{(i)}, y_{t_1}^{(i)})$ correspond to the Cartesian coordinates of the i'th facial feature at ages t_0 and t_1, $k^{(i)}$ corresponds to a facial growth parameter and

$[P_{t_0}^{(i)}]_x, [P_{t_0}^{(i)}]_y$ corresponds to the orthogonal components of the pressure applied on the i'th facial feature at age t_0. Developing the facial growth model using the above formulation amounts to

- Identifying the growth related pressures applied on fiducial features ($[P_{t_0}^{(i)}]_x, [P_{t_0}^{(i)}]_y$) : Attributing the facial feature drifts to the pressures applied by the underlying facial muscles, we develop a parametric muscle model for human faces that helps identify the pressure distribution.

- Identifying the Cartesian coordinates of facial features at ages t_0 and t_1 : Facial growth statistics collected in terms of facial measurements extracted across different fiducial features across ages, helps identify the feature coordinates across age transformation.

- Computing the facial growth parameters $k^{(i)}$ across all fiducial features

4.1.1 Parametric muscle model

We propose a physically based parametric muscle model for human faces that implicitly accounts for the physical properties, geometric orientations and functionalities of each of the individual facial muscles. Drawing inspiration from Waters' muscle model [74], we identify three types of facial muscles namely (i) Linear muscles (ii) Sheet muscles (iii) Sphincter muscles, based on their functionalities. Further, we propose transformation models for each muscle type. The number of parameters needed to completely specify the muscle configurations are much fewer in the proposed model than that in Waters' model [74] and its derived versions ([75], [76]).

Fig. 4.1 illustrates the 18 facial muscles that were identified in developing the model and further illustrates the 'point of origin' and 'point of insertion' of each individual muscle.

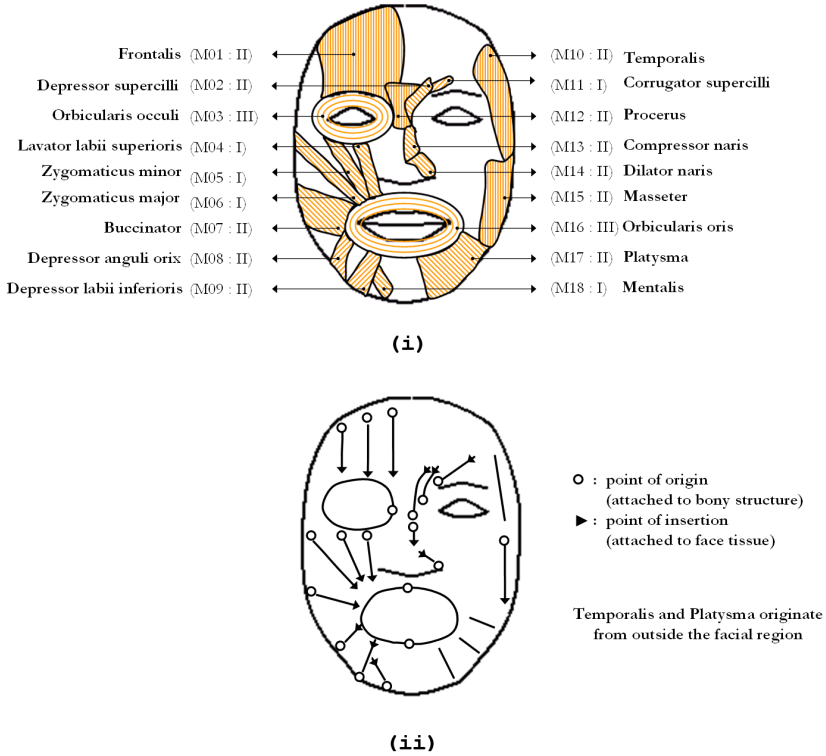

Figure 4.1: (i) Configuration of different facial muscles is illustrated. M01, M02 ... etc. correspond to the muscle tags and I, II and III correspond to the muscle types (ii) The points of origin and insertion of different facial muscles are illustrated.

The following factors are to be taken into consideration while developing the pressure models (i) *Muscle functionality and gravitational forces*: The proposed pressure models reflect the muscle functionalities such as the 'stretch' operation and the 'contraction' operation. The direction of applied pressure reflects the effects of gravitational forces. (ii) *Points of origin and insertion for each muscle*: The degrees

of freedom associated with muscle deformations are minimum at their points of origin (fixed end) and maximum at their points of insertion (free end). Hence, the deformations induced over a facial feature directly depends on the distance of the facial feature from its point of origin of the underlying muscle. The transformation models proposed on each muscle type is illustrated below.

1. **Linear muscle** (α, ϕ)

Linear muscles correspond to the 'stretch operation'. As illustrated in fig. 4.2, linear muscles are described by their attributes namely, the muscle length (α) and the muscle orientation w.r.t to the facial axis (ϕ). The farther a feature is from the muscle's point of origin, the greater the chances that the feature undergoes deformation. Hence, the pressure is modeled such that : $P^{(i)} \propto \alpha^{(i)}$. ($\alpha^i$ is the distance of the i'th from the point of origin). The corresponding shape transformation model is described below :

$$\begin{aligned} x_{t_1}^{(i)} &= x_{t_0}^{(i)} + k\ [\alpha^{(i)} \sin\phi] \\ y_{t_1}^{(i)} &= y_{t_0}^{(i)} + k\ [\alpha^{(i)} \cos\phi] \end{aligned}$$

2. **Sheet muscle**$(\alpha, \phi, \theta, \omega)$

Sheet muscles correspond to the 'stretch operation' as well. As described in fig. 4.3, sheet muscles are described by four of their attributes (muscle length, angles subtended etc.). The pressure applied on a fiducial feature is modeled as $P^{(i)} \propto \alpha^{(i)} \sec\theta^{(i)}$, the distance of the i'th feature from the point(s) of origin of

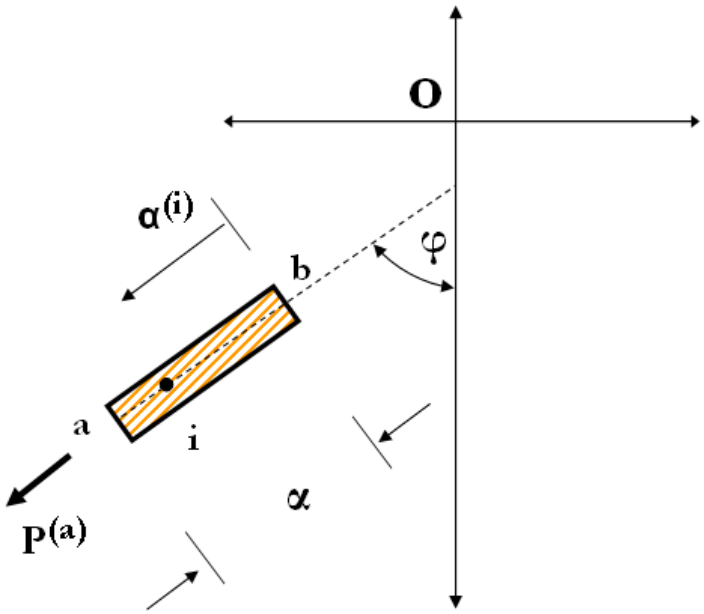

Figure 4.2: Linear muscle model : Points (a) and (b) correspond to the points of origin and points of insertion. (ii) Sheet muscle (points (d,e) and (a,b,c) correspond to the points of origin and points of insertion) (iii) Sphincter muscle (typically, the features along the horizontal axis correspond to the points of origin and those along the periphery correspond to the points of insertion)

the underlying muscles. The shape transformation model is described below :

$$x_{t_1}^{(i)} = x_{t_0}^{(i)} + k\ [\alpha^{(i)} \sec\theta^{(i)} \sin(\phi + \theta^{(i)})]$$

$$y_{t_1}^{(i)} = y_{t_0}^{(i)} + k\ [\alpha^{(i)} \sec\theta^{(i)} \cos(\phi + \theta^{(i)})]$$

3. **Sphincter muscle**(α, β)

The sphincter muscle corresponds to the 'contraction / expansion' operation and is described by two attributes. The pressure modeled as a function of the distance from

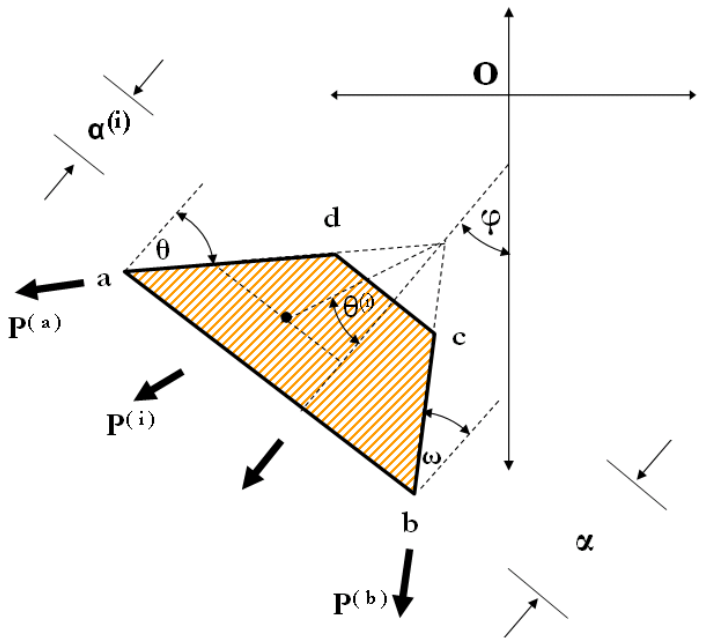

Figure 4.3: Sheet muscle (points (d,e) and (a,b,c) correspond to the points of origin and points of insertion)

the point of origin, $P^{(i)} \propto r^{(i)}(\phi^{(i)}) \cos \phi^{(i)}$, is directed radially inward / outward. Figure 4.4 refers

$$x_{t_1}^{(i)} = x_{t_0}^{(i)} + k\ [r^{(i)}(\phi^{(i)}) \cos^2 \phi^{(i)}]$$

$$y_{t_1}^{(i)} = y_{t_0}^{(i)} + k\ [r^{(i)}(\phi^{(i)}) \cos \phi^{(i)} \sin \phi^{(i)}]$$

Since facial muscle configurations are very well studied [77], the parameters that define the muscle attributes such as the muscle size, its physical location, its geometric orientation etc. are known apriori and only the facial growth parameter needs to be estimated. Fig. 4.5 illustrates the pressure distribution as modeled on different types of facial muscles. Next, we discuss the acquisition of facial growth statistics that helps in computing the facial growth parameters for different age

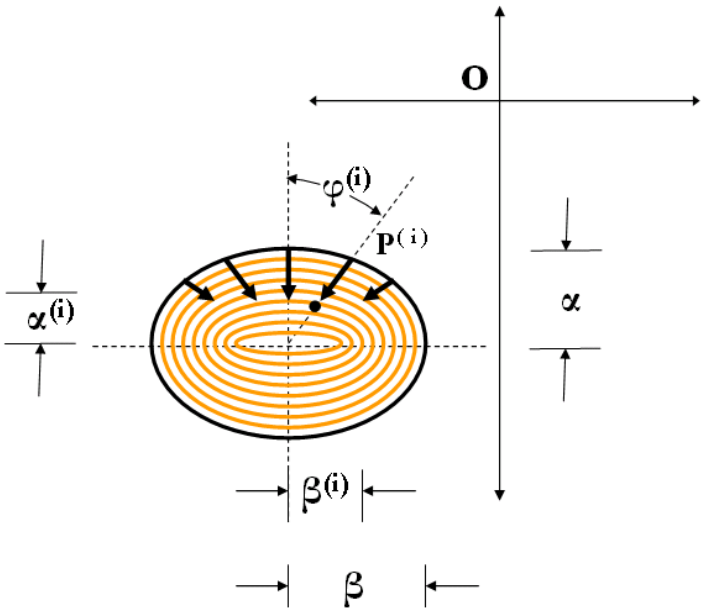

$$r^{(i)}(\phi^{(i)}) = \sqrt{(\alpha^{(i)}\cos\phi^{(i)})^2 + (\beta^{(i)}\sin\phi^{(i)})^2}$$

Figure 4.4: Sphincter muscle (typically, the features along the horizontal axis correspond to the points of origin and those along the periphery correspond to the points of insertion)

transformations.

4.1.2 Facial growth statistics

From a database that comprises of 1200 pairs of age separated face images (predominantly Caucasian), we selected 50 pairs of face images each undergoing the following age transformations (in years): $20's \rightarrow 30's$, $30's \rightarrow 40's$, $40's \rightarrow 50's$, $50's \rightarrow 60's$ and $60's \rightarrow 70's$. The image pairs were compiled from the Passport image database [78]. We selected 48 facial features from each image pair and ex-

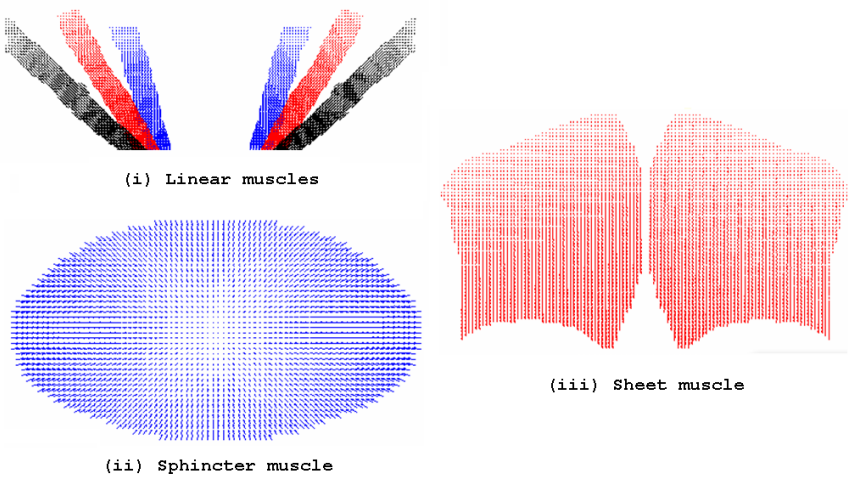

Figure 4.5: The figure illustrates the distribution of pressure on different facial muscles such as (i) Levator labii superioris (M04), Zygomaticus minor (M05) and Zygomaticus major (M06) (ii) Orbicularis Orbis (M16) (iii) Frontalis (M01)

tracted 44 projective measurements (21 horizontal measurements and 23 vertical measurements) across the facial features. Dense facial measurements such as above extracted across age transformation, implicitly capture facial growth patterns and hence are crucial for the shape transformation model. Fig. 4.6 illustrates the 48 facial features that were used in our study. We analyze the intra-pair shape transformations from the perspective of weight-loss, weight-gain and weight-retention and select the appropriate training sets for each case.

4.1.3 Model computation

Consider the facial shape transformations from age t_0 years to t_1 years. Let the training set that was chosen for the experiment comprise of pairs of age separated face images of individuals (from t_0 years to t_1 years) who underwent either

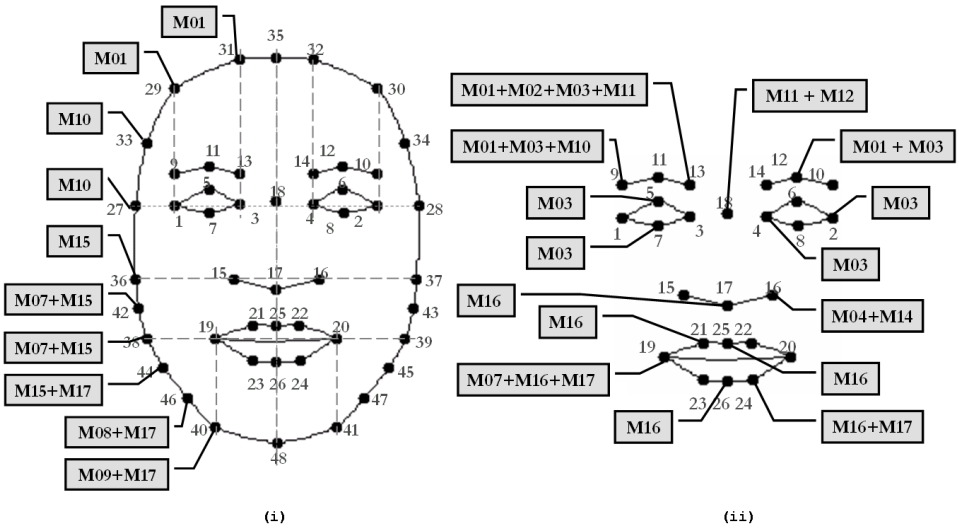

Figure 4.6: The 48 facial features and their correspondences with facial muscles are illustrated (the muscle tags M_{01}, M_{02} etc. follow the nomenclature from fig. 4.1(i))

weight-gain or weight-loss across ages or who retained their weight across age transformation. Let $(\bar{x}_{t_0}^{(i)}, \bar{y}_{t_0}^{(i)})$ and $(\bar{x}_{t_1}^{(i)}, \bar{y}_{t_1}^{(i)})$, $1 \leq i \leq 48$ correspond to the Cartesian coordinates of the 48 facial features on the average faces at ages t_0 years and t_1 years. Let $K_{t_0t_1} = [k_{t_0t_1}(1), k_{t_0t_1}(2), \ldots, k_{t_0t_1}(18)]^T$ denote the growth parameter corresponding to the 18 facial muscles. Developing the shape transformation model amounts to computing $K_{t_0t_1}$, given the average faces for t_0 years and t_1 years and the pressure configurations. Since facial muscles overlap heavily on different facial features, we model the deformations induced over a facial feature as a linear superposition of the deformations induced by the individual facial muscles that act on the facial feature. Figure 4.7 illustrates the overlap of sheet muscles.

Reformulating the shape transformation model, the deformations induced over a facial feature 'i' from t_0 yrs to t_1 yrs, that is influenced by n facial muscles, the

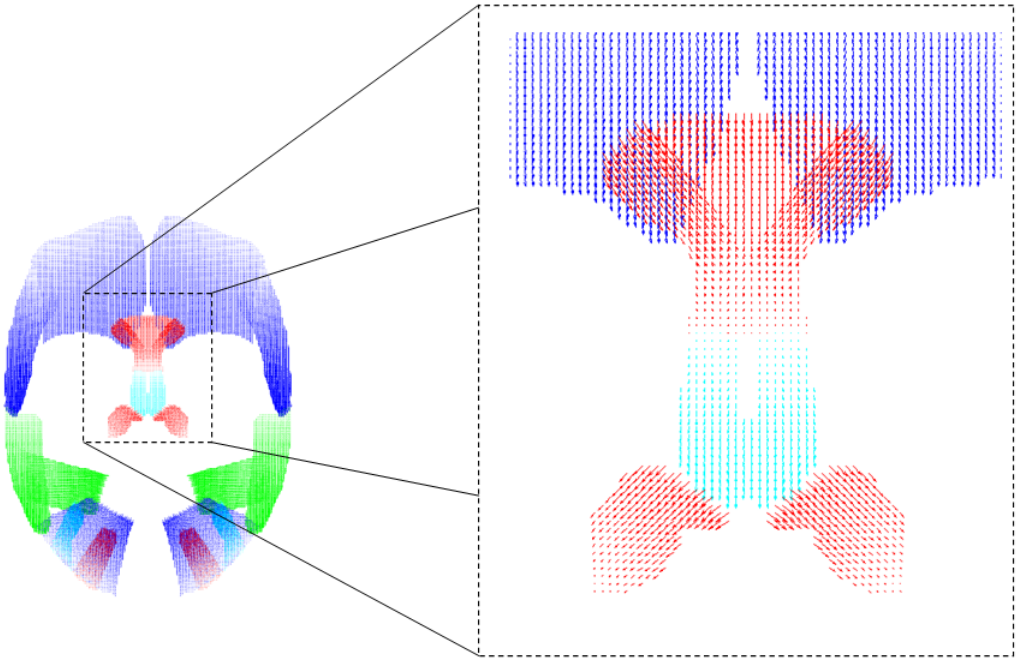

Figure 4.7: An illustration of the overlap observed on sheet muscles

indices of which are denoted as $(m_1, m_2, \ldots, m_n)$, is modeled as

$$\begin{aligned} \bar{x}_{t_1}^{(i)} &= \bar{x}_{t_0}^{(i)} + \sum_{j=1}^{n} [k_{t_0 t_1}(m_j)\ \xi_{t_0}^{(i)}(m_j)] \\ \bar{y}_{t_1}^{(i)} &= \bar{y}_{t_0}^{(i)} + \sum_{j=1}^{n} [k_{t_0 t_1}(m_j)\ \psi_{t_0}^{(i)}(m_j)] \end{aligned} \tag{4.2}$$

where $1 \leq i \leq 48$ and $(\xi_{t_0}^{(i)}(m_j), \psi_{t_0}^{(i)}(m_j)) = ([P_{t_0}^{(i)}(m_j)]_x, [P_{t_0}^{(i)}(m_j)]_y)$ correspond to the orthogonal components of the pressure applied on facial feature 'i' by m_j'th facial muscle. Figure. 4.6(ii) illustrates the correspondences between the facial features and the underlying facial muscles.

Anthropometric studies often characterize facial growth by means of ratios of facial measurements (also addressed as proportion indices). An inherent advantage of using proportion indices to characterize facial growth is that the scale factors corresponding to face images are easily accounted for. In our study, a total of

946 proportion indices are selected from the 44 facial measurements. Studying the transformations corresponding to different proportion indices from t_0 yrs to t_1 yrs, we arrive at a set of linear equations the solution of which helps determine the growth parameters $K_{t_0t_1}$.

Consider the transformations observed on the proportion index $\frac{d_{(15-16)}}{d_{(18-17)}}$ (the nasal index) from t_0 yrs to t_1 yrs, where $d_{(i-j)}$ corresponds to the facial measurement extracted across features 'i' and 'j'. From fig.4.6(ii), the correspondences between the facial features and the indices of the facial muscles that influence them is determined to be $15 \leftrightarrow (04, 14)$, $16 \leftrightarrow (04, 14)$, $17 \leftrightarrow (16)$ and $18 \leftrightarrow (11, 12)$. The resulting transformation equation is

$$\left[\frac{d_{(15-16)}}{d_{(18-17)}}\right]_{t_1} = \left(\frac{\bar{y}_{t_1}^{(16)} - \bar{y}_{t_1}^{(15)}}{\bar{x}_{t_1}^{(17)} - \bar{x}_{t_1}^{(18)}}\right) = c_{t_1} \tag{4.3}$$

$$\begin{aligned} \Rightarrow 2 \times [\bar{y}_{t_0}^{(16)} \ + \ k_{t_0t_1}(4)\ \psi_{t_0}^{(16)}(4) \ + \ k_{t_0t_1}(14)\ \psi_{t_0}^{(16)}(14)] \\ = c_{t_1} \times [\ \bar{x}_{t_0}^{(17)} - \bar{x}_{t_0}^{(18)} \ + \ k_{t_0t_1}(16)\ \xi_{t_0}^{(17)}(16) - \\ k_{t_0t_1}(11)\ \xi_{t_0}^{(18)}(11) \ - \ k_{t_0t_1}(12)\ \xi_{t_0}^{(18)}(12)\ ] \end{aligned}$$

which results in the linear equation

$$\begin{aligned} \lambda_5\ k_{t_0t_1}(5) \ + \ \lambda_{14}\ k_{t_0t_1}(14) \ + \ \lambda_{16}\ k_{t_0t_1}(16) + \\ \lambda_{11}\ k_{t_0t_1}(11) \ + \ \lambda_{12}\ k_{t_0t_1}(12) \ = \ \theta \end{aligned}$$

Thus, the transformations observed over the 946 proportion indices from t_0 yrs to t_1 yrs, result in a system of linear equations : $\Lambda\ K_{t_0t_1} = \ \Theta$, where Λ is the coefficient matrix of size 946×18 and $\Theta = [\theta_1, \theta_2, \ldots, \theta_{946}]^T$ is the constant matrix of size 946×1. The optimal growth parameters $K_{t_0t_1}$ are computed by

solving the system of linear equations using the least squares approach : $K_{t_0t_1} = \arg\min_K ||\Lambda\ K - \Theta||^2$.

Upon computing the growth parameters $K_{t_0t_1}$ corresponding to the 18 facial muscles, we compute the flow of facial features $[\Delta\bar{\mathbf{x}}_{t_0t_1},\ \Delta\bar{\mathbf{y}}_{t_0t_1}]$ over the entire facial region, between the average faces corresponding to ages t_0 yrs and t_1 yrs. Let the average face corresponding to t_0 years comprise of N pixels. Extracting the correspondences between each facial pixel and the underlying facial muscles, the flow of facial features between the average faces at t_0 yrs and t_1 yrs are computed as

$$\begin{aligned} \Delta\bar{x}^{(i)}_{t_0t_1} &= \sum_{j=1}^{n}[k_{t_0t_1}(m_j)\ \xi^{(i)}_{t_0}(m_j)], \quad i = [1,\ldots,N] \\ \Delta\bar{y}^{(i)}_{t_0t_1} &= \sum_{j=1}^{n}[k_{t_0t_1}(m_j)\ \psi^{(i)}_{t_0}(m_j)], \quad i = [1,\ldots,N] \end{aligned} \tag{4.4}$$

Having modeled the shape transformation between average faces at t_0 years and t_1 years, we propose the following steps to induce shape transformations on test face images, that reflect facial aging effects.

Let $I^j_{t_0}$ be the face image of the j'th individual belonging to age group t_0 years. Let $(\mathbf{x}^j_{t_0}, \mathbf{y}^j_{t_0})$ correspond to the coordinates of the N_j pixels on $I^j_{t_0}$. Let $(x^{(i)}_{t_0}, y^{(i)}_{t_0})^j$, $1 \leq i \leq 48$ correspond to the coordinates of the 48 fiducial features on $I^j_{t_0}$. We compute the warping function $\mathbf{w} : (\mathbf{R}^2 \rightarrow \mathbf{R}^2)$ that warps the fiducial features on the average face at age t_0 years to that on the test face. (The warping function is derived using the thin plate spline formulation for interpolation techniques).

$$\mathbf{w} : (\bar{x}^{(i)}_{t_0}, \bar{y}^{(i)}_{t_0}) \rightarrow (x^{(i)}_{t_0}, y^{(i)}_{t_0})^j, 1 \leq i \leq 48$$

The estimated warping function $\mathbf{w}$ is used to map the flow of facial features between

average faces (eq. 4.4) to that corresponding to the test face $I^j_{t_0}$, which can be subsequently used to induce shape variations in the test face.

$$\begin{aligned}[\Delta\bar{\mathbf{x}}_{t_0t_1},\ \Delta\bar{\mathbf{y}}_{t_0t_1}] &\mapsto [\Delta\mathbf{x}^j_{t_0t_1},\ \Delta\mathbf{y}^j_{t_0t_1}] \\ (\hat{\mathbf{x}}^j_{t_0}, \hat{\mathbf{y}}^j_{t_0}) &= (\mathbf{x}^j_{t_0} + \Delta\mathbf{x}^j_{t_0t_1}, \mathbf{y}^j_{t_0} + \Delta\mathbf{y}^j_{t_0t_1})\end{aligned} \tag{4.5}$$

4.2 Texture Transformation

Textural variations observed in human faces with increase in age are often perceived in the form of facial wrinkles, creases and other skin-artifacts. Often, facial wrinkles observed on individuals belonging to the same age group, gender and ethnicity tend to share structural similarities in aspects such as their locations, orientations etc. In spite of such similarities, the density of facial wrinkles tends to be highly subjective. From a modeling perspective, facial wrinkles and other forms of textural variations observed in aging faces can be characterized on the image domain by means of image gradients. In this subsection, we propose a texture variation model that characterizes facial wrinkles and other related facial aging effects, by means of image gradient transformation functions.

Let $(I^{(i)}_{t_1}, I^{(i)}_{t_2})$, $1 \leq i \leq N$ correspond to pairs of age separated face images of N individuals undergoing similar age transformations ($t_1 \rightarrow t_2$). In order to study the facial wrinkle variations across age transformation, we identify four facial regions which tend to have a high propensity towards developing wrinkles, namely (i) the forehead region (W_1) (ii) the eye-burrow region (W_2) (iii) the nasal region (W_3) (iv) the lower chin region (W_4). W_n, $1 \leq n \leq 4$ corresponds to the facial mask that helps isolate the desired facial region. Figure 4.8 illustrates samples of facial wrinkle

patterns observed over the four facial regions mentioned above.

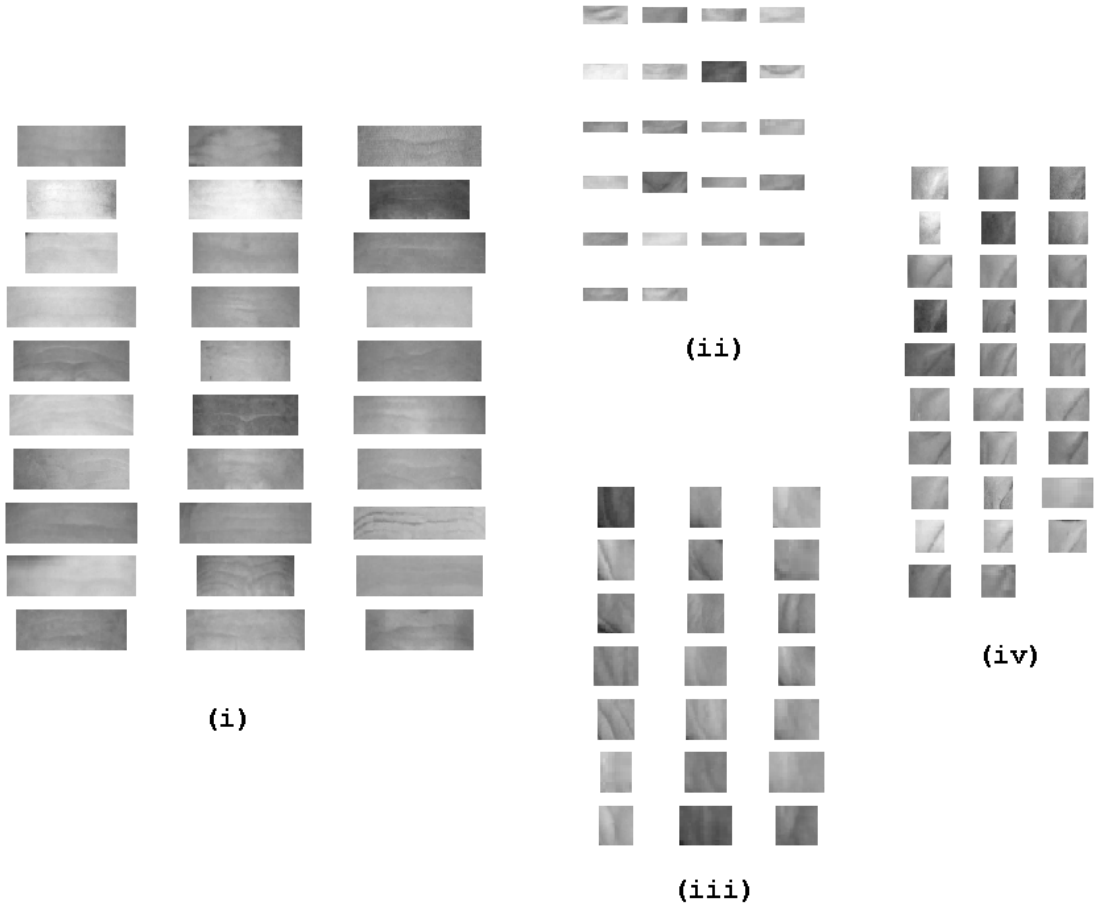

Figure 4.8: Sample facial wrinkle patterns as observed over four facial regions namely (i) Forehead region(ii) Eye-burrow region(iii) Nasal region (iv) Lower chin region are illustrated

Next, we categorize the region-based facial wrinkle variations across age transformation into one of the following three classes : (i) subtle wrinkle change (ii) moderate wrinkle change and (iii) strong wrinkle change. This classification is performed by studying the pixel-based differences in gradient magnitudes and orientations.

Let $\nabla I_{t_1}^{(i)}$ and $\nabla I_{t_2}^{(i)}$ correspond to the image gradients of the i'th image at t_1

and t_2 years, $1 \leq i \leq N$. Let us assume that all the N image pairs fall under the same class of wrinkle variations (subtle / moderate / strong) (ie) all the N image pairs underwent similar textural transformations from t_1 years to t_2 years. Given a test image J_{t_1} at t_1 years, the image gradients of which is ∇J_{t_1}, we induce textural variations by incorporating the region-based gradient differences that were learnt from the set of training images discussed above.

$$\nabla J_{t_2} = \nabla J_{t_1} + \frac{1}{N} \sum_{i=1}^{N} \sum_{n=1}^{4} W_n \cdot (\nabla I_{t_2}^{(i)} - \nabla I_{t_1}^{(i)}) \tag{4.6}$$

The transformed image J_{t_2} is obtained by solving the Poisson equation corresponding to image reconstructions from gradient fields [9]. Figure 4.9 illustrates the subtle, moderate and strong wrinkle pattern changes that were learnt from individuals belonging to the age group 50 - 60 years. Fig. 4.10 provides an overview of the proposed facial aging model. The figure illustrates the muscle-model based facial feature drifts that induce shape transformations for the cases of weight-gain and weight-loss. Further, the figure illustrates the effects of image gradient transformations in inducing facial wrinkles.

4.3 Experiments

4.3.1 Face recognition across ages

On a database that comprises of 87 age separated image pairs of adults, we conducted a face verification experiment. Let the younger of the two images correspond to the gallery image ($[G : g_1, g_2, \ldots, g_{260}]$) and the older counterpart, the

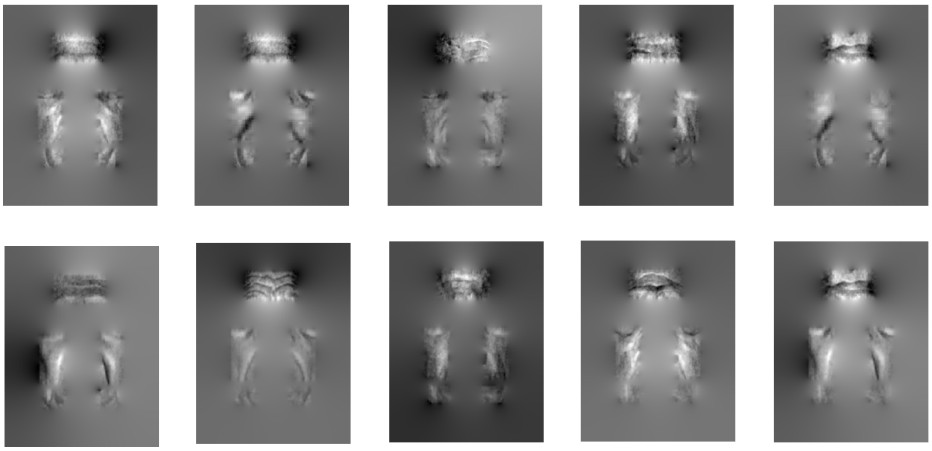

Figure 4.9: The figure illustrates the wrinkle pattern changes learnt from individuals belonging to the age group 50 - 60 yrs. The illustration was obtained by adding the image gradient differences that were learnt from age separated image pairs with a zeros intensity image and subsequently invoking Poisson image reconstruction [9].

probe image ($[P : p_1, p_2, \ldots, p_{260}]$). The objective is to study the face verification rates with and without applying the facial aging model. We divide the dataset into two sets $[(G1, P1), (G2, P2)]$ based on the age difference between the image pairs. The first set $[(G1, P1)]$ comprises of image pairs with an age separation lesser than 9 years. The second set $[(G2, P2)]$ comprises of image pairs with an age separation of 9 years or greater.

Since facial aging patterns depend quite significantly on one's lifestyle, there are many different ways an individual could have aged. Hence, we create nine aged images for each of the gallery images and select that aged image that matches best with the corresponding probe image. The nine aged images are created as explained below : Given a gallery image (g1), we introduce 3 types of shape variations. The

first corresponds to the weight-gain case, the second corresponds to the weight-loss situation and the third corresponds to the weight-retention situation. On top of each of the three types of shape variations, we introduce three types of facial wrinkles (deep, moderate and subtle) that are commonly observed at the individual's age . Thus, for every gallery image g_1, we create 9 images $g_{1,1}, g_{1,2}, \ldots, g_{1,9}$. Figure 4.11 illustrates the nine images that were created from a single gallery image.

Next, we create an eigenspace Ψ [73] using a set of 152 frontal and well illuminated face images from FRGC [10]. We take projections of the original gallery images, the newly generated gallery images and the probe images on the eigenspace Ψ. Let the eigenspace projections for the N gallery images be denoted as $\mathbf{u}_1, \mathbf{u}_2, \ldots, \mathbf{u}_N$ and let the projections for the probe images be denoted as $\mathbf{v}_1, \mathbf{v}_2, \ldots, \mathbf{v}_N$. Let the projections obtained from the newly generated gallery images be $\mathbf{u}_{1,1}, \ldots, \mathbf{u}_{1,9}, \mathbf{u}_{2,1} \ldots, \mathbf{u}_{N,9}$. We compute the Euclidean distance between the projection vectors in measuring their similarity.

When the facial aging model is not used while comparing the gallery images and the probe images, the distance between gallery g_i and probe p_j is computed as $d_1(i,j) = ||\mathbf{u}_i - \mathbf{v}_j||^2$. When the facial aging model is used, the distance between the same gallery and probe is computed as $d_2(i,j) = \min_k ||\mathbf{u}_{i,k} - \mathbf{v}_j||^2$, $1 \leq k \leq 9$. We performed a face verification experiment using the distance matrices thus computed. The results are illustrated in Figure 4.12 and Figure 4.13. It can be observed that the facial aging model when employed on the second set of face images, the set which corresponded to an age separation of 9 years or greater, results in better verification results. For the image pairs from the first set, the set which comprised of image pairs

separated by lesser than 9 years, the face verification results obtained by applying the facial aging model were comparable to that obtained without applying the facial aging model.

4.3.2 Appearance Prediction

Fig 4.14 illustrates the facial shape variations (for the cases of weight-gain, weight-loss and weight-retention) across 6 individuals and further illustrates the three types of textural variations (subtle, moderate, strong) that were induced on the shape transformed face.

4.4 Discussions and Conclusions

The proposed facial aging model poses some unique advantages over other similar methods.

- **Facial growth statistics** : Facial measurements extracted across different facial features across ages provide considerable evidences on facial growth. Computational models that are built using such ground-truth data on facial aging implicitly account for the different rates of growth observed across ages.
- **Gender, Ethnicity** : The facial measurements were extracted from men and women who were predominantly Caucasian. Hence, the model can account for gender-based and ethnicity-based facial growth patterns.
- **Weight loss/gain** : We compute facial growth parameters for each of the instances namely weight-loss / gain / retention separately and hence, account

for this factor successfully.

- **Alternate wrinkle patterns** : The rates at which facial wrinkles are manifested on individuals across different ages is often subjective. The proposed texture variation model can be used to predict the different wrinkle patterns that could have been observed on the individual.

In future, we wish to reduce the redundancy in the required facial features. The proposed facial aging model cannot account for facial hair and hence cannot address hair loss. With the advent of 3D measurements of growing adult faces (by means of laser scans), the proposed shape transformation model can be adopted to characterize facial aging effects in 3D.

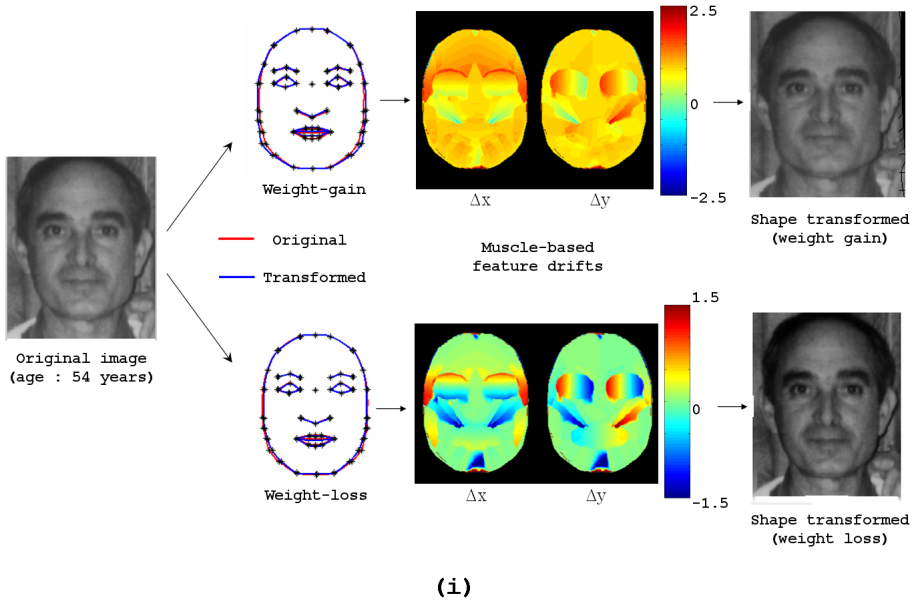

Figure 4.10: An overview of the proposed facial aging model : Facial shape variations induced for the cases of weight-gain and weight-loss are illustrated. Further, the effects of gradient transformations in inducing textural variations are illustrated as well.

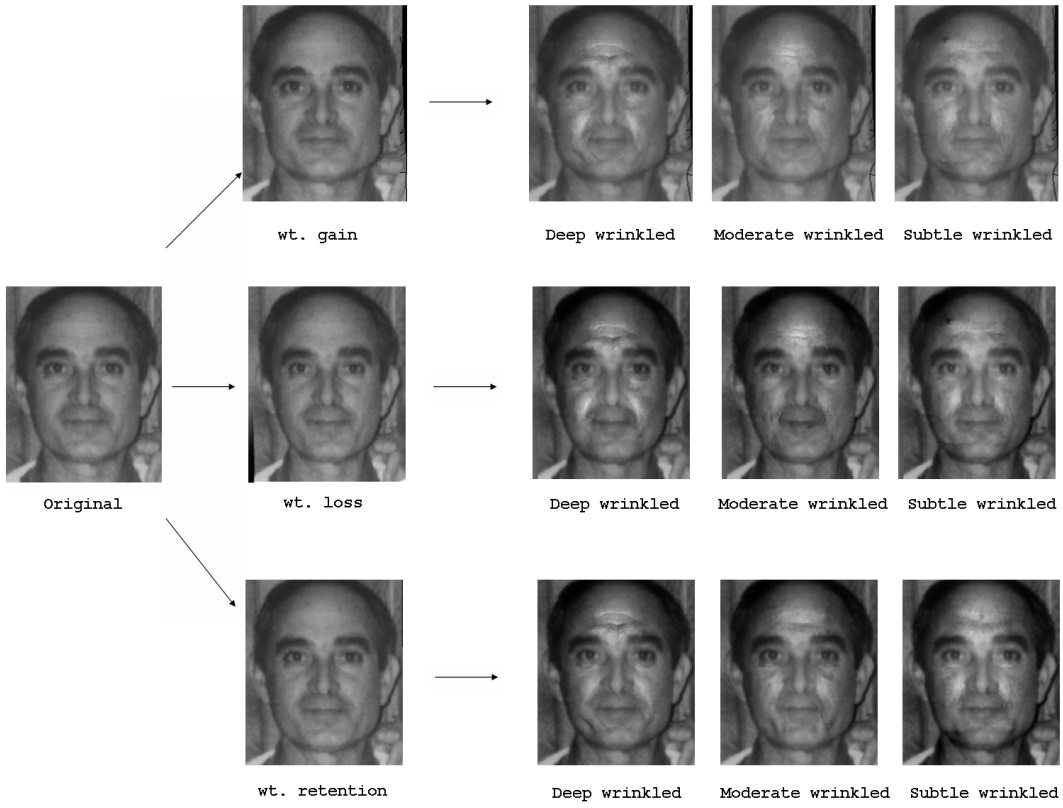

Figure 4.11: Aged images generated from a single image as part of the face verification experiment.

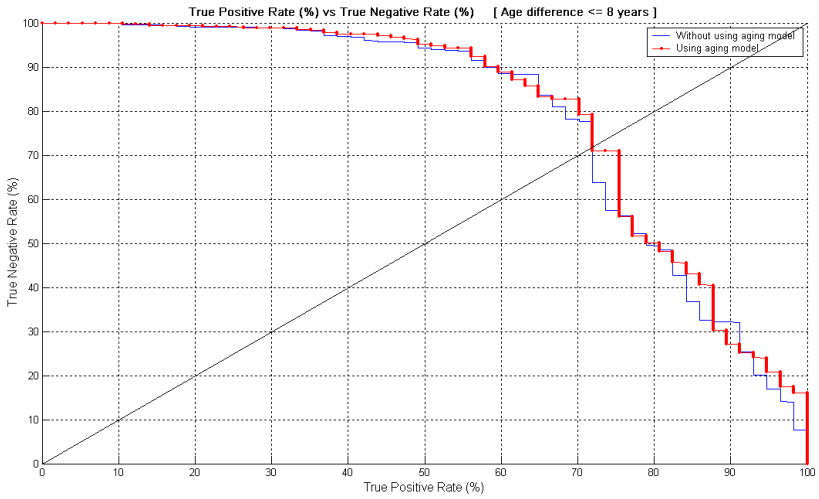

Figure 4.12: True positive rate vs. False negative rate, when age separation is lesser than 9 years.

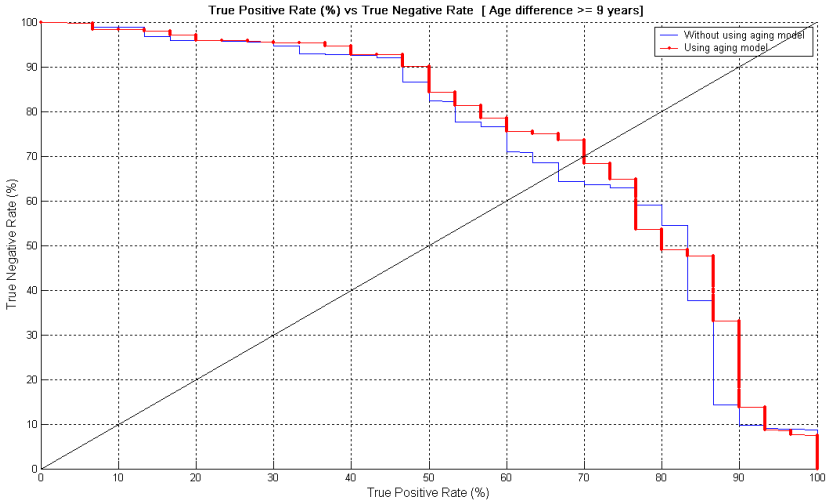

Figure 4.13: True positive rate vs. False negative rate, when age separation is 9 years or greater.

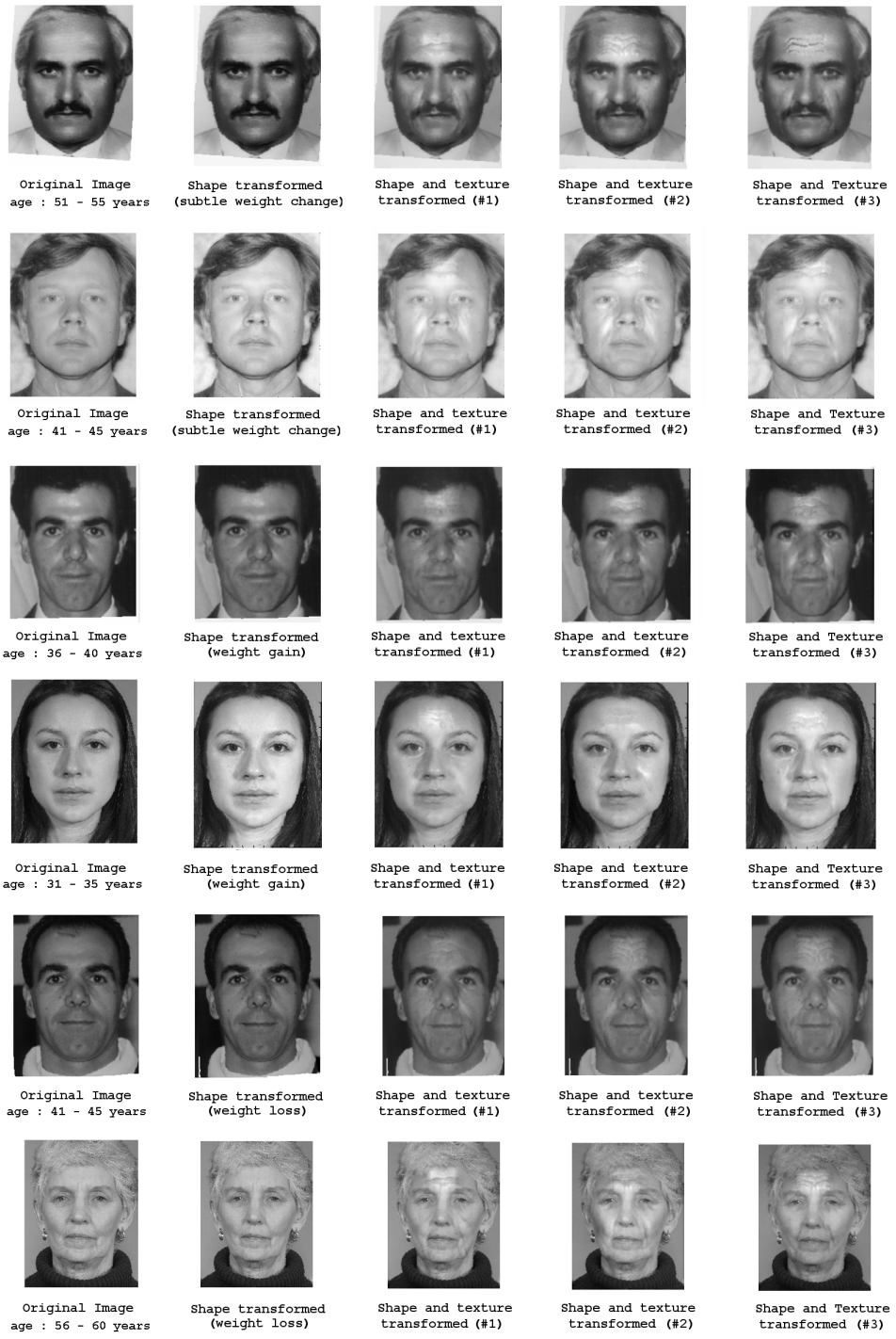

Figure 4.14: Appearance prediction across ages : The 2nd column illustrates the shape transformation results for the three types of weight-change across ages. The 3rd, 4th and 5th columns illustrate the textural variations induced on the shape transformed image, using image gradient transformations that correspond to 'subtle', 'moderate' and 'strong' wrinkles.

Chapter 5

Face Verification across Age Progression

Face recognition systems often encounter images of individuals taken from real-life conditions where facial appearances are affected by the inter play of multiple factors such as illumination, pose, facial expressions, age, occlusions etc. Hence, the robustness to variations due to factors such as illumination, pose, facial expressions, aging etc. is a significant metric in evaluating face recognition systems. In this chapter, we propose a method to perform face verification across age progression.

5.1 Problem Statement

While face images have traditionally been used in identification documents such as passports, driver's licenses, voter ID etc., in recent years, face images are being increasingly used as additional means of authentication in applications such as credit/debit cards and in places of high security. Since faces undergo gradual variations due to aging, periodically updating face databases with more recent images of subjects might be necessary for the success of face recognition systems. Since periodic updating of such large databases would be a tedious task, a better alternative would be to develop face recognition systems that verify the identity of individuals from a pair of age separated face images. Understanding the role of age progression in affecting the similarity between two face images of an individual is important in

such tasks.

How similar is a pair of age separated face images of an individual ? How do inherent changes in a human face due to aging, affect facial similarity ? Given a pair of age separated face images of an individual, what is the confidence measure associated with verifying his/her identity ? Our database comprises of pairs (younger and most recent) of face images retrieved from the passports of 465 individuals. Table 5.1 summarizes the database. The age span of individuals in our database is 20 years to 70 years. Fig. 5.1 shows a few sample images from our database.

Table 5.1: Database of Passport Images

Age Difference	**No: of image pairs**
1-2 yrs	165
3-4 yrs	104
5-7 yrs	81
8-9 yrs	115

Though passport images are generally taken under controlled environments, subtle variations in head pose tend to exist and hence face images are not strictly frontal in pose. Further, we observed many instances where passport images were taken under non-uniform illumination conditions. To study age progression in human faces, it is crucial to reduce variations due to factors such as head pose and

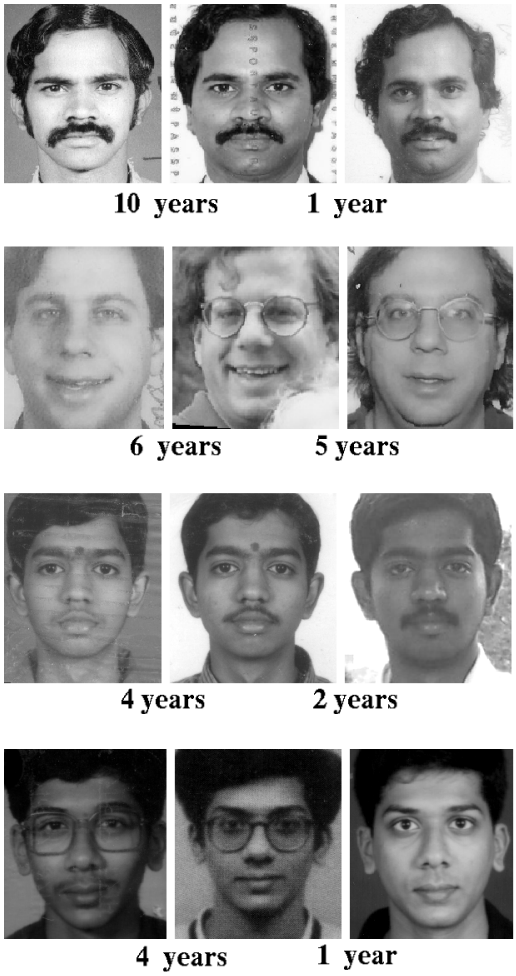

Figure 5.1: A few sample age separated images of individuals retrieved from their passports

illumination. In section II, we propose methods to recover a frontal face from non-frontal face images and to circumvent non-uniform illumination on faces. In section III, we build a Bayesian age-difference classifier that verifies the identity between a pair of age separated face images and estimates the age difference between a pair of face images. In section IV, we study the similarity of faces across age progression and highlight some of the interesting results obtained using the proposed similarity

measure. Section V discusses some directions for future work.

5.2 Frontal face recovery

In this subsection, we propose a method to recover the frontal face of an individual from a non-frontal face image. Blanz and Vetter, in their seminal work on 3D morphable models for faces [79], [18], estimate the 3D shape and texture of faces from a single face image and perform face recognition across varying pose and illumination. Our method draws inspiration from their work. But the computational simplicity of our method coupled with the need for very little manual intervention, if any, makes our approach more suitable to the recovery of frontal faces from non-frontal passport images. Head pose orientations are generally described using three angles, namely, pitch, yaw and roll. Though pose variations in passport images are generally small, in our dataset we observed that the face orientations described by the yaw angle were significantly different from that of frontal faces. Hence, we focus on recovering the frontal face from face images where the yaw angle is non-trivial. The method is trivially extendable to pose correction on rotations about the other two axes. Our approach is described in detail, below.

Our training set comprises of 3D head scans of 100 faces. Let S_1,S_2,.....,S_{100} and T_1,T_2,.....T_{100} be the corresponding shape and texture vectors extracted from the 3D head scans of the 100 faces. The shape vector $S = (x_1, y_1, z_1, ..., x_N, y_N, z_N)^T$ represents the (x, y, z) co-ordinates of N vertices and the texture vector $T = (t_1, t_2, ...t_N)^T$ represents the gray scale intensities at the N corresponding vertices. Let R_θ corre-

spond to the rotation matrix for a yaw angle θ. The 3D faces are rotated by different angles θ and the corresponding textures are extracted by appropriately mapping the frontal face textures to faces rotated by such angles. Let f be the function that maps frontal face textures to faces in different orientations and let $T_i^{(\theta)}$, $i = 1, 2, ..., 100$ correspond to the texture of faces from the training set, rotated by a yaw angle θ. $T_i^{(\theta)}$, $i = 1, 2, ..., 100$ can be computed as below. In eq. (1), P corresponds to the orthographic projection matrix.

$$\begin{aligned} s_i^{(\theta)} &= PR_\theta S_i \\ T_i^{(\theta)} &= f(T_i, s_i^{(\theta)}) \end{aligned} \tag{5.1}$$

There exists an underlying correlation between the shape of a face and the corresponding facial texture. Our approach is based on exploiting the underlying correlation between the two attributes. We apply the principal component analysis [80] on the texture $\{T^{(\theta)}\}_{i=1}^N$ and shape vectors $\{S_i\}_{i=1}^N$ and construct their respective eigenspaces. Let the eigenvectors of the texture space $\mathbf{T}^{(\theta)}$ and shape space $\mathbf{S}$ be $\Phi^{(\theta)} = (\phi_1^{(\theta)}, \phi_2^{(\theta)}, ..., \phi_N^{(\theta)})$ and $\Psi = (\psi_1, \psi_2, ..., \psi_N)$ respectively. By projecting the shape and texture vectors at different orientations onto their respective eigenspaces, we represent them by means of their principal components.

$$T_i^{(\theta)} = \bar{T^\theta} + \sum_{j=1}^{N} \alpha_{ij}^{(\theta)} \phi_j^{(\theta)} \quad i \in (1, 2, .., N) \tag{5.2}$$

$$S_i = \bar{S} + \sum_{j=1}^{N} \beta_{ij} \psi_j \quad i \in (1, 2, .., N) \tag{5.3}$$

Hence each pair of texture and shape vector of a face $[(T_1^{(\theta)}, S_1), (T_2^{(\theta)}, S_2), ...(T_N^{(\theta)}, S_N)]$ is represented by its principal component vector pairs $[(\underline{\alpha}_1^{(\theta)}, \underline{\beta}_1), (\underline{\alpha}_2^{(\theta)}, \underline{\beta}_2), ...(\underline{\alpha}_N^{(\theta)}, \underline{\beta}_N)]$. We assume that the principal components from the respective spaces are jointly Gaussian and estimate the joint probability distribution $p(\underline{\alpha}^{\theta}, \underline{\beta}|\theta)$.

Next, given a non-frontal color image I of an individual, we extract the face region using statistical color models for skin detection [81]. Using a large number of images on which skin and non-skin regions had been manually selected, we construct skin and non-skin histogram models and design a Bayes classifier [80] to perform skin detection. Let s[rgb] and n[rgb] are the pixel counts for skin and non-skin histograms respectively and T_s and T_n, the total pixel counts in the skin and non-skin histograms respectively. The probabilities are defined as

$$P(rgb|skin) = \frac{s[rgb]}{T_s} \quad P(rgb| \sim skin) = \frac{n(rgb)}{T_n} \tag{5.4}$$

$$P(skin|rgb) = \frac{P(rgb|skin)P(skin)}{P(rgb)} \tag{5.5}$$

The detected skin region in the input image serves as a cue to estimate the scale of the input image. To estimate the head pose of the input image, we align the gray scale input image I_{gray} with an appropriately scaled average face $\bar{T^{\theta}}$ about their nose locations and compute the disparity between their edge maps I_e and $\bar{T_e^{\theta}}$ respectively. The orientation θ that minimizes the disparity between the edge maps serves as an estimate of the head pose. Since head pose variations in passport images tend to be small, we limit our search space to the range (-10 to +10) degrees.

$$\tilde{\theta} = \arg\min_{\theta} \left\| I_e - \bar{T}_e^{\theta} \right\| \tag{5.6}$$

Having estimated the pose of the input image as $\tilde{\theta}$, the input image is projected on the texture space $\mathbf{T}^{(\tilde{\theta})}$ spanned by $\Phi^{(\tilde{\theta})}$ and the principal components on the texture space are computed. The principal components on the shape space $\mathbf{S}$ are subsequently estimated as illustrated below.

$$\underline{\alpha}_I^{\tilde{\theta}} = \left\langle I_{gray} - \bar{T}^{\theta}, \Phi^{(\tilde{\theta})} \right\rangle \tag{5.7}$$

$$\underline{\beta}_I = E(p(\beta | \underline{\alpha}_I^{\tilde{\theta}}, \tilde{\theta})) \tag{5.8}$$

Having estimated $\underline{\beta}_I$, we compute the 3D shape of the input face image and recover the frontal face image.

$$S_I = \bar{S} + \sum_{j=1}^{N} \beta_{I,j} \psi_j \tag{5.9}$$

$$I_{frontal} = f^{-1}(I_{gray}, PR_{\tilde{\theta}} S_I) \tag{5.10}$$

To illustrate the performance of our method, we generated non-frontal images of four individuals from our training set at orientations -15 degrees and +15 degrees. For this experiment, the training set that was used to create the eigenspaces comprised of shape and texture of the remaining 96 individuals from the original training set. Fig. 5.2 shows the recovered frontal face images corresponding to the four non-frontal faces. Accurate face localization is a key to the success of our method. Since the eigenspaces for shape and texture can be computed off-line, the method is computationally simple. The presence of dark glasses or facial hair affects

pose estimation and hence affects the performance of our method.

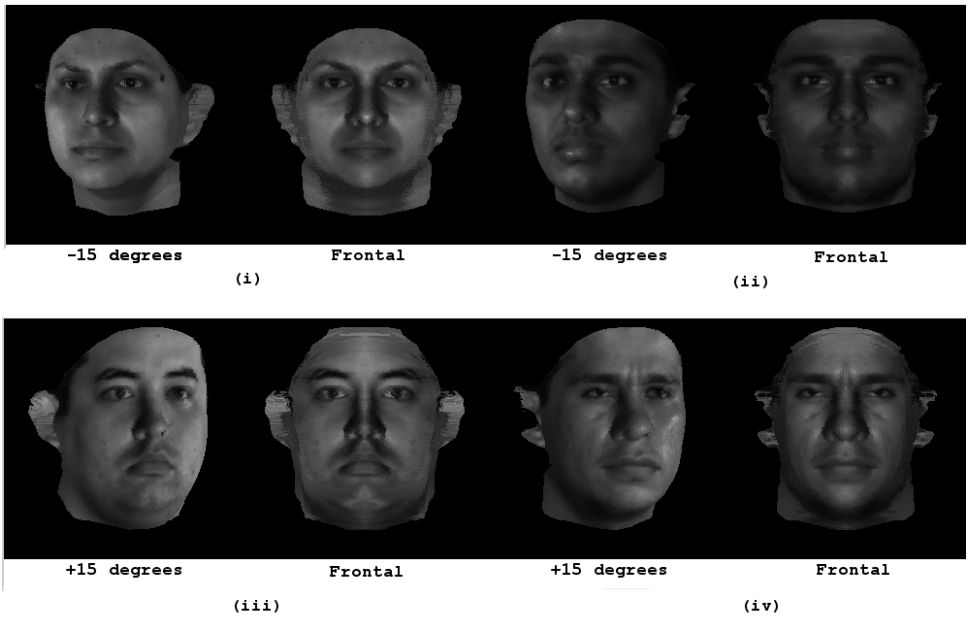

Figure 5.2: Recovery of frontal faces : Images in the top and the bottom row illustrate the recovery of frontal faces from non-frontal faces with a yaw = -15 degrees and yaw = +15 degrees respectively.

5.3 Illumination Compensation

While most face recognition systems perform commendably well on faces taken under uniform illumination conditions, their performance drops when presented with faces that were non-uniformly illuminated. Belhumeur et al. [82] discuss subspace methods for face recognition and cite that ignoring the first few principal components improves recognition performance in the presence of non-uniform illumination. Georghiades et al. [17] proposed the illumination cone model for face recognition. From a set of training images for each face, 3D models are reconstructed and

subsequently used to create synthetic images of faces under different illumination conditions and poses. The Lambertian surface approximation of faces enables the illumination cone to be well-approximated by a low-dimensional linear subspace. Basri and Jacobs [83] have shown that the set of images of a convex Lambertian object under arbitrary illumination conditions can be approximated by a low dimensional linear subspace. They construct the spherical harmonic basis images for faces and subsequently propose a simple scheme to perform face recognition. Lee et al. [84] proposed an effective approximation to the basis images using nine single light source images of a face and reported good recognition performance. Recently, Aggarwal and Chellappa [23] proposed methods to perform face recognition in the presence of multiple light sources.

However, most of these approaches need a set of training images for each subject or 3D scans of the subjects in the database. Real-life face images often contain specular reflections and hence, do not strictly exhibit the properties of a Lambertian surface. In the case of face images retrieved from passports, neither are multiple face images per subject available nor are the face images free from specular reflections. The non-uniformity in illumination in passport images is often due to imbalances in the illumination on either sides of the face. Self-shadows and specular reflections are some of the most common effects of uncontrolled illumination on faces. Given the aforementioned constraints, we propose a simple approach towards circumventing non-uniform illumination in face images retrieved from passports. We assume that faces are bilaterally symmetric and represent non-uniformly illuminated faces with the better illuminated half and discard the poorly illuminated half. Bilateral

symmetry of human faces has been used earlier in SFS problems [85]. Further, psychophysical experiments conducted by Troje and Bulthoff [86] illustrate the role of bilateral symmetry of human faces in recognizing faces across novel views. On the contrary, Liu et al. [29] and Martinez [87] studied the asymmetries in either halves of the human face and used the same for studying facial expressions.

Figure 5.3: Images of an individual under each of nine different illumination conditions from the PIE dataset [11]. With images from each of f_i, i $\in 02, 03, ...22$ as the gallery and images from f_j, j$\neq$i as the probe, a round-robin recognition experiment was performed

From a recognition perspective, how effective is the assumption of bilateral symmetry of human faces to circumvent non-uniform illumination across faces ? To answer this question, we performed an eigenface based recognition experiment on the PIE dataset [11]. The details of the experiments are as follows : Frontal faces of 68 individuals in 9 different illumination conditions ($(f_{02}, f_{03}, f_{04}, f_{05}, f_{10}, f_{13}, f_{15}, f_{16}, f_{22})$ under the PIE nomenclature) were selected. Face recognition is performed in a round-robin fashion (f_i comprises the gallery set and f_j, $i \neq j$ comprises the probe set) and the performance of full-faces as against better illuminated half-faces was studied. The eigenspaces for full-faces and half-faces were created using well illuminated frontal face images from the Yale Face Database B [17]. Table 5.4 reports

Figure 5.4: Evaluation of Half-faces : Rank 1 recognition score using Eigenfaces on Full faces and Half-faces.

Half-faces vs Full faces [a]: Rank 1 recognition scores (%)

Gallery		f_{02}	f_{03}	f_{04}	f_{05}	f_{10}	f_{13}	f_{15}	f_{16}	f_{22}
	f_{02}	-	c{97}	93{60}	38{29}	41{26}	29{4}	38{3}	35{3}	32{4}
	f_{03}	99{c}	-	c{c}	60{38}	62{41}	43{4}	41{3}	38{3}	46{3}
P	f_{04}	72{44}	c{91}	-	c{84}	97{79}	56{4}	51{1}	40{1}	57{3}
r	f_{05}	29{12}	47{21}	99{41}	-	c{c}	50{6}	37{4}	26{1}	51{6}
o	f_{10}	26{10}	54{16}	97{49}	c{c}	-	56{6}	37{4}	18{4}	51{6}
b	f_{13}	21{3}	41{3}	51{7}	53{6}	65{7}	-	97{68}	57{32}	c{c}
e	f_{15}	44{3}	51{4}	51{4}	28{4}	26{4}	99{90}	-	97{82}	c{c}
s	f_{16}	46{3}	46{4}	32{4}	18{4}	22{4}	82{49}	99{96}	-	90{65}
	f_{22}	29{3}	46{3}	54{4}	49{6}	37{7}	99{c}	c{c}	66{47}	-
Mean		46{22}	61{30}	72{54}	56{34}	56{34}	64{33}	63{35}	47{22}	66{36}

[a]Scores within {} are rank 1 recognition scores using full faces. In the table, entry 'c' corresponds to 100% recognition rates

the rank 1 recognition scores under both the settings. Figure 5.3 shows the face images from each of the 9 illumination conditions. The non-trivial improvement in recognition performance on experiments such as (f_{04} *vs.* f_{13}), (f_{10} *vs.* f_{13}) illustrate the effectiveness of the proposed approach in challenging environments.

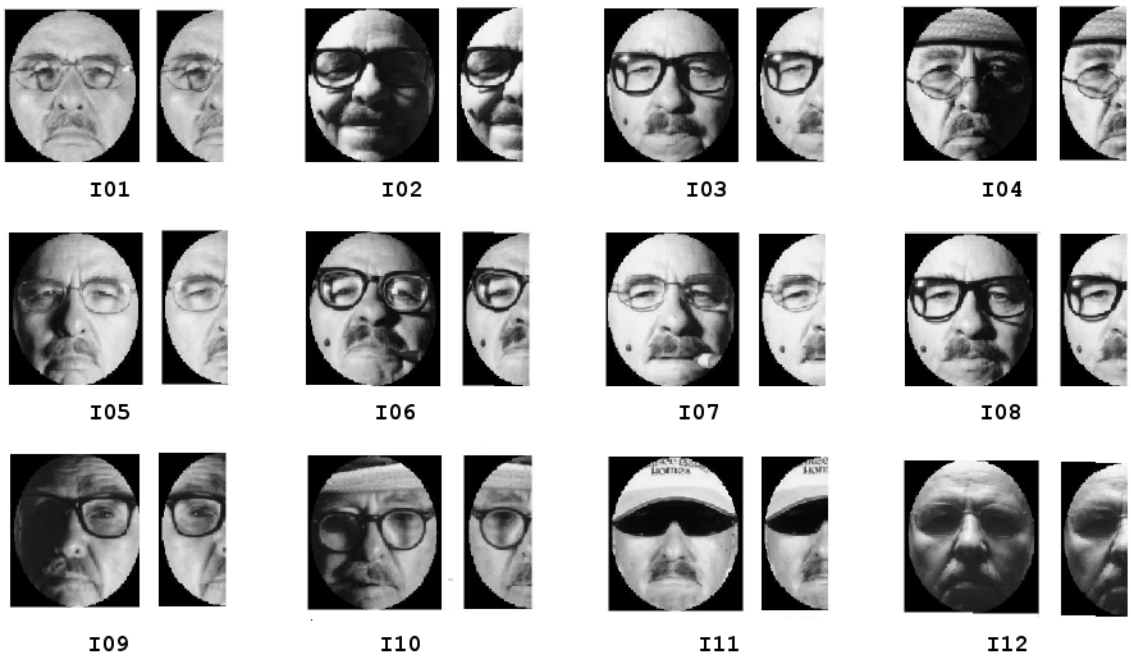

Figure 5.5: Facial similarity experiment : Images of an individual taken under different illumination conditions and their corresponding half-faces with better illumination

For the verification problem, we illustrate the significance of half-faces in computing a similarity measure on images of an individual taken under varying illumination conditions. Figure 5.5 displays the 12 test images of an individual and their respective half-faces with better illumination. We create an eigenspace Φ using a large number of well illuminated frontal faces and an eigenspace Ω using their half-faces. The full-faces and half-faces from the test set are projected on to their

respective spaces. Defining a similarity measure between two images based on the correlation between their eigenspace coefficients, we compute the similarity measure between the first test image and the remaining 11 test images. The similarity scores computed using full faces (Set I) and half-faces (Set II) are tabulated in Table 5.2. On the image samples where one half of the face was better illuminated, half-faces performed better.

Next, we define a criterion function towards the automatic selection of the better half-faces from regular face images. Given I, a frontal face image of size m x n we extract I_1 and I_2, the right half and the mirror reflected left half of I. Let $X^i = [x_1, x_2, ..., x_{n/2}]$ denote the column-wise mean intensity of I_i. The mean intensity curve of I_i, $\bar{X}^{(i)}_{MIC}$ is defined as :

$$\bar{X}^{(i)}_{MIC} = \frac{(X^{(i)} - \bar{X}^{(i)})}{\parallel X^{(i)} - \bar{X}^{(i)} \parallel} \tag{5.11}$$

where $\bar{X}^{(i)}$ denotes the mean of $X^{(i)}$ and $\parallel . \parallel$ denotes the Euclidean norm. The difference between the mean intensity curves of either halves of the face is a measure of the disparity in the spread of illumination between the two halves of the face.

$$MIC_d = \parallel \bar{X}^{(1)}_{MIC} - \bar{X}^{(2)}_{MIC} \parallel \tag{5.12}$$

A low MIC_d indicates that the spread of illumination across either halves of the face is comparable.

Next, using the above measure we compute the *optimal mean intensity curve* for frontal face images. We compute the MIC_d on face images from a large gallery of faces. If $MIC_d < \alpha$, where α is a pre-defined threshold, then the face image is

classified as optimally illuminated. From N such optimally illuminated face images, we compute the *optimal mean intensity curve* as

$$\bar{X}_{OptimalMIC} \triangleq \frac{1}{2N} \sum_{i=1}^{N} (\bar{X}^{(1)}_{MIC_i} + \bar{X}^{(2)}_{MIC_i}) \tag{5.13}$$

The criterion function for the selection of the better half face is defined as follows :

$$j = \min_{i=1,2} \quad \| \bar{X}_{OptimalMIC} - \bar{X}^{(i)}_{MIC} \| \tag{5.14}$$

$$I_{opt} = I_j \tag{5.15}$$

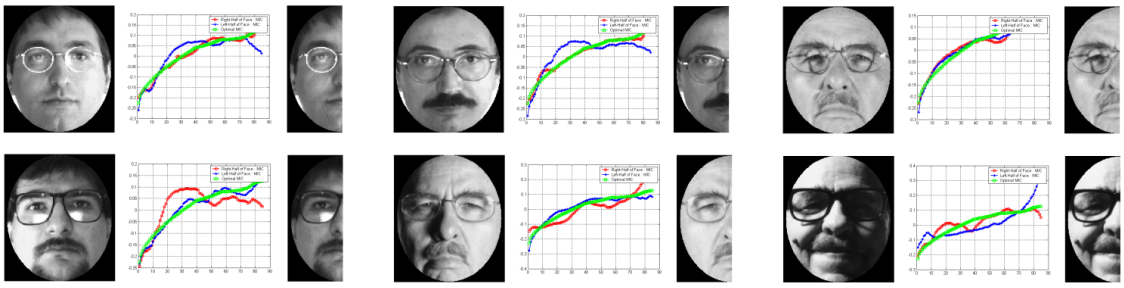

Figure 5.6: Half-faces selection criterion : Green - Optimal Mean Intensity Curve; Red - Mean Intensity Curve from the right half of the face; Blue - Mean Intensity Curve from the mirror reflected left half of the face. Some of the images from the AR Face database [12] were used for illustration purposes

Figure 5.6 illustrates the mean intensity curves for both halves of faces under different illumination conditions.

5.4 Classifier

In this section, we develop an age difference classifier designed primarily for the purpose of establishing the identity between a pair of age separated face images

and for estimating the age separation between the pair of face images. It has been observed that while faces undergo significant variations in shape from infancy to teenage years, they undergo considerably lesser variations in shape during adulthood. During adulthood, aging effects in faces are more commonly observed in the form of textural variations such as wrinkles and other skin artifacts. Facial wrinkles are primarily attributed to factors such as loss of skin elasticity (due to lesser production of collagen), habitual facial expressions, effects of gravity on facial muscles, over exposure to sun's rays etc.

Since the database of passport images comprises of individuals in the age range (20 years to 70 years), the age difference classifier is developed primarily to verify adult face images across age progression. Hence, in our formulation the age-difference based classification of face images is based on textural variations that are commonly observed in faces due to aging. Across each pair of face images, we compute the difference image by subtracting the more recent image from the older image. The difference image, when computed between age separated images of the same individual (intra-personal images), captures facial variations due to aging effects. Intuitively, the difference images obtained from the intra-personal image pairs (image pairs of the same individual) with lesser age separation would be less exaggerated than that obtained from the intra-personal image pairs with larger age separation. Further, one would expect the difference images obtained from images belonging to different individuals (extra-personal images) to be different from the ones obtained from intra-personal images due to the large mismatch in facial features. Fig. 5.7 illustrates the average difference images computed from

intra-personal images with an age separation of $1-2\ yrs,\ 3-4\ yrs,\ 5-7\ yrs,$ $8-9\ yrs$ and that computed from extra-personal images. The sagging of facial features becomes prominent in the average difference images obtained from intra-personal images as the age difference increases. Prior to classification of faces based on age differences, we perform the pre-processing steps discussed in the previous section to reduce variations due to pose and illumination.

Figure 5.7: Average difference images from the intra-personal (under each of the four age-difference categories) and extra-personal classes.

5.4.1 Bayesian Framework

We propose a Bayesian age-difference classifier that is built on a probabilistic eigenspaces framework [88]. The framework proposed in [88] was adopted primarily to estimate complex density functions in high dimensional image spaces and subsequently to compute class conditional density functions. The classification of pairs of face images based on their age-differences, consists of two stages. In the first stage of classification, the identity between the pair of face images is established. In the second stage, the pairs of age separated face images that were identified as

intra-personal images are further classified based on their age differences.

Let Ω_I denote the intra-personal space and let Ω_E denote the extra-personal space. Let I_{11}, I_{12}, I_{21}, I_{22} ,..., I_{M1}, I_{M2} be the set of N x 1 vectors formed by the lexicographic ordering of pixels in each of the M pairs of half-faces. The intra-personal image differences $\{\mathbf{x}_i\}_{i=1}^{M}$ are obtained by the difference of individuals' pairs of half-faces.

$$\mathbf{x}_i = I_{i1} - I_{i2},\ 1 \leq i \leq M \tag{5.16}$$

The extra-personal image differences $\{\mathbf{z}_i\}_{i=1}^{M}$ are obtained by the difference of half-faces of different individuals.

$$\mathbf{z}_i = I_{i1} - I_{j2}\ ,\ j \neq i,\ 1 \leq i, j \leq M \tag{5.17}$$

Firstly, from a set of intra-personal image differences $\{\mathbf{x}_i\}_{i=1}^{M} \in \Omega_I$ we estimate the likelihood function for the data $P(\mathbf{x}_i|\Omega_I)$. We assume the intra-personal difference images to be Gaussian distributed. Upon performing a Karhunen Loeve Transform [89] on the training data we get the basis vectors $\{\Phi_i\}_{i=1}^{N}$ that span the intra-personal space. But due to the high dimensionality of data such a computation is infeasible. We perform PCA [80], and extract the k basis vectors $\{\Phi_i\}_{i=1}^{k}$ that capture 99% variance in the data. The space spanned by $\{\Phi_i\}_{i=1}^{k}$ corresponds to the principal subspace or the feature space F. The remaining basis vectors $\{\Phi_i\}_{i=k+1}^{N}$ span the orthogonal complement space or the error space $\bar{F}$. The likelihood function

$P(x_i|\Omega_I)$ is estimated as

$$\begin{aligned} P(\mathbf{x}|\Omega_I) &= \frac{\exp(-\frac{1}{2}(\mathbf{x}-\bar{\mathbf{x}})^T\Sigma^{-1}(\mathbf{x}-\bar{\mathbf{x}}))}{(2\pi)^{N/2}|\Sigma|^{1/2}} \\ &= \frac{\exp(-\frac{1}{2}\sum_{i=1}^{N}\frac{y_i^2}{\lambda_i})}{(2\pi)^{N/2}\prod_{i=1}^{N}\lambda_i^{1/2}} \\ &\simeq \left[\frac{\exp(-\frac{1}{2}\sum_{i=1}^{k}\frac{y_i^2}{\lambda_i})}{(2\pi)^{k/2}\prod_{i=1}^{k}\lambda_i^{1/2}}\right] \cdot \left[\frac{\exp\left(-\frac{\epsilon^2(\mathbf{x})}{2\rho}\right)}{(2\pi\rho)^{(N-M)/2}}\right] \\ &= P_F(\mathbf{x}|\Omega_I)\ .\ \hat{P}_{\bar{F}}(\mathbf{x}|\Omega_I) \end{aligned} \tag{5.18}$$

where $y_i = \Phi_i^T(x - \bar{x})$ are the principal component feature vectors and λ_i are the eigenvalues. The marginal density in the orthogonal complement space $\hat{P}_{\bar{F}}(\mathbf{x}|\Omega_I)$ is estimated using the error in PCA reconstruction $\epsilon^2(\mathbf{x}) = \|\tilde{\mathbf{x}}^2\| - \sum_{i=1}^{k} y_i^2$ and the estimated variance along each dimension in the orthogonal subspace, $\rho = \frac{1}{N-k}\sum_{i=k+1}^{N}\lambda_i$. The sum $\sum_{i=k+1}^{N}\lambda_i$ is estimated by fitting a cubic spline function on the computed eigenvalues $\{\lambda_i\}_{i=1}^{k}$ and subsequently extrapolating the function.

Next, from a set of extra-personal image differences $\{\mathbf{z}_i\}_{i=1}^{M} \in \Omega_E$, we estimate the likelihood function $P(\mathbf{z}_i|\Omega_E)$. Adopting a similar approach as before, the extra-personal space is decomposed into two complementary spaces : the feature space and the error space. Since the assumption of Gaussian distribution of extra-personal image differences may not hold, we adopt a parametric mixture model (mixture of Gaussian) to estimate the marginal density in the feature space and follow a similar approach to estimate the marginal density in the orthogonal complement space. We estimate the likelihood for the data as

$$\hat{P}(\mathbf{z}|\Omega_E) = P(\mathbf{y}|\Theta^*)\ .\ \hat{P}_{\bar{F}}(\mathbf{z}|\Omega_E)$$

where

$$P(\mathbf{y}|\Theta) = \sum_{i=1}^{N_c} w_i N(\mathbf{y}; \mu_i, \Sigma_i) \tag{5.19}$$

$$\Theta^* = argmax \left[\prod_{i=1}^{M} P(\mathbf{y}_i|\Theta) \right] \tag{5.20}$$

$N(\mathbf{y}; \mu_i, \Sigma_i)$ is Gaussian with parameters (μ_i,Σ_i) and w_i correspond to the mixing parameters such that $\sum_{i=1}^{N_c} w_i = 1$. We solve the estimation problem using the Expectation-Maximization algorithm [90].

During the first stage of classification, given a pair of age separated face images, we extract the well illuminated half-faces I_1 and I_2 and compute the difference image $\mathbf{x} = I_1 - I_2$. The *a posteriori* probability $P(\Omega_I|\mathbf{x})$ is computed using the Bayes rule.

$$P(\Omega_I|\mathbf{x}) = \frac{P(\mathbf{x}|\Omega_I)P(\Omega_I)}{P(\mathbf{x}|\Omega_I)P(\Omega_I) + P(\mathbf{x}|\Omega_E)P(\Omega_E)} \tag{5.21}$$

The classification of the image difference as intra-personal or extra-personal is based on a maximum *a posteriori* (MAP) rule. For operational conditions, $P(\Omega_I)$ and $P(\Omega_E)$ are set equal and the difference image $\mathbf{x}$ is classified as intra personal if $P(\Omega_I|\mathbf{x}) > \frac{1}{2}$.

The second stage of classification deals with classifying the intra-personal image pairs into one of many age difference categories. For each of the four age-difference categories ($1-2\ yrs$, $3-4\ yrs$, $5-7\ yrs$ and $8-9\ yrs$), we build the intra-personal spaces denoted as Ω_1 , Ω_2 , Ω_3 , Ω_4. Next, from a set of age-difference based intra-personal difference images we estimate the likelihood function $P(\mathbf{x}|\Omega_j)$, j $\in$ 1,2,3,4 for each of the four age-difference categories. Given a difference image $\mathbf{x}$ that has been classified as intra-personal, we compute the *a posteriori* probability $P(\Omega_i|\mathbf{x})$ with $i = 1, 2, 3, 4$ as :

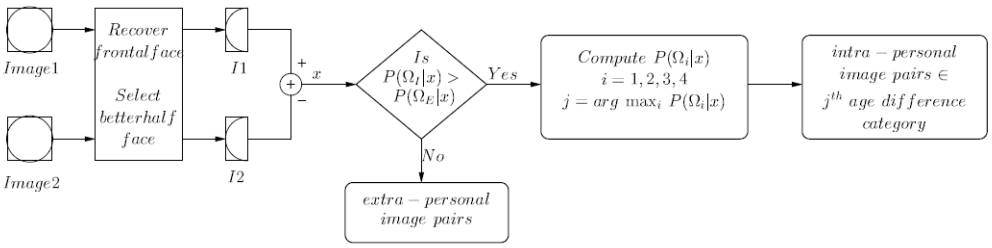

Figure 5.8: An Overview of the Bayesian Age-Difference Classifier

$$P(\Omega_i|\mathbf{x}) = \frac{P(\mathbf{x}|\Omega_i)P(\Omega_i)}{\sum_{j=1}^{4} P(\mathbf{x}|\Omega_j)P(\Omega_j)} \tag{5.22}$$

Thus if $P(\Omega_i|\mathbf{x}) > P(\Omega_j|\mathbf{x})$ for all $j \neq i$, $i, j = 1, 2, 3, 4$, then Ω_i is identified to be the class to which the difference image $\mathbf{x}$ belongs. Figure 5.8 gives a complete overview of the age-difference classifier.

5.4.2 Experimental Results

Using the above formulation, we performed classification experiments on the passport database. We selected pairs of better illuminated half-faces of 200 individuals from the database. Using their intra-personal image differences, we created the intra-personal space Ω. Computing the extra personal difference images (by randomly selecting two images of different individuals from the 200 pairs of images) we created the extra-personal space Ψ. We created two sets of image differences : Set I comprised of intra-personal difference images computed from the half-faces of 465 image pairs from the database and Set II comprised of 465 extra-personal difference images computed by a random selection of half-faces of different individuals from the database. The image pairs from Set I and Set II were classified as either

intra-personal or extra-personal.

During the second stage of classification, 50 pairs of half-face images from each of the following age-difference categories $1-2\ yrs$, $3-4\ yrs$, $5-7\ yrs$ and $8-9\ yrs$ were randomly selected and their corresponding difference image subspaces namely, Ω_1, Ω_2, Ω_3, Ω_4, were created. The image pairs from Set I that were classified as intra-personal were further classified into one of the four age-difference categories using the formulation discussed previously. The classification experiment was repeated many times using different sets of images from each age-difference category to create the intra-personal spaces. The classification results are reported in Table 5.3 in the form of percentage of images under each category that were classified into one of the four classes. The means and the standard deviations of the classification results generated from the many iterations are reported in table 5.3. The bold entries in the table correspond to the percentage of image pairs that were correctly classified to their age-difference category. The entries within parenthesis denote the standard deviations.

The classification results can be summarized as follows :

- At the operating point, 99 % of the difference images from Set I were correctly classified as intra-personal. 83 % of the difference images from Set II were correctly classified as extra-personal. It was observed that the image pairs from Set I that were misclassified as extra-personal differed from each other significantly either in facial hair or glasses. Moreover, the average age difference of intra-personal images that were misclassified was 7.4 years. The ROC plot

in fig. 5.9 was generated by varying the thresholds adopted for classification. The equal error rate is 8.5%.

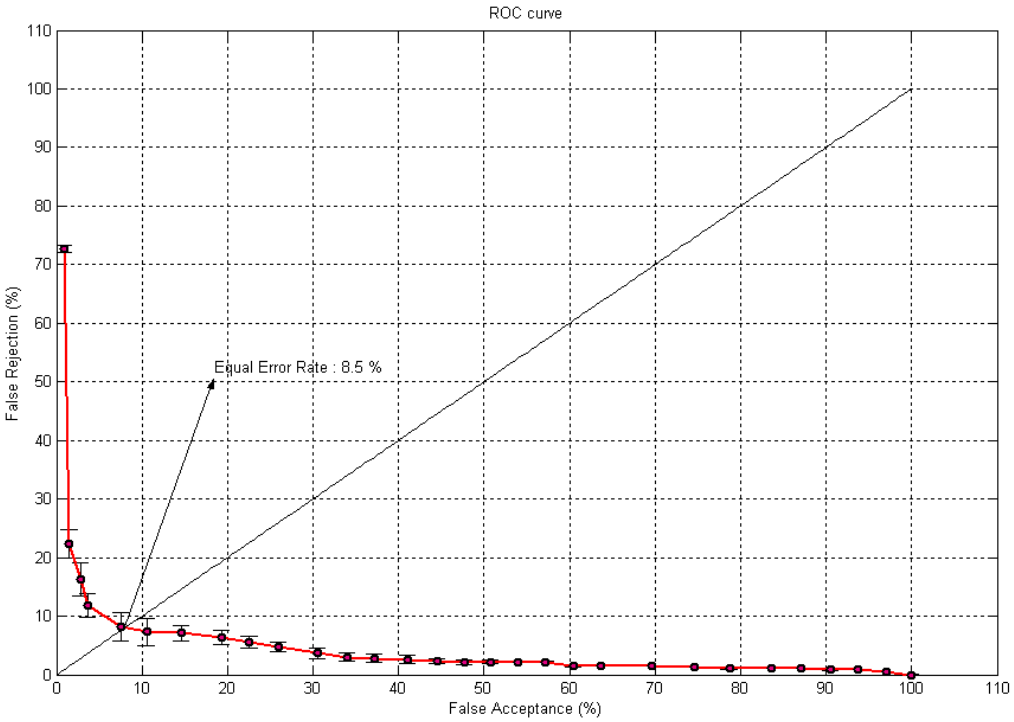

Figure 5.9: Face verification results : ROC curve

- When the image pairs from Set I that were correctly classified as intra-personal were classified further based on age-differences, it was observed that image pairs with little variations due to factors such as facial expressions, glasses and facial hair were more often classified correctly to their respective age-difference category.

- Image pairs, that belong to the age difference categories $1-2$ yrs or $3-4$ yrs or $5-7$ yrs, with significant differences in facial hair or expressions or glasses, were misclassified under the category $8-9$ yrs. Since Ω_4 was built using images from the age difference category $8-9$ yrs, it spans more intra pair

variations than those compared with the other three age difference categories and hence the above trend is observed.

To study the effects of external variations such as facial hair, glasses and facial expressions on classification accuracy, images with such variations were identified and classified separately. The images from the database were divided into four sets - ones with differences in facial hair, differences in glasses, differences in facial expressions and finally, ones with little external variations (henceforth, addressed as non-variate images). Those images with variations due to multiple external factors were classified based on the most dominant factor that caused the variations. Classification results for non-variate images are reported in Table 5.4. The classification results on images pairs with variations in facial expressions, glasses, facial hair are reported in Tables 5.5, 5.6, 5.7 respectively.

- A comparison of the classification results in Table 5.3 and Table 5.4 highlights the bias introduced by external factors such as facial hair, glasses and facial expression on age-difference based classification. While classification results improved in the age-difference categories 1-2 yrs, 3-4 yrs and 5-6 yrs on image pairs with little variations, classification results in the 8-9 yrs category were less accurate when compared to that obtained on the original image set.

- As observed in Tables 5.5, 5.6, 5.7, age-difference based classification suffers heavily in the presence of factors such facial hair, glasses and facial expressions. Since the variations induced by these factors mask variations due to aging effects, image pairs with lower age-differences were more often classified into

the age-difference category 8-9 yrs.

The eigenspace decomposition which forms an inherent part of the density estimation process reduces computational complexities significantly. Further, since the estimation of the class conditional density functions is an off-line process, the real-time computations involved in classifying image pairs based on age differences are simple.

We designed the following experiment to study how age progression affects the measure of facial similarity. We created an eigenspace using 200 half-faces retrieved from the database of passport images. The 465 pairs of half-faces were projected onto the space of eigenfaces and were represented by the projections along the eigenfaces that correspond to 95% of the variance. We adopt the similarity measure proposed in section II. Since illumination and pose variations across each pair of half-faces is minimal, the similarity score between each pair would be affected by factors such as age progression, facial expression variations and occlusions due to facial hair and glasses. We divided our database into two sets : the first set comprised of those images where each pair of passport images had similar facial expressions and similar occlusions if any, due to glasses and facial hair. The second set comprised of those pairs of passport images where differences due to facial expressions or occlusions due to glasses and facial hair were significant.

The distribution of similarity scores across the age-difference categories $1-2\ yrs$, $3-4\ yrs$, $5-7\ yrs$ and $8-9\ yrs$, is plotted in Figure 5.10. The statistical variations in the similarity scores across each age-difference category and across each

set of passport images are tabulated in Table 5.8.

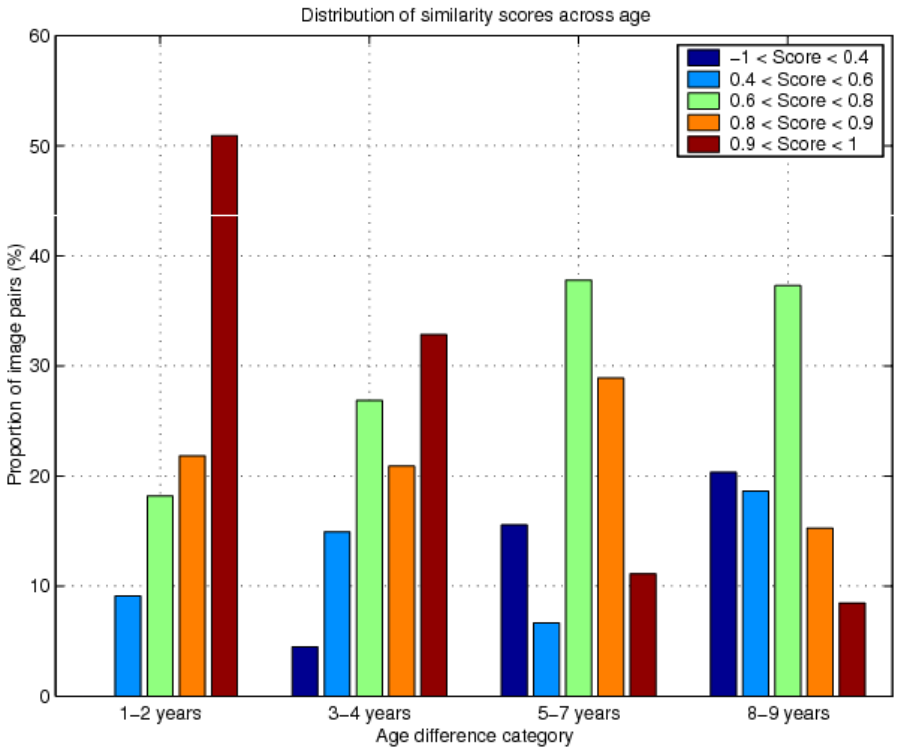

Figure 5.10: Facial similarity across time : Distribution of Similarity scores across age

- From Figure 5.10 we note that as the age difference between the pairs of images increases, the proportion of images with high similarity scores decreases.
- While the distribution of similarity scores has a strong peak for category $1-2yrs$, it flattens out gradually as the age difference increases.
- From Table 5.8 we note that as the age difference increases, across both the sets of images and across all the variations such as expressions, glasses and

facial hair, the mean similarity score drops gradually and the variance of the similarity scores increases.

- Within each age-difference category, we see a notable drop in similarity scores when variations due to expressions and facial hair are more pronounced.

5.5 Conclusion

From a face recognition perspective, understanding the process of age progression in human faces is crucial towards the development of face recognition systems that are robust to aging effects and in the successful deployment of such systems. Some of the limitations one faces while addressing age progression in human faces :

- Human faces undergo complex variations due to aging. Modeling the complex shape variations human faces undergo during one's younger years or the textural variations that are observed during the later years is a very challenging task. Apart from biological factors, since factors as diverse as ethnicity, climatic conditions, food intake, mental stress etc. also contribute towards aging effects, it is natural to expect different individuals to age differently.

- Manifestations of aging effects in human faces such as shape and textural variations can be best understood using 3D scans of human heads. With 3D head scans becoming increasingly available, we anticipate the development of more robust methods to address age progression.

- Lack of databases of age progressed face images of individuals is another reason

for lesser research on this topic. Only recently, the FG-Net aging database [2] that contains real life images of many individuals across ages, has become publicly available. Since real life images are often taken under uncontrolled environments, the age separated images in this database differ significantly in other aspects such as illumination and pose. Such external variations need to be minimized before studying aging effects.

Our primary objective was to study the effects of age progression on facial similarity measure and to develop systems that can perceive age separation between a pair of images of an individual. The relatively well controlled environments under which passport images are taken, make them ideally suited for studying the effects of age progression in human faces. We presented a Bayesian age-difference classifier that identifies the age separation between a pair of face images of an individual. In our formulation, the difference images obtained from a pair of intra-personal age separated face images formed the primary basis for classification. While the characterization of the intra-personal difference images were based on their age-differences, the age group to which the image pairs belonged to, were not considered primarily due to lack of sufficient samples to characterize such variations for each age group. While the method presented in this chapter is suitable to handle age progression in adult face images, since it does not account for shape variations in faces, it may not be effective for handling age progression in face images of children. We also studied facial similarity across age progression and highlighted the role of age progression in affecting similarity scores.

Table 5.2: Facial Similarity Scores : Set I corresponds to full faces and Set II corresponds to half-faces faces.

Similarity Score(I_{01}, I_n)			
Image	Set I	Set II	Remark
I_{02}	-0.43	0.33	
I_{03}	-0.13	0.79	
I_{04}	-0.44	0.81	
I_{05}	0.11	0.90	half-faces
I_{06}	-0.45	0.77	in set II perform
I_{07}	0.14	0.95	better
I_{08}	-0.16	0.84	
I_{09}	-0.32	0.22	
I_{10}	-0.34	0.16	
I_{11}	0.58	0.49	No Distinct
I_{12}	-0.48	-0.37	Advantage

Table 5.3: The overall results of the Bayesian Age-difference Classifier

Type	Class	1-2 yrs	3-4 yrs	5-7 yrs	8-9 yrs
Original set of images	Ω_1	**41.0 (1.1)**	12.0 (6.9)	9.0 (5.0)	38.0 (7.2)
	Ω_2	8.0 (5.0)	**46.0 (5.6)**	8.0 (4.9)	37.0 (9.2)
	Ω_3	10.0 (3.3)	8.0 (6.3)	**53.0 (4.4)**	28.0 (6.9)
	Ω_4	10.0 (2.3)	12.0 (7.3)	5.0 (5.4)	**73.0 (8.2)**

Table 5.4: Classification results on Non-Variate images pairs

Type	Class	1-2 yrs	3-4 yrs	5-7 yrs	8-9 yrs
Images with less external variations	Ω_1	**53.0 (3.8)**	14.0 (2.3)	12.0 (5.0)	21.0 (7.2)
	Ω_2	9.0 (3.0)	**53.0 (4.0)**	10.0 (6.1)	29.0 (8.0)
	Ω_3	11.0 (4.9)	8.0 (4.5)	**62.0 (2.9)**	19.0 (7.2)
	Ω_4	14.0 (4.3)	13.0 (6.5)	6.0 (6.1)	**67.0 (8.9)**

Table 5.5: Classification results on images pairs with facial expressions

Type	Class	1-2 yrs	3-4 yrs	5-7 yrs	8-9 yrs
Images with variations in facial expressions	Ω_1	**33.0 (2.7)**	11.0 (14.3)	5.0 (4.9)	51.0 (13.5)
	Ω_2	10.0 (10.0)	**39.0 (9.3)**	9.0 (5.7)	42.0 (12.2)
	Ω_3	13.0 (4.2)	6.0 (8.9)	**57.0 (9.1)**	24.0 (2.0)
	Ω_4	8.0 (4.4)	12.0 (6.5)	6.0 (4.1)	**74.0 (8.9)**

Table 5.6: Classification results on images pairs with glasses

Type	Class	1-2 yrs	3-4 yrs	5-7 yrs	8-9 yrs
Images with variations in	Ω_1	**25.0 (1.9)**	12.0 (10.5)	5.0 (9.9)	58.0 (11.9)
	Ω_2	4.0 (5.2)	**51.0 (7.6)**	5.0 (6.7)	40.0 (6.7)
	Ω_3	9.0 (3.1)	8.0 (9.1)	**42.0 (6.4)**	41.0 (10.6)

Table 5.8: Similarity Measure

Age Based Similarity Measure								
Age Difference	First Set		Second Set					
			Expression		Glasses		Facial Hair	
	μ	σ^2	μ	σ^2	μ	σ^2	μ	σ^2
1-2 yrs	0.85	0.02	0.70	0.021	0.83	0.01	0.67	0.04
3-4 yrs	0.77	0.03	0.65	0.07	0.75	0.02	0.63	0.01
5-7 yrs	0.70	0.06	0.59	0.01	0.72	0.02	0.59	0.10
8-9 yrs	0.60	0.08	0.55	0.10	0.68	0.18	0.55	0.10

Chapter 6

Conclusions and Future Work

6.1 Conclusions

The many interesting studies on facial aging have provided a good understanding of the multifaceted problem and further have highlighted the many challenges associated with the problem. Given the critical stage the problem has reached, establishing a formal platform that enables the evaluation of different algorithms is critical to the success of the problem. Creating a formal facial aging dataset, identifying a set of aging-related challenge problems in varying levels of difficulty, establishing formal evaluation protocols etc. are bound to formalize the solutions proposed to the problem.

Unlike other problems in face recognition such as illumination variations, pose variations, facial expressions etc., the temporal nature of the facial aging problem introduces numerous challenges in creating a formal dataset for the problem. The success of any learning-based method that is employed on facial aging, invariably depends on how thoroughly the facial aging datasets represent the problem. In other words, with multiple factors such as ethnicity, gender, age group etc. being identified as factors that affect facial aging effects [91], it is critical that face datasets assembled for this problem span the complete spectrum of the problem. In addition, the faces that comprise the aging dataset should ideally be devoid of variations due

to other factors such as illumination, head pose, facial expressions, occlusions etc.

Some of our recommendations for future work on this topic are listed below :

- From a practical standpoint, age estimation methods should focus on identifying the age range that a face image belongs to rather than the actual age. It will be interesting to study the contributions of shape-based features and texture-based features in estimating the age of a face.

- Age-based anthropometric measurements have been shown to play a critical role in modeling facial growth during formative years [92]. To the best of our knowledge, similar such anthropometric data collected on adult faces is not available easily. With the advent of such data, developing computational models for facial aging during adulthood might be a more tractable task.

- An unusual problem that is often encountered (but ignored) while handling face images of children, is the progressive change that is observed on their facial sizes across years. Solutions that are proposed for facial aging during formative years should implicitly account for the gradual change in feature dimensions across ages. For instance, a typical preprocessing step that is often used for adult images is that of aligning the face images using a set of fiducial features such as eyes, nose, mouth etc. With intra-personal variations in facial shape being subtle during adulthood, such a pre-processing step may not directly affect different algorithms. The same may not be the case for face images in the age-range 0 to 18 years.

- Faces being 3D objects, 3D facial aging methods need to be explored. Again,

sufficient data in the form of laser scans obtained from many individuals across different ages would significantly help model the shape variations in 3D that are observed with increase in age.

6.2 Future Work : Familiarity in Face Recognition

Familiarity under the context of facial appearances has been an actively researched topic in the fields of psychophysics, human perception and neurology (prosopagnasia). From a face recognition perspective, familiarity of a human face can be described as the ability to generalize across different appearances of the same individual due to various factors using prior knowledge, which in turn helps in recognizing the individual. Familiarity of faces could be described from two perspectives.

- Familiarity with individual-specific facial characteristics
- Familiarity with the facial characteristics of the class of human faces

Studies suggested that the recognition of a familiar face was often based upon both the visual information and the broad semantic information, while the recognition of an unfamiliar face was predominantly based on the visual information. Bartlett *et al.* [93] studied the typicality of faces and suggested that distinctive faces tend to gain more familiarity than typical faces. Bruce and Young [94] proposed a functional architecture of face processing. They identified 7 distinct types of information that are derived from known faces namely pictorial codes, structural codes, visually derived semantic codes, identity specific semantic codes, name related codes, expression related codes and facial speech codes. They suggested that

the recognition of familiar faces involves a match between the product of structural encoding and the previously stored structural codes that describe the appearances of familiar faces. Vokey and Read [95], [96] addressed the role of 'typicality of a face' (a subjective rating of the difficulty of picking a particular face out of a crowd) in face recognition. They identified two orthogonal components of typicality namely 'attractiveness and familiarity' and 'memorability'. Attractiveness and familiarity were said to be context-free and structurally induced. Memorability of faces was attributed to prior exposure.

Allinson *et al.* [97] proposed a connectionist model that uses self-organizing maps in characterizing facial features in order to perform face recognition. They address familiarity of faces by means of training samples (face images taken from 5 different poses). Uttal *et al.* [98], [99] suggested that information that underlies discrimination of faces may reside mainly in the higher spatial frequencies and that familiarity and memorability were attributes belonging to two different spatial frequencies. Schwaninger *et al.* [100] and Sinha *et al.* [101] study the role of holistic features as against local features contributing to the familiarity of faces.

6.2.1 Problem Statement

We wish to incorporate the notion of 'familiarity' in developing face recognition systems. A system that is familiar with an individual's facial characteristics should ideally be able to override problems due to poor illumination, non-frontal pose, poor image resolution etc. A system that is familiar with the characteristics of the class of

human faces should ideally be able to decipher more information about an individual such as gender, age group, the presence or absence of facial occlusions etc. from the individual's appearance. We illustrate our notion by means of the figure 6.1 below :

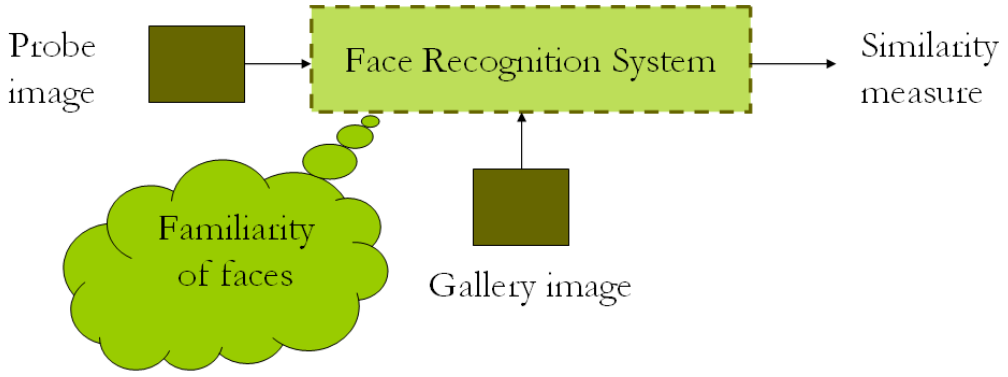

Figure 6.1: Familiarity in face recognition : Let $S_1(G, P)$ and $S_2(G, P)$ correspond to the similarity scores obtained from the gallery image G and the probe image P with and without incorporating the notion of familiarity. In the ideal scenario, $S_1(G, P) > S_2(G, P)$, when G and P correspond to the images of the same individual and $S_1(G, P) < S_2(G, P)$, when they correspond to the images of different individuals. In other words, the ROC curves obtained from the familiar face recognition system should be better than that obtained from the regular system.

6.2.2 Preliminary Experiments

The objective of this experiment was to develop a face recognition system that generalizes well across different illumination conditions. Does incorporating a face recognition system the ability to generalize across illumination changes amount to increasing the size of the training set of face images ? How does the composition of

the training set affect the system's generalizing capability ? For our experiments, we used the PIE dataset [11] and the LDA (Linear Discriminant Analysis) framework for performing recognition.

The PIE dataset comprises of images of 68 individuals taken in 21 different illumination conditions. Figure 6.2 illustrates the 21 illumination conditions. The 10 highlighted illumination conditions were chosen for our study. Our objective is to identify the best combination of illumination conditions that when comprising the training set, result in the best overall recognition performance, across images from the 10 illumination conditions. Performing an exhaustive search on the 10 highlighted illumination conditions we identify the best 'n-training set' ($2 \leq n \leq 10$). The initial observations were such that the training set that corresponds to the four illumination conditions illustrated in figure 6.3 corresponded to the best training set. Figure 6.4 illustrates the recognition rates that were obtained for each of the training sets that were identified as the best 'n-Training sets'.

6.2.3 Discussions

The above experiment illustrates that both over training and under training can affect the generalizing ability of the recognition system. The best training set was identified to be the face images that corresponded to four different illumination conditions. None of the four illumination conditions that comprised the best '4-Training Set' corresponded to frontal illumination. It is to be studied if the illumination conditions that were identified as the ones that best help the face recognition

Figure 6.2: The 21 illumination conditions from the PIE dataset are illustrated above. Different combinations of the 10 highlighted illumination conditions were used to create the training set for the LDA classifer.

system in generalizing across different illumination conditions, dependent on the nature of the recognition algorithm.

Numerous interesting studies can be performed under the context of 'familiarity' in face recognition. Can familiarity with an individual's facial appearance help in constructing a high resolution image of the individual from his or her low resolution images ? Can familiarity with gender-based facial cues or age-based facial cues help in reducing the search space for the right identity match ? How do we build quantifying measures for the 'typicality' and 'memorability' of human faces ? These are some of the topics that I would like to work on, in future.

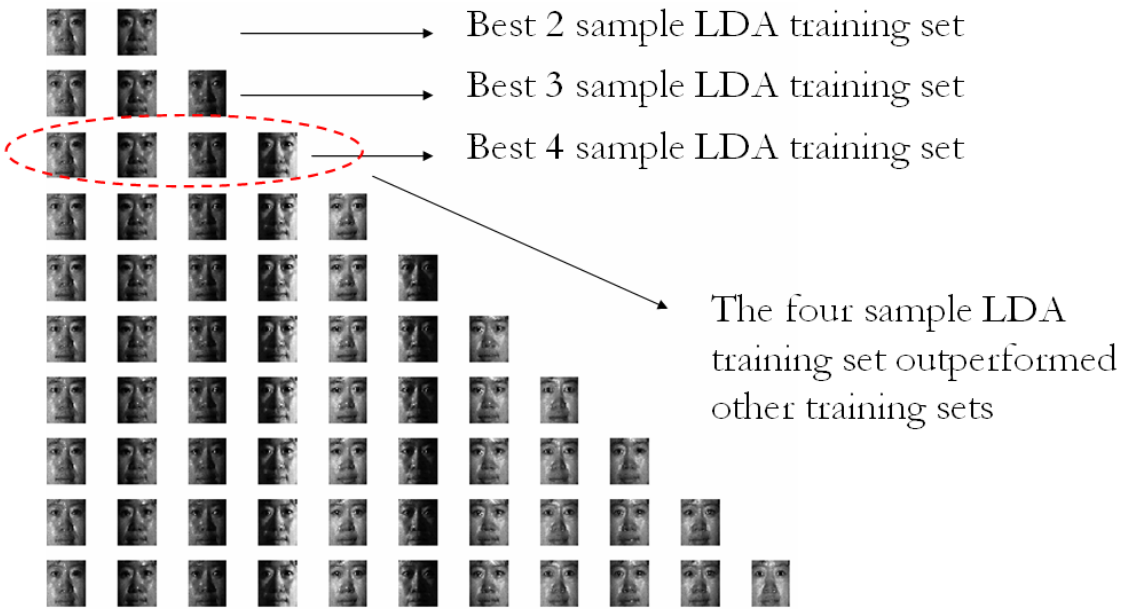

Figure 6.3: The 'n-Training set' ($2 \leq n \leq 10$) that generalizes best across all the 21 illumination conditions are illustrated.

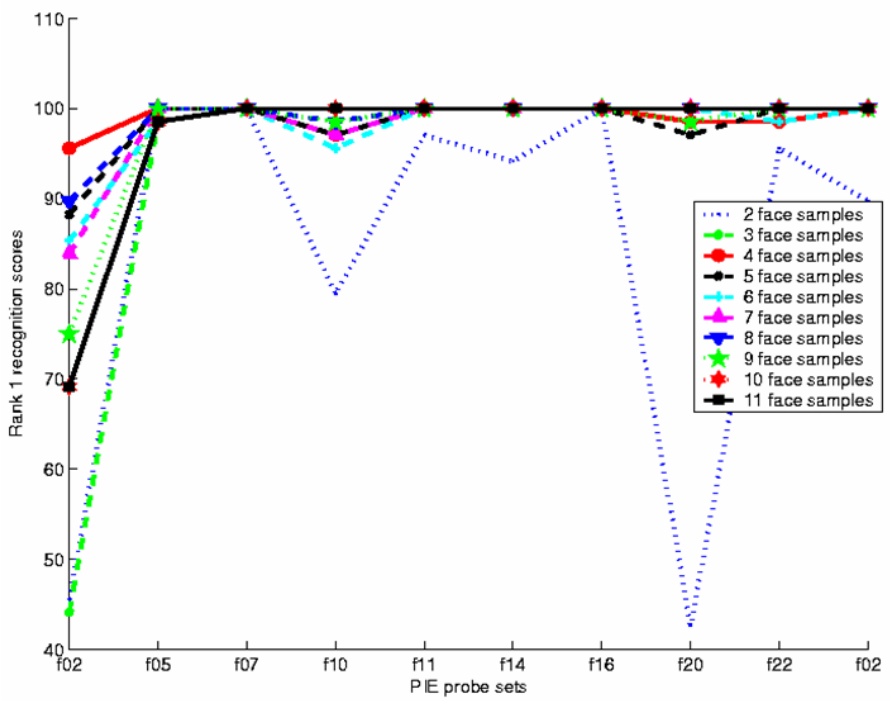

Figure 6.4: The 'n-Training set' ($2 \leq n \leq 10$) that generalizes best across all the 21 illumination conditions are illustrated.

Bibliography

[1] L. S. Mark, J. T. Todd, and R. E. Shaw, "Perception of growth : A geometric analysis of how different styles of change are distinguished," *Journal of Experimental Psychology : Human Perception and Performance*, vol. 7, pp. 855–868, 1981.

[2] FG-Net aging database. [Online]. Available: http://sting.cycollege.ac.cy/~alanitis/fgnetaging/

[3] A. J. O'Toole, T. Vetter, H. Volz, and E. M. Salter, "Three-dimensional caricatures of human heads: distinctiveness and the perception of facial age," *Perception*, vol. 26, pp. 719–732, 1997.

[4] M. Burt and D. I. Perrett, "Perception of age in adult caucasian male faces: computer graphic manipulation of shape and colour information," *Journal of Royal Society*, vol. 259, pp. 137–143, Febraury 1995.

[5] B. Tidderman, D. M. Burt, and D. Perrett, "Prototyping and transforming facial texture for perception research," *IEEE Computer Graphics and Applications*, vol. 21(5), pp. 42–50, September/October 2001.

[6] L. G. Farkas, *Anthropometry of the Head and Face.* New York: Raven Press, 1994.

[7] J. T. Todd, L. S. Mark, R. E. Shaw, and J. B. Pittenger, "The perception of human growth," *Scientific American*, vol. 242(2), pp. 132–144, 1980.

[8] FG-Net aging database. [Online]. Available: http://sting.cycollege.ac.cy/~alanitis/fgnetaging/

[9] P. Perez, M. Gangnet, and A. Blake, "Poisson image editing," *SIGGRAPH*, pp. 313–318, 2003.

[10] J. Phillips, P. J. Flynn, T. Scruggs, K. W. Bowyer, J. Chang, K. Hoffman, J. Marques, J. Min, and W. Worek, "Overview of the face recognition grand challenge," in *CVPR*, San Diego, June 2005.

[11] T. Sim, S. Baker, and M. Bsat, "The CMU pose illumination and expression database," *IEEE Transactions on Pattern Analysis and Machine Intelligence*, vol. 25(12), pp. 1615–1618, December 2003.

[12] A. M. Martinez and R. Benavente, "The AR face database CVC technical report," Tech. Rep., june 1998.

[13] W.-Y. Zhao, R. Chellappa, P. J. Phillips, and A. Rosenfeld, "Face recognition : A literature survey," *ACM Computing Surveys*, vol. 35(4), pp. 399–458, December 2003.

[14] P. J. Phillips, H. Moon, and P. J. R. S. A. Rizvi, "The FERET evaluation methodology for face recognition algorithms," *IEEE Transactions on Pattern Analysis and Machine Intelligence*, vol. 22(10), pp. 1090–1104, 2000.

[15] S. A. Rizvi, P. J. Phillips, and H. Moon, "The FERET verification protocol and statistical performance analysis for face recognition algorithm," in

IEEE Conference on Computer Vision and Pattern Recognition, Santa Barbara, U.S.A, June 1998, pp. 833–838.

[16] P. Phillips, P. Grother, R. Micheals, D. Blackburn, E. Tabassi, and J. Bone, "Frvt 2002: Overview and summary," Tech. Rep., March 2003. [Online]. Available: http://www.frvt.org

[17] A. S. Georghiades, P. N. Belhumeur, and D. J. Kriegman, "From few to many: Illumination cone models for face recognition under variable lighting and pose," *IEEE Transactions on Pattern Analysis and Machine Intelligence*, vol. 23(6), pp. 643–660, June 2001.

[18] V. Blanz and T. Vetter, "Face recognition based on fitting a 3d morphable model," *IEEE Transactions on Pattern Analysis and Machine Intelligence*, vol. 25(9), pp. 1063–1074, September 2003.

[19] R. Gross, S. Baker, I. Matthews, and T. Kanade, *Handbook of Face Recognition*. Springer, December 2004, ch. Face Recognition across Pose and Illumination.

[20] S. K. Zhou, "Unconstrained face recognition," Ph.D. dissertation, Univ. of Maryland, College Park, June 2004. [Online]. Available: http://www.umiacs.umd.edu/~shaohua/

[21] L. Zhang and D. Samaras, "Face recognition from a single training image under arbitrary unknown lighting using spherical harmonics," *IEEE Transactions*

on Pattern Analysis and Machine Intelligence, vol. 28(3), pp. 351–363, March 2006.

[22] S. K. Zhou and R. Chellappa, "Image-based face recognition under illumination and pose variations," *Journal of the Optical Society of America*, vol. 22, pp. 217–229, Febraury 2005.

[23] G. Aggarwal and R. Chellappa, "Face recognition in the presence of multiple light sources," in *IEEE International Conference on Computer Vision*, Beijing,China, October 2005, pp. 1169–1176.

[24] I. Kemelmacher and R. Basri, "Molding face shapes by example," in *European Conference on Computer Vision*, vol. 1, Graz, Austria, May 2006, pp. 277–288.

[25] P. Ekman and W. Friesen, "Facial action coding system : A technique for the measurement of facial movement," *Consulting Psychologists Press*, 1998.

[26] Y. Yacoob and L. Davis, "Recognizing human facial expressions from long image sequences using optical flow," *IEEE Transactions on Pattern Analysis and Machine Intelligence*, vol. 18(6), pp. 636–642, June 1996.

[27] I. Essa and A. Pentland, "Coding, analysis, interpretation and recognition of facial expressions," *IEEE Transactions on Pattern Analysis and Machine Intelligence*, vol. 19(7), pp. 757–763, July 1997.

[28] Y.-L. Tian, T. Kanade, and J. F. Cohn, *Handbook of Face Recognition*. Springer, December 2004, ch. Facial Expression Analysis.

[29] Y. Liu, K. L. Schmidt, J. F. Cohn, and S. Mitra, "Facial asymmetry quantification for expression invariant human identification," *Computer Vision and Image Understanding*, vol. 91(1/2), pp. 138–159, July 2003.

[30] L. S. Mark, R. E. Shaw, and J. B. Pittenger, *Social and Applied Aspects of Perceiving Faces*. NJ: Lawrence Erlbaum Associates, Inc, 1998, ch. Natural Constraints, Scales of Analysis, and Information for the Perception of Growing Faces.

[31] R. Alley, *Social and Applied Aspects of Perceiving Faces*. NJ: Lawrence Erlbaum Associates, Inc, 1998.

[32] D. W. Thompson, *On Growth and Form*. Dover Publications, 1992 (original publication - 1917).

[33] R. E. Shaw, M. McIntyre, and W. Mace, "The role of symmetry in event perception," *Perception: Essays in honor of James J. Gibson*, pp. 276–310, 1974.

[34] J. B. Pittenger and R. E. Shaw, "Aging faces as viscal-elastic events : Implications for a theory of nonrigid shape perception," *Journal of Experimental Psychology : Human Perception and Performance*, vol. 1(4), pp. 374–382, 1975.

[35] J. B. Pittenger, "The early years of Robert Shaw's craniofacial growth project," *Ecological Psychology*, vol. 17(3/4), pp. 147–159, 2005.

[36] L. S. Mark, "Developing formative models of craniofacial growth and workplace design : Personal reflections on the work and the influence of robert e. shaw," *Ecological Psychology*, vol. 17(3/4), pp. 161–191, 2005.

[37] D. H. Enlow, *The Human Face : An account of the postnatal growth and development of the craniofacial skeleton.* New York: Harper and Row : Hoeber Medical Division, 1968.

[38] M. M. Gerasivmov, *Face Finder.* Hutchinson and Co., 1971.

[39] J. B. Pittenger, R. E. Shaw, and L. S. Mark, "Perceptual information for the age level of faces as a higher order invariant to growth," *Journal of Experimental Psychology : Human Perception and Performance*, vol. 5, pp. 478–493, 1979.

[40] L. S. Mark, J. B. Pittenger, H. Hines, C. Carello, R. E. Shaw, and J. T. Todd, "Wrinkling and head shape as coordinated sources of age level information," *Journal of Perception and Psychophysics*, vol. 27(2), pp. 117–124, 1980.

[41] L. S. Mark and J. T. Todd, "The perception of growth in three dimensions," *Journal of Perception and Psychophysics*, vol. 33(2), pp. 193–196, 1983.

[42] V. Bruce, M. Burton, T. Doyle, and N. Dench, "Further experiments on the perception of growth in three dimensions," *Perception and Psychophysics*, vol. 46(6), pp. 528–536, 1989.

[43] A. J. O'Toole, T. Price, T. Vetter, J. C. Bartlett, and V. Blanz, "3d shape and 2d surface textures of human faces : The role of 'averages' in attractiveness and age," *Image and Vision Computing*, vol. 18, pp. 9–19, 1999.

[44] A. Lanitis, C. J. Taylor, and T. F. Cootes, "Toward automatic simulation of aging effects on face images," *IEEE Transactions on Pattern Analysis and Machine Intelligence*, vol. 24(4), pp. 442–455, April 2002.

[45] A. Lanitis, C. Draganova, and C. Christodoulou, "Comparing different classifiers for automatic age estimation," *IEEE Transactions on Systems, Man and Cybernetics - Part B*, vol. 34(1), pp. 621–628, February 2004.

[46] X. Geng, Z. H. Zhou, and K. Smith-Miles, "Automatic age estimation based on facial aging patterns," *IEEE Pattern Analysis and Machine Intelligence*, vol. 29 (12), pp. 2234–2240, December 2007.

[47] X. Geng, Z. H. Zhang, G. Li, and H. Dai, "Learning from facial aging patterns for automatic age esimation," in *Proc. 14th ACM International Conference on Multimedia*, 2006, pp. 307–316.

[48] Y. Fu and T. S. Huang, "Human age estimation with regression on discriminative aging manifold," *IEEE Transactions on Multimedia*, vol. 10(4), pp. 578–584, 2008.

[49] G. Guo, Y. Fu, C. R. Dyer, and T. S. Huang, "Image-based human age estimation by manifold learning and locally adjusted robust regression," *IEEE Transactions on Image Processing*, vol. 17(7), pp. 1178–1188, July 2008.

[50] J. Suo, F. Min, S. Zhu, S. Shan, and X. Chen, "A multi-resolution dynamic model for face aging simulation," in *IEEE Conference on Computer Vision and Pattern Recognition*, Minnesota, U.S.A., June 2007.

[51] U. Park, Y. Tong, and A. K. Jain, "Face recognition with temporal invariance : A 3d aging model," in *IEEE Conference on Automatic Face and Gesture Recognition*, 2008 (to appear).

[52] M. Gandhi, "A method for automatic synthesis of aged human facial images," Master's thesis, McGill University, September 2004.

[53] H. Ling, S. Soatto, N. Ramanathanan, and D. Jacobs, "A study of face recognition as people age," in *IEEE International Conference on Computer Vision*, Rio De Janeiro, Brazil, October 2007.

[54] Z. Yang and H. Ai, "Demographic classification with local binary patterns," in *International Conference on Biometrics*, 2007, pp. 464–473.

[55] Y. H. Kwon and N. da Vitoria Lobo, "Age classification from facial images," *Computer Vision and Image Understanding*, vol. 74, pp. 1–21, April 1999.

[56] S. Biswas, G. Aggarwal, and R. Chellappa, "A non-generative approach for face recognition across aging," in *IEEE Second International Conference on Biometrics : Theory, Application and Systems*, 2008 (under review).

[57] Y. H. Kwon and N. da Vitoria Lobo, "Age classification from facial images," in *IEEE Conference on Computer Vision and Pattern Recognition*, Seatle, U.S.A, June 1994, pp. 762–767.

[58] Y. Wu, N. Thalmann, and D. Thalmann, "A dynamic wrinkle model in facial animation and skin aging," *Journal of Visualization and Computer Animation*, vol. 6, pp. 195–205, 1995.

[59] M. Kass, A. Witkin, and D. Terzopolous, "Snakes: Active contour models," *International Journal of Computer Vision*, pp. 321–331, 1987.

[60] T. F. Cootes, G. J. Edwards, and C. J. Taylor, "Active appearance models," *IEEE Transactions on Pattern Analysis and Machine Intelligence*, vol. 23(6), pp. 681–685, June 2001.

[61] C. M. Bishop, *Pattern Recognition and Machine Learning*. Springer, 2006.

[62] T. Ahonen, A. Hadid, and M. Pietikainen, "Face description with local binary patterns: Application to face recognition," *IEEE Transactions on Pattern Analysis and Machine Intelligence*, vol. 28(12), pp. 2037–2041, 2006.

[63] Z. Xu, H. Chen, and S.-C. Zhu, "A high resolution grammatical model for face representation and sketching," in *IEEE Conference on Computer Vision and Pattern Recognition*, vol. 2, 2005, pp. 470–477.

[64] http://www.face-rec.org/databases/.

[65] A. M. Albert and K. Ricanek, "The MORPH database: Investigating the effects of adult craniofacial aging on automated face-recognition technology," in *Forensic Science Communications*, vol. 10(2), April 2008.

[66] K. Ricanek and T. Tesafaye, "MORPH : A longitudinal image database of normal adult age-progression," in *IEEE International Conference on Automatic Face and Gesture*, 2006, pp. 341–345.

[67] L. G. Farkas and I. R. Munro, *Anthropometric Facial Proportions in Medicine*. Springfield, Illinois, USA: Charles C Thomas, 1987.

[68] D. DeCarlo, D. Metaxas, and M. Stone, "An anthropometric face model using variational techniques," *SIGGRAPH*, pp. 67–74, 1998.

[69] K. Kahler, "A head model with anatomical structure for facial modeling and animation," Master's thesis, der Universitat des Saarlendes, 2003.

[70] D. M. Bates and D. G. Watts, *Nonlinear Regression and its Applications*. New York: Wiley, 1988.

[71] H. Moon, R. Chellappa, and A. Rozenfeld, "Optimal edge-based shape detection," *IEEE transactions on Image Processing*, vol. 11(11), pp. 1209–1226, 2002.

[72] F. L. Bookstein, "Principal warps: Thin-plate splines and the decomposition of deformations," *IEEE Transactions on Pattern Analysis and Machine Intelligence*, vol. 11(6), pp. 567–585, June 1989.

[73] M. Turk and A. Pentland, "Eigenfaces for recognition," *Journal of Cognitive Neuroscience*, vol. 3, pp. 72–86, 1991.

[74] K. Waters, "A muscle model for animating three-dimensional facial expression," *SIGGRAPH*, vol. 21, pp. 17–24, July 1987.

[75] B. Choe, H. Lee, and H.-S. Ko, "Performance-driven muscle-based facial animation," *The Journal of Visualization and Computer Animation*, vol. 12(2), 2001.

[76] Y. Zhang, E. C. Prakash, and E. Sung, "A new physical model with multilayer architecture for facial expression animation using dynamic adaptive mesh," *IEEE Transactions on Visualization and Computer Graphics*, vol. 10, no. 3, may/june 2004.

[77] C. Jarmey, *The atlas of musculo-skeletal anatomy.* Lotus Publishing, October 2004.

[78] N. Ramanathan and R. Chellappa, "Face verification across age progression," *IEEE Transactions on Image Processing*, vol. 15(100), pp. 3349–3362, 2006.

[79] V. Blanz and T. Vetter, "A morphable model for the synthesis of 3d faces," in *Computer Graphics Proc. SIGGRAPH*, Los Angeles, U.S.A, 1999, pp. 187–194.

[80] R. O. Duda, P. E. Hart, and D. G. Stork, *Pattern Classification*, 2nd ed. New York: John Wiley and Sons. Inc., 2001.

[81] M. J. Jones and J. M. Regh, "Statistical color models with application to skin detection," *International Journal of Computer Vision*, vol. 46(1), pp. 81–96, January 2002.

[82] P. N. Belhumeur, J. P. Hespanha, and D. J. Kriegnan, "Eigenfaces vs. fisherfaces : Recognition using class specific linear projection," *IEEE Transactions on Pattern Analysis and Machine Intelligence*, vol. 19(7), pp. 711–720, July 1997.

[83] R. Basri and D. W. Jacobs, "Lambertial reflectance and linear subspaces," *IEEE Transactions on Pattern Analysis and Machine Intelligence*, vol. 25(2), pp. 218–233, febraury 2003.

[84] K.-C. Lee, J. Ho, and D. J. Kriegman, "Acquiring linear subspaces for face recognition under variable lighting," *IEEE Transachtions on Pattern Analysis and Machine Intelligence*, vol. 27(5), pp. 684–698, may 2005.

[85] W.-Y. Zhao and R. Chellappa, "Symmetric shape from shading using self ratio images," *International Journal of Computer Vision*, vol. 45, pp. 55–75, 2001.

[86] N. Troje and H. Bulthoff, "How is bilateral symmetry of human faces used for recognition of novel views," *Vision Research*, vol. 38(1), pp. 79–89, 1998.

[87] A. M. Martinez, "Recognizing imprecisely localized, partially occluded and expression variant faces from a single sample per class," *IEEE Transactions on Pattern Analysis and Machine Intelligence*, vol. 24(6), pp. 748–763, June 2002.

[88] B. Moghaddam and A. Pentland, "Probabilistic visual learning for object representation," *IEEE Transactions on Pattern Analysis and Machine Intelligence*, vol. 19(7), pp. 696–710, July 1997.

[89] M. Loeve, *Probability Theory.* New Jersey: Von Nostrand Company, Inc., 1955.

[90] G. McLachlan and T. Krishnan, *The EM Algorithm and Extensions.* New York: John Wiley and Sons. Inc., 1996.

[91] E. Patterson, A. Sethuram, M. Albert, K. Ricanek, and M. King, "Aspects of age variation in facial morphology affecting biometrics," in *IEEE International Conference on Biometrics : Theory, Applications and Systems*, Crystal City, VA, 2007.

[92] N. Ramanathan and R. Chellappa, "Modeling age progression in young faces," in *IEEE Conference on Computer Vision and Pattern Recognition*, vol. 1, New York, U.S.A, June 2006, pp. 387–394.

[93] J. Bartlett, S. Hurry, and W. Thorley, "Typicality and familiarity of faces," *Memory and Cognition*, vol. 12, pp. 219–228, 1984.

[94] V. Bruce and A. Young, "Understanding face recognition," *Journal of British Psychology*, vol. 77, pp. 305–327, 1986.

[95] J. R. Vokey and J. D. Read, "Familiarity, memorability and the effect of typicality on the recognition of faces," *Memory and Cognition*, vol. 20, pp. 291–302, 1992.

[96] J. R. Vokey and J. Read, "Typicality, familiarity and the recognition of male and female faces," *Canadian Journal of Psychology*, vol. 42, pp. 489–495, 1988.

[97] N. M. Allinson, A. W. Ellis, B. M. Flude, and A. J. Luckman, "A connectionist model of familiar face recognition," *IEE Coloquium on Machine Storage and Recognition of Faces*, vol. 24, 1992.

[98] W. Uttal, T. Baruch, and L. Allen, "The effect of combinations of image degradations in a discrimination task," *Perception and Psychophysics*, vol. 57, pp. 668–681, 1995.

[99] ——, "Combining image degradations in a recognition task," *Perception and Psychophysics*, vol. 57, pp. 682–691, 1995.

[100] A. schwaninger, C. Wallraven, and H. H. Bulthoff, "Computational modeling of face recognition based on psychophysical experiments," *Swiss Journal of Psychology*, vol. 63(3), pp. 207–215, 2004.

[101] P. Sinha, B. Balas, Y. Ostrovksy, and R. Russel, "Face recognition by humans : 19 results all computer vision researchers should know about," *Proceedings of the IEEE*, vol. 94(11), pp. 1948–1962, November 2006.